# DEVELOPMENT OF ALCOHOL BIOSENSOR WITH PORPHYRIN FOR ALCOHOLIC BEVERAGE

BY

MISS JITTIMA KHORUNGKUL

A DISSERTATION SUBMITTED IN PARTIAL FULFILLMENT
OF THE REQUIREMENTS FOR THE DEGREE OF
DOCTOR OF PHILOSOPHY (BIOTECHNOLOGY)
DEPARTMENT OF BIOTECHNOLOY
FACULTY OF SCIENCE AND TECHNOLOGY
THAMMASAT UNIVERSITY
ACADEMIC YEAR 2023

THAMMASAT UNIVERSITY

FACULTY OF SCIENCE AND TECHNOLOGY

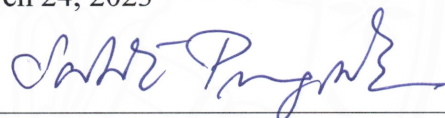DISSERTATION

BY

MISS JITTIMA KHORUNGKUL

ENTITLED

DEVELOPMENT OF ALCOHOL BIOSENSOR WITH PORPHYRIN FOR
ALCOHOLIC BEVERAGE

was approved as partial fulfillment of the requirements for

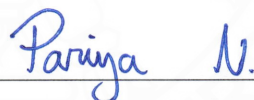the degree of Doctor of Philosophy program (Biotechnology)

on March 24, 2023

Chairman _____

(Associate Professor Sehanat Prasongsuk, Ph.D.)

Member and Advisor _____

(Assistant Professor Pariya Na Nakorn, Dr.rer.nat)

Member and co-Advisor _____
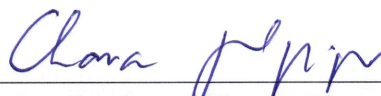
(Associate Professor Supakorn Boonyuen, Ph.D.)

Member _____

(Associate Professor Theppanya Charoenrat, Ph.D.)

Member _____

(Assistant Professor Chanan Phonprapai, Ph.D.)

Dean _____

(Associate Professor Supet Jirakajohnkool, Ph.D.)

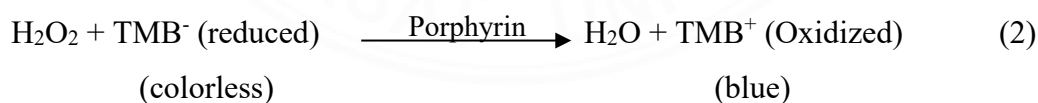| | |
|---|---|
| Dissertation Title | DEVELOPMENT OF ALCOHOL BIOSENSOR WITH PORPHYRIN FOR ALCOHOLIC BEVERAGE |
| Author | Jittima Khorungkul |
| Degree | Doctor of Philosophy program (Biotechnology) |
| Major Field/Faculty/University | Biotechnology |
| | Science and Technology |
| | Thammasat University |
| Dissertation Advisor | Assistant Professor Pariya Na Nakorn, Dr.rer.nat |
| Dissertation Co-Advisor | Associate Professor Supakorn Boonyuen, Ph.D. |
| Academic Year | 2023 |

## ABSTRACT

Hydrometry and rudimentary testing are conventional methods for ethanol detection. These methods are limited by lacking precision and accuracy resulting inability to detect trace ethanol concentrations. The data derived from those methods provide less suiTable for quality control and regulatory in the current scenario.

The researcher was trying to develop new method to measure the ethanol content. Biosensors are being considered promising approaches for the detection of ethanol due to their enhanced specificity and simplified sample treatment. Normally the ethanol was identified through the reaction of alcohol in the presence of alcohol oxidase (AOX), which is operated by oxygen ($O_2$) consumption and hydrogen peroxide ($H_2O_2$) production. The amount of $H_2O_2$ is directly proportional to the ethanol content. Furthermore, the $H_2O_2$ react with colorless form of the reduced 3,3',5,5'-tetramethylbenzidine (TMB), turning into blue oxidized TMB under the influence of peroxidase. To further improve the detection of ethanol content, the researcher investigated porphyrin and metalloporphyrin complexes as mimetic catalyst inspired by nature and possessing peroxidase-like properties.

This study investigates the catalytic properties of ethanol reduction using AOX, porphyrin and metalloporphyrin complexes. The innovative approach offers potential benefits in terms of ethanol stability, and specificity when compared with

traditional approaches. In this study, a representative porphyrin and metalloporphyrin complexes were selected including TPP, CuTPP, TOBPP, CuTOBPP, TOMPP, CuTOMPP and FeTOMPP, which were utilized for reacting with oxidized TMB in order to quantifying ethanol content in local beverages. All compounds were tested for their peroxidase-like activity. The obtained results showed that TPP and FeTOMPP exhibited better performance than CuTPP, TOBPP, CuTOBPP, TOMPP, and CuTOMPP. Furthermore, the FeTOMPP demonstrated outstanding detection properties than TPP, due to the higher activity ($0.0977 \ \mu M^{-1}$) lower $H_2O_2$ detection limit ($2.4 \ \mu M$) and low amount at $35 \ \mu g/ml$ by the mean of absorbances at 652 nm.

By harnessing the Alcohol oxidase (AOX)/FeTOMPP/TMB system, a novel colorimetric biosensor for alcohol detection was developed. This biosensor demonstrated good response and sensitivity towards ethanol detection within the range of 0-15% (v/v), with a lower detection limit of 0.0524% (v/v) and sensitivity at 0.0535% (v/v). The comparison of ethanol content in different market alcoholic beverages sample using gas chromatography (GC) and this developed biosensor reveal that ethanol values were differed less than 5%. These findings emphasize the potential applications of the AOX/FeTOMPP/TMB system for alcohol detection especially with a local beverage with rapid response (30 minutes) and precision method, moreover, it provides the possibility usage for other ethanol analytical in many applications was illustrated in reactions 1 and 2.

$$CH_3CH_2OH + O_2 \xrightarrow{AOX} CH_3CHO + H_2O_2 \quad (1)$$

$$H_2O_2 + TMB^- \text{ (reduced)} \xrightarrow{Porphyrin} H_2O + TMB^+ \text{ (Oxidized)} \quad (2)$$
$$\text{(colorless)} \qquad\qquad\qquad\qquad \text{(blue)}$$

**Keywords:** Porphyrins; FeTOMPP; Alcohol oxidase; Ethanol biosensor

# ACKNOWLEDGEMENTS

# TABLE OF CONTENTS

CHAPTER 4 RESULTS

# LIST OF TABLES

# LIST OF FIGURES

# LIST OF ABBREVIATIONS

| Symbols/Abbreviations | Terms |
|---|---|
| ABTS | 2,2'-azinobis-(3-ethylbenzthiazoline-6-sulfonic acid) |
| ABV | Alcohol by volume |
| ADH | Alcohol dehydrogenase |
| AOX | Alcohol oxidase |
| C | Celsius |
| DMSO | Dimethylsulfoxide |
| GC | Gas chromatography |
| $H_2O_2$ | Hydrogen peroxide |
| HRP | Horseradish Peroxidase |
| LOD | Limit of detection |
| $O_2$ | Oxygen |
| Porphyrin | |
| CuTOBPP | Tetrakis(4-butyloxyphenyl) phenylporphyrinatocopper(II) |
| CuTOMPP | Tetrakis(4-methoxyphenyl) phenylporphyrinatocopper(II) |
| CuTPP | Tetraphenylporphyrinatocopper(II) |
| FeTOMPP | Tetrakis(4-methoxyphenyl) phenylporphyrinatoiron(III) |
| NaOAC | Sodium acetate |
| TOBPP | Tetrakis(4-butyloxyphenyl)porphyrin |
| TOMPP | Tetrakis(4-methoxyphenyl)porphyrin |
| TPP | Tetraphenylporphyrin |
| TABs | Traditional alcoholic beverages |
| TMB | 3,3',5,5'-Tetramethylbenzidine |
| UV-Vis | Ultraviolet-Visible |

# CHAPTER 1

# INTRODUCTION

## 1.1 Statement of the problem

Fermented beverage ethanol production has a rich historical significance and is deeply rooted in various cultures worldwide. Indigenous communities play a vital role in every aspect of traditional alcohol fermentation, showcasing their invaluable knowledge and expertise in this ancient tradition. The process of producing fermented alcoholic beverages involves crucial steps that greatly influence the final product's characteristics and overall quality. In the realm of alcoholic beverage production, monitoring the concentration of ethanol throughout the fermentation process is of utmost importance (Egea *et al.*, 2016). Accurate measurement and control of ethanol levels ensure that the desired flavor profiles, alcohol content, and overall quality of the beverages are achieved. This aspect is particularly vital to meet consumer expectations and comply with industry standards. The accurate determination of ethanol concentration extends beyond the domain of beverage production. Forensic laboratories and clinical chemistry heavily rely on precise ethanol measurements for a variety of purposes (Heymann & Ebeler, 2017). Ethanol detection plays a crucial role in legal investigations, such as assessing blood alcohol levels in cases of accidents or suspected driving under the influence. In clinical settings, measuring ethanol levels aids in diagnosing and monitoring alcohol-related medical conditions. Furthermore, a broad spectrum of industries, including beverages, food, and pulp, have a growing need for fast, easy, and reliable a range of analytical techniques to oversee their manufacturing processes and guarantee product quality (Wen *et al.*, 2007). Efficient ethanol measurement techniques are vital to monitor fermentation, optimize production parameters, and ensure consistent product characteristics. These methods enable industries to maintain high standards and meet consumer demands. Additionally, ethanol determination holds significance in agricultural and environmental analyses. For instance, assessing ethanol levels at spill sites or in groundwater provides valuable information for environmental assessments and remediation efforts. Understanding the

presence and distribution of ethanol in various environmental settings aids in managing potential risks and safeguarding ecosystems (Heymann & Ebeler, 2017).

Accurate measurement of ethanol is crucial in numerous fields, requiring the advancement of reliable and robust analytical approaches. Established techniques, including oxidation-reduction titrations, colorimetric assays, density, and optical density measurements., as well as chromatographic and spectroscopic techniques, have traditionally been employed for ethanol quantification (Azevedo *et al.*, 2005). While chromatography coupled with spectrometric techniques has been widely employed for sensitive alcohol detection (Wen *et al.*, 2007), these methods often suffer from complexity, time-consuming procedures, the need for prior separations, expensive equipment, and skilled operators. The drawbacks associated with the lack of specificity in conventional chemical and physical methods have sparked a growing interest in the application of biosensors for ethanol detection. Biosensors, comprising biorecognition elements and transducers, provide a viable solution due to their exceptional specificity and performance in mild experimental conditions. This has prompted researchers to explore biosensors as promising alternatives for accurate and reliable ethanol detection. Enzymes, in particular, are highly selective and catalytically active, making them valuable tools for chemical analysis. Their ability to catalyze multiple substrate molecules provides amplification, enhancing sensitivity. Spectroscopic and electrochemical methods provide convenient means for monitoring enzyme-catalyzed reactions. In the field of alcohol detection, researchers have made significant advancements in the development of biosensors utilizing enzymes, including alcohol oxidase (AOX) and alcohol dehydrogenase (ADH), as key components for recognition and detection purposes (Azevedo *et al.*, 2005). AOX is particularly effective in catalyzing the oxidation of short-chain aliphatic alcohols, including ethanol, while ADH displays lower selectivity and can catalyze the oxidation of both aromatic and aliphatic alcohols (Barman, 1969).

In the development of alcohol sensors utilizing AOX, the detection of hydrogen peroxide, an intermediate product of AOX-catalyzed reactions, is a critical step. While the direct oxidation of hydrogen peroxide at an electrode surface is a conventional approach, recent studies have investigated alternative strategies to enhance the detection performance. These approaches involve the utilization of

peroxidase enzymes and suiTable mediators for electrochemical reduction, leading to improved sensitivity and selectivity (Akin *et al.*, 2010). The colorimetric detection of alcohols has been achieved using various biosensors based on AOX, peroxidase enzymes, and dyes such as 2,2'-azinobis-(3-ethylbenzthiazoline-6-sulfonic acid) (ABTS). These biosensors offer sensitive assays for the detection of alcohols, with sensitivities ranging from 0.05 to 1.0 μg/mL of ethanol (Magos and Haas, 1996). In recent studies, researchers have developed amperometric biosensors capable of accurately determining ethanol levels in crude plant samples. These biosensors utilize *Hansenula sp.* AOX, horseradish peroxidases (HRP), and a mediating agent as key components. The sensitivity of these biosensors rivals that of gas chromatography/mass spectrometry, making them a reliable and effective alternative for ethanol analysis (Hasunuma *et al.*, 2004). Most AOX-based biosensors reported thus far rely on monitoring either $O_2$ consumption or $H_2O_2$ formation for alcohol detection (Azevedo *et al.*, 2005). The utilization of AOX, peroxidase, and dyes such as ABTS allows for the colorimetric detection of alcohols, as illustrated in reactions 1 and 2. These biosensor systems offer promising avenues for accurate and efficient ethanol determination, addressing the need for reliable and user-friendly analytical methods in various fields of application.

$$CH_3CH_2OH + O_2 \xrightarrow{\text{AOX}} CH_3CHO + H_2O_2 \tag{1}$$

$$H_2O_2 + ABTS - [2H] \text{ (reduced)} \xrightarrow{\text{Peroxidase}} H_2O + ABTS \text{ (Oxidized)} \tag{2}$$
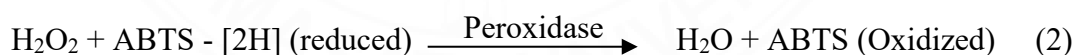
Porphyrins, being aromatic heterocyclic compounds, have garnered considerable attention in the field of biomimetic chemistry owing to their distinctive spectroscopic and chemical attributes (Milgrom, 1997). With their extensive conjugated electronic molecular structures, these compounds have become highly sought-after in materials research. Porphyrins have demonstrated diverse applications in physics, chemistry, medicine, and biology, playing pivotal roles in dye-sensitized solar cells, antibacterial activities, and sensor devices (Li *et al.*, 2004; Martelli *et al.*, 2009). The optical properties of porphyrins can be altered by undergoing chemical interactions or forming complexes with diverse molecules and ions, resulting in

significant spectral changes. This characteristic makes porphyrins and their derivatives promising candidates for the development of optical sensor elements. Recent research has emphasized the use of porphyrins as sensing materials for the detection of glucose, metal ions, pesticides, and other analytes. These studies highlight the versatility and potential applications of porphyrins in the field of optical sensing (Fenefen *et al.*, 2016; Li *et al.*, 2014; Wu *et al.*, 2008).

Moreover, researchers have explored the use of composite materials and hybrids incorporating porphyrins to replicate the catalytic functionality observed in natural enzymes and peroxidases. This approach involves modifying porphyrins with materials such as NiO, $Fe_3O_4$, and $Co_3O_4$, leading to enhanced peroxidase-like activity. These modified porphyrins are capable of catalyzing reactions with dye substrates under the influence of $H_2O_2$, resulting in noticeable color changes that can be easily observed without the need for sophisticated equipment (Liu *et al.*, 2015(a); Liu *et al.*, 2015(b); Liu *et al.*, 2014). In a recent investigation by Wu L. *et al.*, an innovative approach was employed to create an ethanol biosensor. The biosensor was constructed by immobilizing alcohol oxidase (AOX) on an electrode modified with carbon nanofiber (CNF) and FeTMPyP. The electrochemical signal generated from the reduction of oxygen at the surface of the CNF-FeTMPyP modified electrode was utilized to monitor the oxygen consumption during the ethanol oxidation catalyzed by AOX. This strategy demonstrates the potential of porphyrin-based materials in the development of biosensors and offers a promising avenue for ethanol detection (Wu *et al.*, 2008).

The requirements for alcohol monitoring in traditional alcoholic beverage demand sensitive, low-cost, and selective detection system. To address this requirement, the combination of the catalytic reaction of ethanol with alcohol oxidase (AOX) and the peroxidase-like, porphyrin, mimetics will be studied for the development of a colorimetric method for ethanol detection that will be facilitated future local beverage products analysis and further related applications.

**1.2 Research objectives**

1.2.1 To study the properties and peroxidase-like activity of porphyrin and metalloporphyrins.

1.2.2 To develop and characterize an alcohol biosensor model incorporating alcohol oxidase and peroxidase-like, selected porphyrin evaluate.

1.2.3 To evaluate alcoholic beverage samples using developed alcohol biosensor model of AOX-FeTOMPP

**1.3 Scope and limitations of study**

1.3.1 Investigation of suitable porphyrin for alcohol biosensor.

1.3.2 The optimization condition of ethanol detection will be studied, those are porphyrin concentrations, optimum pH and temperature and stability of FeTOMPP-TMB.

1.3.2 The proposed alcohol biosensor model will be characterized, linear range, sensitivity, and specificity.

1.3.4 The commercial or alcoholic beverage sample will be tested with this developed alcohol biosensor comparing with conventional method (Gas chromatographic).

**1.4 Expected results**

1.4.1 The model of AOX-FeTOMPP will be able to use as catalytic couple in alcohol biosensor.

1.4.2 The developed alcohol biosensor will exhibit exceptional sensitivity and selectivity, moreover with lower detection limit than previous report.

1.4.3 This developed alcohol biosensor will be able to use for ethanol detection of real beverage samples.

# CHAPTER 2
# REVIEW OF LITERATURE

## 2.1 Alcoholic beverage

Alcoholic beverages are produced through the fermentation of sugars found in various ingredients such as fruits, berries grains, and other substances like plate saps, tubers, honey, and milk. These sugars, which can be naturally present or generated from raw materials by breaking down starches and dextrins, are converted into ethanol by yeast during the fermentation process. This fermentation results in a liquid with alcohol content ranging from 3% to 14%. Distillation, a later introduction to liquor production, is a process that can further increase the alcohol concentration. Distilled beverages, as opposed to undistilled or fermented drinks, undergo a separation process where alcohol is separated from water through vaporization and condensation (Britanica, 2020; Britanica, 2023; "Type of alcohol," 2023; Werner, 2008).

There is a wide variety of alcoholic drinks, each with its own alcohol content. Wine and beer are examples of fermented, undistilled alcoholic beverages. Wine is an alcoholic beverage that is predominantly produced by fermenting the juice of grapes or other fruits, including apples (cider), cherries, berries, or plums. Yeast consumes the sugar in the juice and converts it into ethanol and carbon dioxide, with different grape varieties and yeast strains contributing to the distinct styles of wine ("Wine," 2023). Standard wine generally contains less than 14% alcoholic by volume (ABV), while champagne, a well-known sparkline wine, typically has an alcohol concentration of about 10% to 12%. Some wines are fortified by adding distilled alcohol, resulting in fortified wines with an ABV of around 20% ("Type of alcohol," 2023). Beer being one of the oldest and most popular alcoholic beverages worldwide, is brewed and fermented using starches, typically from malted barley, but other grains can also be used (Werner, 2008). The fundamental components of beer consist of water, a starch source, brewer's yeast and botanical additives such as hops, which collectively contribute to the distinctive flavors found in various beer varieties. Malted barley is commonly utilized due to the activation of crucial enzymes such as $\alpha$-amylase and $\beta$-

amylase enzymes during the germination process, aiding in the breakdown of starch ("Beer," 2023). Hops, derived from the flowers or cones of the hopvine, are added to provide flavor and aroma. During fermentation, specific strains of brewer's yeast, including *Saccharomyces cerevisiae, Saccharomyces uvarum*, and *Brettanomyces*, convert glucose into ethanol as showed in Figure 2.1 (Maicas, 2020). The fermentation of carbohydrates derived from raw materials such as barley, wheat, corn, or rice is responsible for the production of ethanol and carbonation, leading to the creation of beer. Typically, beer has as alcohol content ranging from 4% to 6% ABV. When beer is distilled, it transforms into a form of whisky ("Type of alcohol," 2023).
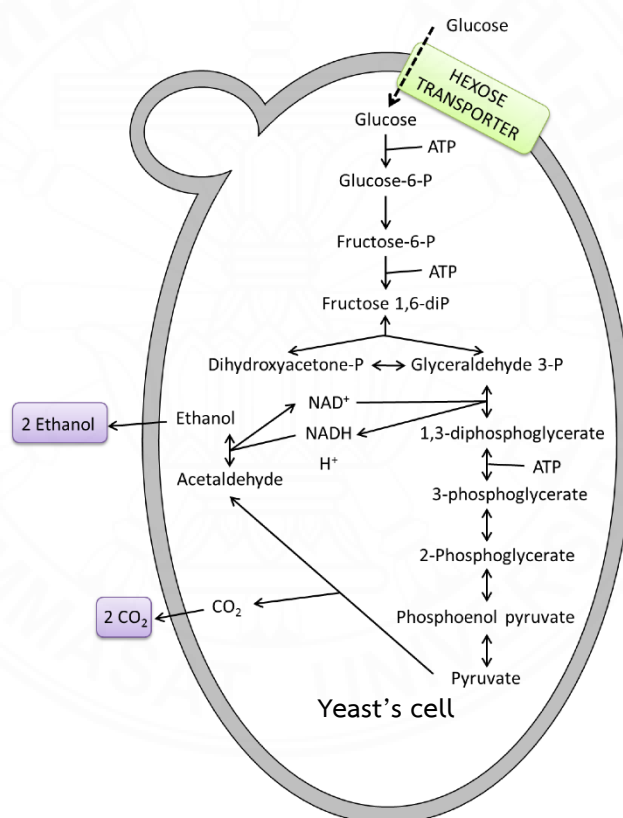


**Figure 2.1** Schematic representation of the fermentation process of glucose to ethanol by brewer's yeast (Maicas, 2020)

Distillation is a widely recognized physical process employed for the separation of mixtures based on their varying volatilities. In the context of alcoholic beverages, distillation plays a vital role in concentrating the ethanol that is produced during the fermentation process. By subjecting the mixture to heat, the ethanol, with its

lower vapor pressure compared to water, can be vaporized and subsequently condensed, leading to an increase in its concentration. Through continuous or batch distillation methods, the initial ethanol content of 5-10% obtained from fermentation can be raised to as high as 95% ABV ("Type of alcohol," 2023). Distilled spirits, such as brandy, whisky, rum, or arrack, are derived from distilling wine or other fermented fruit juices, as well as from starchy materials that have undergone brewing. These spirits typically exhibit higher alcohol content compared to beer or wine. Distilled beverages such as brandy, liqueurs, whiskey, gin, vodka, rum, or cordials generally range in alcoholic content from 40% to 50% ABV, although concentrations higher or lower can be encountered ("Type of alcohol," 2023).

Alcoholic beverages have played a significant role in various cultures throughout history, serving as a focal point for celebrations and special occasions (Egea *et al.*, 2016). These beverages, known as traditional alcoholic beverages (TABs), are typically prepared at the local or family level, giving them a unique cultural and social significance. The World Health Organization (WHO) recognizes TABs as part of the "unrecorded alcohol" category, acknowledging their global importance from cultural, social, and economic perspectives. In fact, it is estimated that around 24.8% of global alcohol consumption falls under the category of unrecorded alcohol, with certain regions such as Southeast Asia and the Eastern Mediterranean surpassing 50% (World Health Organization [WHO], 2014). TABs offer a wide range of options, each reflecting the specific traditions and customs of the respective regions. Therefore, understanding the social context surrounding the production and consumption of TABs is of great interest.

In Thailand, there is a long-standing tradition of creating and consuming alcoholic beverages using traditional and often secretive processes and tools. The knowledge of local alcoholic beverages production is typically passed down from experienced individuals or elders within the community. Thailand boasts a range of traditional alcoholic beverages that reflect local wisdom, including Sato, Lao U, Krahae, and Lao Khao (White spirits) (Kruwanna, 2001) as mentioned below:

### 2.1.1 Lao U

Lao U is made by fermented steamed rice mixed with chaff that steamed with "Loogpang" without water added in closed small water jar for 2-3 weeks. When the fermentation ready, the water jar was opened and added clean water into the fermented mixture. The bamboo straw is usually used for drinking the Lao U from the water jar. Lao U has the light brown color, fragrance, and bittersweet taste. Lao U is also called Lao Hai. Lao is alcohol, U is "cradle" in the sense of holding something under construction (Pimpen & Nitiya, n.d.).

### 2.1.2 Krachae

Krachae is fermented sugar. It is an alcoholic beverage from palm juice fermentation. Palm juice get from palm tree or coconut tree. The fermentation process takes about 7 days to complete. Krachae is turbid, bittersweet in taste (Pimpen, & Nitiya, n.d.).

### 2.1.3 Sato

Sato is produced by fermenting a mixture of glutinous rice and a solid-state starter called "Loogpang". The Loogpang starter is comprised of a blend of different microorganisms that are cultivated on rice or rice flour. The molds and yeasts present in Loogpang play crucial roles in the fermentation process. They convert the starch present in the rice into simple reducing sugars and further metabolize these sugars into ethanol. Various species of molds, including *Rhizopus* sp*., Mucor* sp*., Amylomyces* sp*.,* and *Aspergillus* sp have been reported in Sato starters and play a vital role in the initial enzymatic breakdown of starch into sugars (Kanlayakrit & Boornansawettatham, 2004). Additionally, Sato starters have been found to contain various yeast species, such as *Pichia sp., Saccharomycopsis sp., Issatchenkia sp., Saccharomyces sp*., and *Candida sp.* These yeasts ferment the sugars produced by the molds, converting them into ethanol. In addition to molds and yeasts, Sato starters also contain bacteria, with lactic acid bacteria (LAB) being the primary type. LAB species belonging to the genera *Pediococcus spp., Lactobacillus spp*., and *Lactococcus spp.* are commonly found in Sato starters (Kanlayakrit & Boornansawettatham, 2005). These bacteria contribute to the fermentation process by producing lactic acid, which helps in the development of the characteristic flavors and acidity in the final product. The combined activity of molds, yeasts, and bacteria in the Sato starter creates a complex

microbial ecosystem that transforms the rice into a unique alcoholic beverage with its own distinct flavors and characteristics.

### 2.1.3.1 The traditional production process of Sato

(Sanpamongkolchai, n.d.)

The production of Sato is a simple and accessible process, making it suiTable for household production, especially in countryside areas. The production process of Sato is illustrated in Figure 2.2.

Glutinous rice

↓

Soaked in water to soften (6-12 hr.)

↓

Cooked for 30-60 min

↓

Allow to cool to room temperature

↓

Washing with water

↓

Discharging

↓

Loogpang power
0.1-0.2 % of total weight of glutinous rice ——→ Mixing

↓

t in fermentation vessel

↓

Ferment for 24-48 hr.

↓

Sterile water added

↓

Ferment for 2 weeks

↓

Filter

↓

Sato product (alcohol 7-10% (v/v))
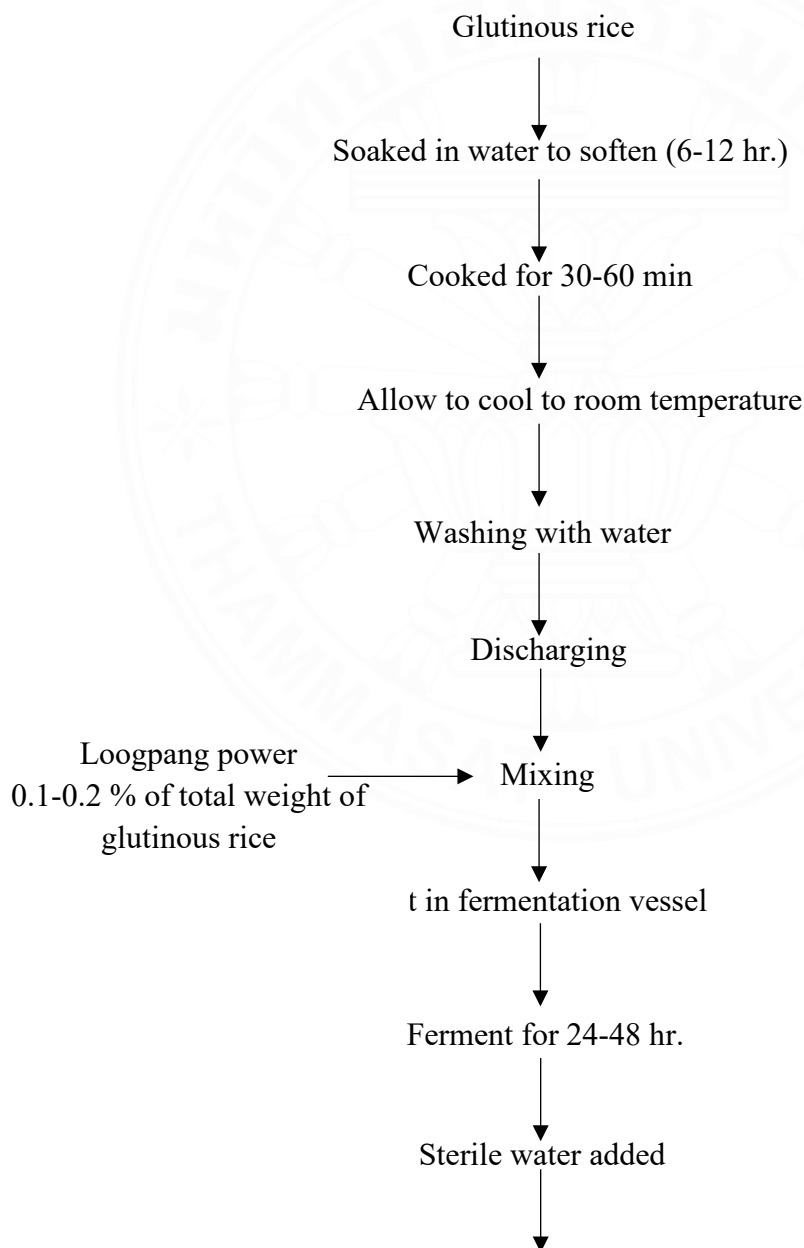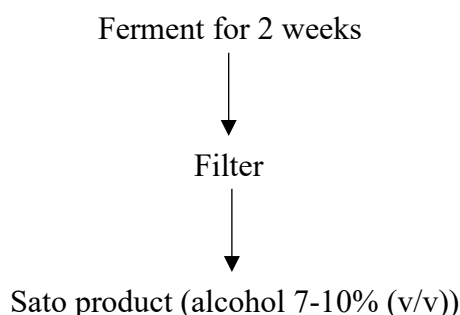
**Figure 2.2** Traditional Sato production process (Sanpamongkolchai, n.d.)

The fermentation process contributes to the alcohol content of Sato, typically ranging from 7-10% v/v (Luangkhlaypho *et al.*, 2014). During fermentation, organic acids are produced as byproducts of metabolism. The specific types and concentrations of organic acids can be influenced by the particular origin of the Loogpang starter culture used. Research studies have identified a range of organic acids, including citric acid, succinic acid, lactic acid, acetic acid, and glycerol, in Sato products prepared using various types of Loogpang starters (Luangkhlaypho *et al.*, 2014).

### 2.1.4 Lao Khao (White spirit)

"Lao Khao" is a type of Thai spirit or liquor. It's a distilled alcoholic beverage that is popular in Thailand. Lao Khao is typically made from fermented glutinous rice or sticky rice, which is distilled to produce a clear and strong spirit. It has a high alcohol content and is often consumed as a shot or used in cocktails (Pimpen, & Nitiya, n.d.).

## 2.2 Alcohol Determination

The determination of ethanol concentration holds significant importance in various industrial and biotechnology processes, including the production of foodstuffs, cosmetics, and pharmaceuticals (Wen & Choi, 2013). In additional, it is particularly crucial for alcoholic beverages due to the stringent regulations governing the labeling of such drinks. Accurate measurement of ethanol content is essential to ensure

compliance with these regulations and provide consumers with reliable information about the alcohol content of the beverages.

### 2.2.1 Conventional method for alcohol detection

Several analytical methods can be utilized to quantify the ethanol content in alcoholic beverages. These methods include gas-diffusion flow injection analysis (FIA system), electroanalysis, FIA-electroanalytical detection, infrared (IR) spectroscopy, pulse amperometry, direct injection gas chromatography (GC)/Flame ionization detection (FID), headspace injection GC/FID, high-performance liquid chromatography (HPLC)/Fourier transform (FT) IR, headspace GC/mass spectrometry (MS), FT-near infrared (NIR) spectrometry, and FT-Raman spectrometry (refer to Table 2.1) (Heymann & Ebeler, 2017). By employing these various techniques, the ethanol concentration in alcoholic beverages can be determined accurately and with high reliability. While some of these methods offer precision and reliability, they often come with drawbacks such as complexity, time consumption, requirement of prior separation processes (such as distillation or vapor permeation), costly equipment and the need for skilled personnel (Azevedo *et al.*, 2005).
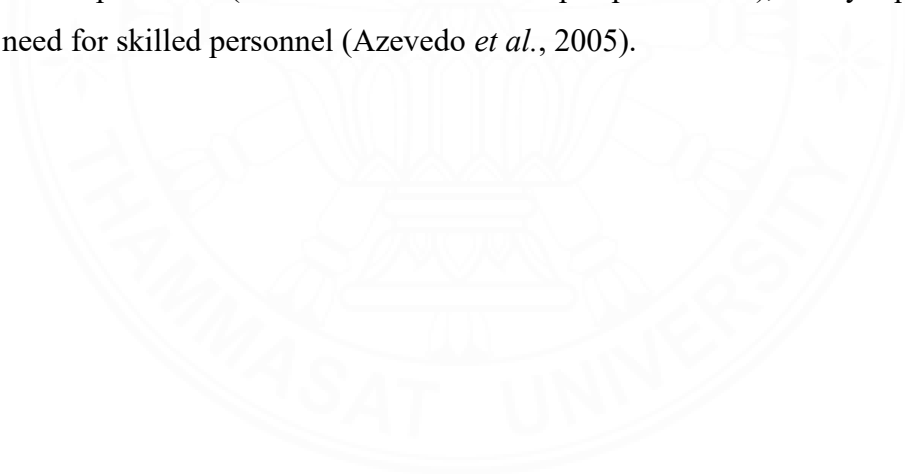
**Table 2.1**. Quantification techniques for alcohol in various sample types (Azevedo *et al.*, 2005).

| Technique | Sample | LOD | Linear range |
|---|---|---|---|
| GC/FID direct injection | Biological fluids | 0.1 ppm | 0.1-5000 mg/l |
| GC/FID headspace injection | Blood | 0.3 ppm | |
| Headspace GC/MS | Botanical medicines | | |
| HPLC/FTIR | Wine | 1-10 mg/ml | |
| HPLC/FID | Alcoholic beverages | | |
| FT-NIR spectrometry | Alcoholic beverages, Fuel | 0.05%(w/w) | |
| FT-Ramen spectrometry | Alcoholic beverages, Fuel | 0.2%(w/w) | |
| NIR spectrometry, flow injection | Liqour | 10 g/l | 200-500 g/l |
| Pulse amperometry, pt electrodes | Alcoholic beverages | 0.02 mM | 0.02-1700 mM |
| Photometry, pervaporation | Wines | 1% | |
| Photometry, Cr(IV) → Cr(III) at 600 nm | Spirits | 5% | 5-40% |

GC = gas chromatography; FID = flame-ionisaion detection; MS = mass spectroscopy; HPLC = high performance liquid chromatography; IR = infrared; NIR = near infrared; FT = Fourier transform

**2.2.2 Chemical sensor for alcohol detection**

Commonly, a chemical sensor is comprised of two main components: a receptor system and a transducer. The receptor system facilitates various interactions between the analyte and itself, including binding, adsorption, catalysis, and other relevant interactions. These interactions are responsible for the observed physiochemical changes in the system. The transducer part of the sensor then converts the resulting change into analytical signal that is measurable and quantifiable (Heymann & Ebler, 2017). There are several types of chemical alcohol sensors according to transducer as depicted below:

**2.2.2.1 Optical sensors**

An optical sensor designed for alcohol detection represents a biosensor variant utilizing optical methodologies to identify and measure alcohol concentrations across diverse sample types. These sensors operate based on the interplay between alcohol molecules and dedicated recognition elements, such as enzymes or specific chemical compounds, culminating in the generation of a quantifiable optical signal. The alteration in this optical signal serves as a direct indicator of the alcohol concentration within the tested sample (Hernandez *et al.*, 2002). There are several types of optical sensors, each designed for specific applications. Here are some common types of optical sensors:

**(1) Colorimetry based sensors**

Numerous colorimetric techniques for ethanol determination involve the oxidation of alcohol using an oxidizing agent. Common oxidizing agents used in these methods include potassium dichromate, permanganate, vanadic acid, and ceric ammonium nitrate. The oxidation reaction converts ethanol to acetic acid. The excess oxidant remaining after the reaction can be quantified either through titration or photometric measurement (Eq. (1)) (Lau & Luk, 1994; Williams & Reese, 1950).

$$2K_2Cr_2O_7 + 8H_2SO_4 + 3CH_3CH_2OH \longrightarrow 2K_2SO_4 + 2Cr_2(SO_4)_3 + 3CH_3COOH + 11H_2O \quad (1)$$

Colorimetric methods have proven to be a convenient and straightforward means of ethanol determination. These methods rely on measuring the resulting color change or the absorbance of reaction products to quantify the ethanol

content in a sample. Due to their simplicity and versatility, colorimetric methods have found extensive application in diverse fields, such as quality control in the beverage industry, forensic analysis, and research settings.

**(2) Sensors based on fluorescence**

Detection of alcohol using solvatochromic fluorescence relies on the use of a fluorescent probe or dye that exhibits a variation in fluorescence emission in response to changes in solvent polarity (Simon, 1995; Kessler *et al.*, 1991). When alcohol is present, it can modify the solvent polarity, causing a shift in the fluorescent emission of the probe. The observed change in fluorescence can be quantitatively measured and correlated with the concentration of alcohol present in the sample. Fluorescence-based sovatochromic detection is a highly responsive and specific approach for alcohol identification, offering the advantage of real-time monitoring and non-destructive analysis. It has been employed in various applications, including the analysis of alcoholic beverages, environmental monitoring, and forensic investigations (Smith *et al.*, 2020).

**(3) Infrared spectroscopy based sensors**

The Inoxilyzer, manufactured by CMI Inc., is a widely utilized alcohol sensor based on infrared (IR) spectroscopy. This device utilizes the principle of specific infrared light absorption by the bonds within ethanol molecules for identification. By analyzing the absorbed wavelengths, the Inoxilyzer can detect the presence of ethanol, while changes in IR intensity are utilized to quantify the ethanol concentration in a given sample. Additionally, short wavelength near IR spectroscopy has been reported as a method for noninvasive determination of ethanol levels (Cavinato *et al.*, 1990). This approach utilizes near IR light in the short-wavelength range to measure ethanol concentration without the need for direct contact or invasive sampling.

However, it is essential to emphasize that the methods based on IR spectroscopy, including those used by the Intoxilyzer and short-wavelength near IR spectroscopy, may suffer from limitations in terms of precision. Factors such as interferences from other compounds, variations in sample matrix, and instrumental factors can contribute to measurement uncertainties and affect the precision of the results obtained. Therefore, careful calibration and validation procedures are necessary

to ensure accurate and reliable alcohol concentration measurements using these methods (Smith & Johnson, 2018).

## (4) Sensors based on luminescence

Under acidic conditions, the interaction between ethanol and permanganate ions can lead to the generation of chemiluminescence, a phenomenon characterized by the emission of light resulting from a chemical reaction. The employment of this chemiluminescent reaction has demonstrated its efficacy in the accurate and expedient quantification of ethanol content specifically in gin (Montalvo & Ingle, 1993).

While chemiluminescence-based methods can provide a sensitive and rapid approach for ethanol determination, it is important to note that they do not distinguish between different alcohols. This means that the method cannot differentiate ethanol from other types of alcohols that may be present in a sample.

### 2.2.2.2 Electrochemical sensors

Incorporating nano and micro-technology into electrochemical sensors can significantly enhance their performance. The breath alcohol measurement sensor is a well-known example of an electrochemical sensor. Fuel cells are particularly popular for real-time breath alcohol measurement due to their portability and ease of use. In order to develop fuel cell-based sensors for analyzing alcohol content in simulated human breath, a combination of solid polymer electrolyte membrane (such as Naifon) and carbon-supported Pt catalyst has been employed (Modijtahedi *et al.*, 2016).

### 2.2.2.3 Electrical sensors

Electrical alcohol sensors, include gas sensing alcohol sensors, utilize semiconducting materials for gas detection. Among these materials, metal oxide nanostructures like $SnO_2$ and ZnO are widely employed due to their unique physical properties that make them suiTable for optoelectronic devices (Chen *et al.*, 2008; Zhang *et al.*, 2008). However, it is crucial to acknowledge that metal oxide gas sensors utilizing semiconductor materials still encounter inherent challenges that necessitate further investigation and resolution.

### 2.2.2.4 Mass sensitive sensors

Piezoelectric sensors operate by utilizing thin organic films deposited on the surface of a quartz crystal, which interact with the analyte. This interaction results in a mass change, consequently affecting the fundamental resonance frequency of the crystal. Alcohol sensing has utilized a variety of coatings, such as polymers (Otles, 2023), cyclodextrin derivatives (Tetyana *et al.*, 2021), nanomaterials (Kissinger, 2005), ionic liquids (Chaubey & Malhotra, 2002), bithiophenes (Bhalla *et al.*, 2016), and phosphonates (Castillo *et al.*, 2004). However, it is important to note that reactive analytes such as acetaldehyde can interfere with the sensor's regeneration process.

### 2.2.3 Biosensor for alcohol detection

Alcohol biosensors have gained considerable interest as a viable and promising alternative to conventional methods and non-specific chemical and physical techniques in the field of alcohol detection. These biosensors combine biorecognition elements with transducers to enable accurate and sensitive detection. Enzymes have emerged as highly suitable biorecognition elements in alcohol biosensors owing to their exceptional selectivity and robust activity under gentle experimental conditions (Reisner *et al.*, 2014). Enzymes are readily accessible and can be engineered to exhibit precise substrate specificity through molecular techniques. Alcohol biosensors have found extensive applications in diverse fields, including clinical analysis, where they are utilized for the assessment of alcohol levels in biological samples such as blood, serum, saliva, urine, breath, and sweat. Additionally, they have been utilized in the food and beverage industry to analyze wine, beer, and spirits (Patel *et al.*, 2001).

Alcohol dehydrogenase (ADH) and Alcohol oxidase (AOX) are extensively employed enzymes in the quantification of alcohol, particularly ethanol. Enzyme-based biosensors offer a straightforward and efficient approach for ethanol measurement, characterized by their simplicity in terms of assembly and operation. One of the most promising advancements in ethanol biosensors is the utilization of bi-enzymatic systems, where AOX and horseradish peroxidase (HRP) are immobilized in combination (Patel *et al.*, 2001). These biosensors offer a reliable and effective means of detecting ethanol, showcasing the potential of enzyme-based systems in alcohol determination as explained below.

### 2.2.3.1 ADH-based biosensor

ADH, also known as Alcohol:NAD+ oxidoreductase (EC 1.1.1.1), is an enzyme responsible for the reversible oxidation of primary aliphatic and aromatic alcohols, excluding methanol. The reaction is expressed in Figure 2.3.
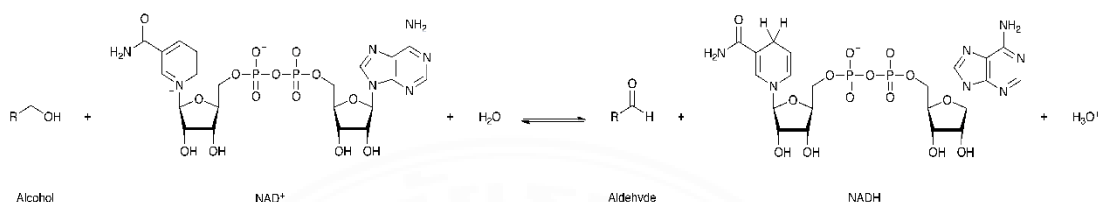


**Figure 2.3** Alcohol dehydrogenase reaction (Azevedo *et al.*, 2005)

Ethanol biosensors utilizing ADH have been recognized for their enhanced stability and specificity compared to those based on AOX. However, ADH-based biosensors require the addition of the coenzyme nicotinamide adenine dinucleotide ($NAD^+$), which acts as a cofactor for the enzymatic reaction catalyzed by ADH. $NAD^+$ facilitates the oxidation of ethanol by ADH, and it is essential to ensure its proper presence in proximity to the enzyme for efficient enzymatic activity. However, caution must be exercised to prevent the irreversible trapping or binding of the cofactor, as this could have adverse effects on the biosensor's performance. Careful optimization and design considerations are necessary to maintain the availability and functionality of $NAD^+$ in ADH biosensors, thereby ensuring accurate and reliable detection of ethanol (Azevedo *et al.*, 2005).

The ADH-catalyzed reaction is widely utilized in the detection of alcohol, employing both electrochemical and optical methods. Electrochemical transducer-based alcohol biosensors have garnered considerable interest due to their exceptional sensitivity, compatibility with *in-situ* analysis, and minimal reagent consumption. These biosensors utilize the electrochemical signal generated by the ADH-catalyzed oxidation of alcohol for quantitative detection (Hua *et al.*, 2013). In contrast, optical biosensors utilizing ADH have predominantly centered around the utilization of the fluorescence signal emitted by NADH at a wavelength of approximately 459 nm (Smith & Johnson, 2018).

Researcher have investigated various experimental setups to improve the efficiency of ADH-based optical biosensors for the detection of alcohol. One such approach involves the use of fluorescence capillary analysis in conjunction with portable UV light-emitting diodes (LEDs). This setup allows for the efficient excitation of fluorescence in the reaction mixture and the subsequent measurement of emitted light. By utilizing portable UV LEDs, the biosensors become more compact and portable, making them suitable for on-site or point-of-care applications. The combination of fluorescence capillary analysis and UV LEDs provides a convenient and effective means of detecting and quantifying alcohol using ADH-based optical biosensors (Cabaleiro *et al.*, 2012; Kudo *et al.*, 2010).

### 2.2.3.2 AOX-based biosensor

AOX, also referred to as Alcohol: $O_2$ oxidoreductase (EC 1.1.2.13), is an enzyme composed of eight identical subunits organized in a quasi-cubic arrangement. The enzyme's structure allows it to exhibit oligomeric properties. Within each subunit, there is a cofactor known as flavin adenine dinucleotide (FAD) that is tightly bound. The presence of FAD is crucial for the enzyme's catalytic activity in the oxidation of alcohols (Yang *et al.*, 2016). AOX is primarily produced by methylotrophic yeast species such as *Hansenula, Pichia,* and *Candida*, within subcellular organelles called peroxisomes, during growth on methanol as a carbon source. AOX demonstrates its capability to oxidize a range of short-chain alcohols, such as ethanol, propanol, and butanol. The enzymatic reaction facilitated by AOX leads to the transformation of these alcohols into the corresponding aldehydes, utilizing molecular oxygen ($O_2$) as the electron acceptor. This oxidation process enables the conversion of the alcohol substrates into their respective aldehyde products by removing hydrogen atoms from the alcohol molecules (Yang *et al.*, 2016). This exothermic and irreversible oxidation process is driven by the strong oxidizing properties of $O_2$, as depicted in Figure 2.4. The presence of AOX facilitates the efficient metabolism of low molecular weight alcohols in organisms that are suitable for use methanol as both a carbon source and an energy source. The specific structure and function of AOX, along with its ability to catalyze the oxidation of different alcohols, make it a valuable biocatalyst for various applications, including alcohol biosensing and bioconversion processes (Vonck & Bruggen, 1990).
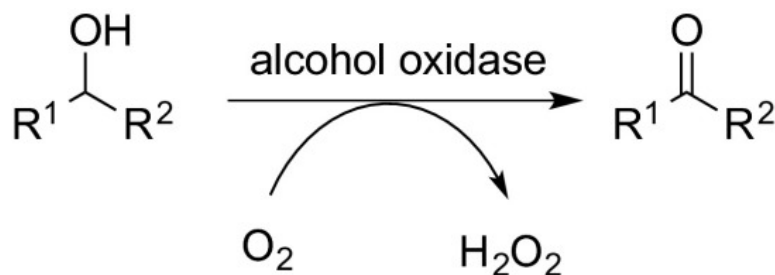
**Figure 2.4** Alcohol oxidase reaction (Pickl *et. al.*, 2015)

Conventional approaches for monitoring oxidase-catalyzed reactions typically involve quantifying the reduction in oxygen ($O_2$) levels or the accumulation of $H_2O_2$ concentration. However, detecting $H_2O_2$ has become a widely adopted alternative to address limitations associated with $O_2$ detection (Azevedo *et al.*, 2005). By measuring the concentration of $H_2O_2$, the enzymatic activity can be indirectly assessed, providing valuable information about the catalytic reaction. $H_2O_2$ detection offers several advantages, including improved sensitivity, selectivity, and stability compared to direct $O_2$ measurement. It has found extensive use in various applications, including biosensors, where $H_2O_2$ serves as a key analyte for the quantification of target substances (Smith & Johnson, 2019) as mentioned below.

**(1) $H_2O_2$ detection**

AOX biosensors provide the ability to detect the generation of hydrogen peroxide ($H_2O_2$) and can employ optical or electrochemical detection techniques for analysis. The electrochemical method involves the use of amperometric electrodes to detect the $H_2O_2$ produced by AOX. These electrodes enable the measurement of current resulting from the oxidation or reduction of $H_2O_2$ at the working electrode's surface. Two sensing schemes can be employed for $H_2O_2$ detection using AOX biosensors: direct and indirect detection as depicted in Figure 2.5. In direct detection, the AOX biosensor directly measures the electrochemical response of $H_2O_2$ (Azevedo *et al.*, 2005). The $H_2O_2$ molecules generated through the activity of AOX undergo oxidation or reduction at the working electrode, causing a detectable change in current that is directly varies in proportion to the concentration of $H_2O_2$ present. In indirect detection, the AOX biosensor utilizes $H_2O_2$ as a substrate for an enzyme that catalyzes a subsequent reaction, leading to the generation of a detectable product. This

product can be electroactive or possess other optical properties, and it is measured using appropriate techniques. The choice between direct and indirect detection methods depends on factors such as the specific application requirements, the availability of suitable enzymes, and the required level of sensitivity and specificity of the biosensor. Both optical and electrochemical detection methods provide reliable and sensitive means for $H_2O_2$ detection in AOX-based biosensors, enabling the accurate quantification of alcohol concentration (Goswami *et al*., 2013).
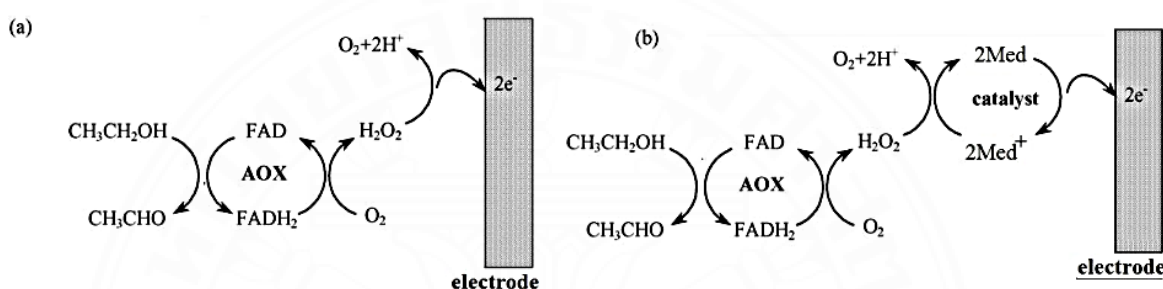


**Figure 2.5** Schematic representation of two sensing schemes for $H_2O_2$ detection by AOX electrodes: (a) Direct $H_2O_2$ detection and (b) Indirect $H_2O_2$ detection. (Azevedo *et al.*, 2005)

Hydrogen peroxide ($H_2O_2$) detection offers significant advantages in sensor technology, including ease of fabrication and miniaturization. $H_2O_2$ sensors are known for their wide linear range and high upper linearity. However, electrochemical detection of $H_2O_2$ presents challenges due to the high potential required for its oxidation, which can result in interference from reducing compounds found in real sample matrices (such as ascorbic acid and uric acid) as they are also oxidized at the same potential (Pickl *et al*., 2015). Optical biosensors offer an alternative approach, such as the fiber-optic chemiluminescence method proposed for ethanol determination in beverages. This method measures the luminescence generated from the oxidation of luminol by $H_2O_2$, utilizing $K_3FeIII(CN)_6$ as a catalyst. This approach offers a reliable method for detecting and quantifying ethanol through the analysis of the chemiluminescent signal it generates (Xie *et al*., 1992). Another method for monitoring alcohol oxidation by AOX involves the use of polyaniline (PANI). In this approach,

H$_2$O$_2$ produced in the AOX reaction oxidizes the PANI film, resulting in a noticeable color transition from green to blue. This dipstick-format biosensor allows for visual and user-friendly applications, making it suitable for on-site analysis (Kuswandi *et al.*, 2014). These examples showcase diverse strategies for H$_2$O$_2$ detection in alcohol biosensors, highlighting the versatility and potential of these sensors in applications such as beverage analysis, environmental monitoring, and quality control.

AOX sensors that rely on H$_2$O$_2$ production can utilize spectroscopic or electroanalytical detection methods. In electroanalytical detection, amperometric electrodes are employed to measure the current generated from the oxidation or reduction of H$_2$O$_2$ at the surface of the working electrode. These enzyme electrodes, which directly detect H$_2$O$_2$, are commonly known as first-generation biosensors. Spectroscopic methods, including colorimetric, chemiluminescent, and fluorescent techniques, can also be utilized for the detection of H$_2$O$_2$ production by AOX during the oxidation of alcohols (Goswami *et al.*, 2013). Colorimetric methods depend on the formation of a product that exhibits a color change, which can be quantified using spectrophotometric analysis. Chemiluminescence is characterized by the production of light through a chemical reaction, while fluorescent techniques involve the measurement of the intensity of fluorescence. In various spectrometric methods used to determine ethanol and methanol, a bi-enzymatic system incorporating AOX and a peroxidase enzyme is employed. This system facilitates the reduction of H$_2$O$_2$ to water using hydrogen donor molecules (Xie *et al.*, 1992).

### 2.2.3.3 Oxidase-peroxidase biosensor

Peroxidases, classified under the EC number 1.11.1.x, are a diverse group of enzymes capable of catalyzing the oxidation of various substrates, including both inorganic and organic compounds, utilizing H$_2$O$_2$ as the oxidizing agent (Bansal & Kanwar, 2013). The catalytic mechanism of peroxidases involves a two-electron oxidation-reduction process, which occurs in three distinct steps. These enzymes are naturally abundant and can be found in various organisms, including eukaryotes and prokaryotes. Peroxidases are essential enzymes found in various biological systems, where they perform critical functions. These include the metabolism of toxins, the detoxification of heavy metals, and the regulation of hormone levels, among other important biological processes (Adewale & Adekunle, 2018). In

addition to their biological significance, peroxidases have found wide-ranging applications in different industries and scientific fields. They serve as valuable catalysts in industrial processes, clinical biochemistry, and enzyme immunoassays. Moreover, peroxidases are employed in the elimination of peroxides from industrial waste and are utilized in the synthesis of aromatic chemicals (Bansal & Kanwar, 2013; Pandey *et al.*, 2017; Dragana *et al.*, 2017).

Peroxidases play a crucial role in the antioxidative defense system (Opwia *et al.*, 2016) and participate in the breakdown of various substrates, such as ferricyanides and ascorbate, by facilitating the transfer of oxygen from $H_2O_2$ or other peroxides (Bansal & Kanwar; Adewale & Adekunle, 2018; Pandey *et al.*, 2017; Shigeto & Tsutsumi, 2016). The catalytic cycle of peroxidases involves a three-step process, including the formation of distinct intermediate enzyme forms (Twala *et al.*, 2020): The catalytic cycle of peroxidases involves three main steps:

Step (i): The peroxidase enzyme reacts with $H_2O_2$ to form Compound I and water.

$$\text{Peroxidase} + H_2O_2 \rightarrow \text{Compound I} + H_2O_2$$
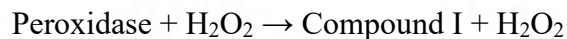
Step (ii): Compound I react with a peroxidase substrate (PS) to form Compound II and a free-radical product (FRP).

$$\text{Compound I} + PS \rightarrow \text{Compound II} + FRP$$
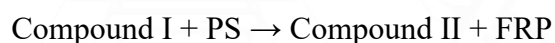
Step (iii): Compound II further reacts with a peroxidase substrate (PS) to regenerate the peroxidase enzyme, releasing the free-radical product (FRP) and generating more hydrogen peroxide ($H_2O_2$).

$$\text{Compound II} + PS \rightarrow \text{Peroxidase} + FRP + H_2O_2$$

Overall, in the presence of peroxidase and hydrogen peroxide, two substrate molecules (reduced form) are oxidized to produce two product molecules (oxidized form) and two water molecules.

$$2\text{ Substrate (reduced)} + H_2O_2 \rightarrow 2\text{ Product (oxidized)} + 2H_2O$$
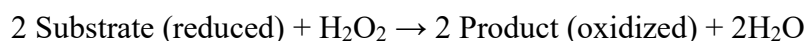
This cycle allows peroxidases to efficiently catalyze oxidation reactions, using hydrogen peroxide as the oxidizing agent, and generate free radicals as byproducts.

The catalytic cycle of peroxidases involves several steps that facilitate their enzymatic activity. The cycle begins with the oxidation of the native

ferric enzyme by $H_2O_2$, leading to the formation of an unstable intermediate called Compound I. In this state, the heme group of the enzyme contains a ferryl-oxo species (FeIV = O) and a porphyrin cation radical. Compound I, a key intermediate in the catalytic cycle of peroxidases, is composed of a heme structure with FeIV = O (ferryl-oxo) and a porphyrin cation radical. This unique structure enables Compound I to effectively reduce peroxide to water. In the subsequent step of the catalytic cycle, Compound I interact with an electron donor substrate (referred to as PS). This interaction leads to the formation of Compound II and the simultaneous release of a free radical product (FRP). The electron transfer from the substrate to Compound I facilitate the reduction of peroxide, contributing to the overall enzymatic activity of peroxidases. Subsequently, Compound II undergoes reduction by a second substrate molecule, leading to the restoration of the iron (III) state within the enzyme and the production of an additional FRP (Pandey *et al.*, 2017; Shigeto & Tsutsumi, 2016).

To overcome the challenges associated with $H_2O_2$ detection, a commonly employed strategy involves utilizing a bi-enzyme system consisting of AOX and a peroxidase enzyme, such as horseradish peroxidase (HRP) (Azevedo *et al.*, 2005). Figure 2.6 depicts the catalytic process of AOX in which alcohols are oxidized, resulting in the production of $H_2O_2$ as a byproduct. The generated $H_2O_2$ is then enzymatically reduced to $H_2O$ by HRP. Figure 2.7 illustrates the oxidation-reduction reaction taking place in the system, which can be detected using either electrochemical techniques or optical spectroscopy. Amperometric bi-enzyme electrodes, incorporating AOX and HRP or other peroxidases, can utilize direct or mediated electron transfer as shown in the Figure. Unmediated enzyme electrodes typically exhibit lower sensitivities and higher detection limits. To overcome these limitations, mediated electrodes have been employed to enhance the electron transfer between the electrode and HRP, resulting in increased sensitivity and lower detection limits. By facilitating efficient electron transfer, mediated electrodes significantly enhance the performance of the biosensor for $H_2O_2$ detection (Kawai *et al.*, 2019). This approach, utilizing a bi-enzyme system and mediated electrodes, offers an effective solution for accurate and sensitive $H_2O_2$ detection in alcohol biosensors. It enables reliable measurements of alcohol concentrations in various applications, including breath analysis, clinical diagnostics, and quality control in the food and beverage industry.
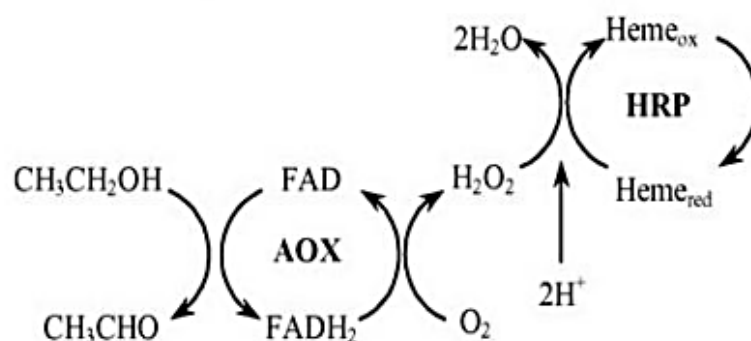
**Figure 2.6** Bi-Enzyme system for alcohol oxidation and $H_2O_2$ reduction. (Azevedo *et al.*, 2005)
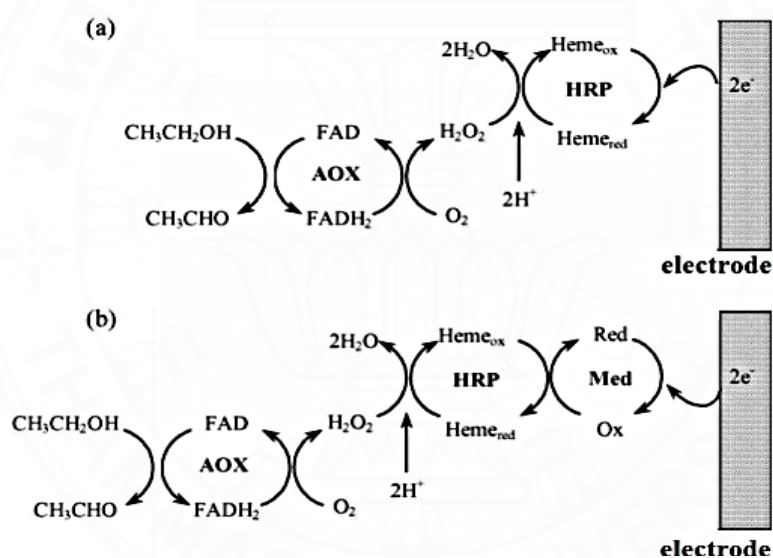


**Figure 4.7** Schematic of bi-enzyme electrodes with AOX and HRP for Direct (a) and Mediated (b) electron transfer. (Azevedo *et al.*, 2005)

Colorimetric methods are commonly employed, which involve the transformation of a chromogenic substrate into a colored product that absorbs light within the visible spectrum. The magnitude of the color change observed in the biosensor is directly linked to the concentration of $H_2O_2$ present, enabling accurate detection and quantification of this analyte. Upon excitation with shorter wavelength radiation, fluorescent methods rely on the formation of a fluorophore product that emits

visible light. A chemical reaction results in the emission of visible light in the process known as chemiluminescence (Bansal & Kanwar, 2013). Several optical approaches reported in the literature for ethanol analysis make use of a bi-enzymatic system consisting of AOX and a peroxidase enzyme. This system efficiently converts $H_2O_2$ to $H_2O$ with the aid of hydrogen donor molecules. Optical biosensors make use of a range of substrates, such as chromogenic, fluorigenic, and luminogenic substrates, to facilitate the detection of target analytes. The well-known substrate in this regard is ABTS and TMB (Ukeda *et al.*, 1999). Upon addition of ethanol-containing samples to the microtiter plate immobilized with AOX, a reaction takes place resulting in the generation of $H_2O_2$. Subsequently, a sample from the AOX plate is transferred to the HRP plate, where it encounters the chromogenic substrate ABTS. The oxidized form of ABTS produces a bluish-green color, which can be detected at around 415 nm (Figure 4.8). The biosensor exhibits a linear response over a range of ethanol concentrations from 0.1 to 1 mM, which allows for accurate detection and quantification of ethanol in multiple assays (Ukeda *et al.*, 1999). 4-Aminoantipyrine (4-APP) is a commonly employed chromogenic substrate in alcohol biosensors. It demonstrates the ability to be used with various reducing substrates like phenol (Salgado *et al.*, 2000), 4-hydroxybenzosulfonate (Azevedo *et al.*, 2004), and 8-hydroxyquinoline (Rodionov *et al.*, 2002). The growing need for rapid, cost-effective, sensitive, and uninterrupted analysis techniques with efficient sample throughput has led to the adoption of enzyme-based biosensors in flow system-based analysis. Different analytical approaches, including continuous flow analysis, segmented flow analysis, and flow injection analysis, can be explored to meet these demands effectively. The utilization of packed bed (Salgado *et al.*, 2000) and rotating bioreactor (Matsumoto & Waki, 1999) configurations is prevalent for the immobilization of AOX in biosensor applications. Another approach involves the implementation of a flow system, where the detection of $H_2O_2$ is achieved through the HRP-catalyzed chemiluminescence of luminol, presenting a potential method. These optical methods provide valuable options for the detection of $H_2O_2$ produced by AOX during ethanol oxidation (Figure 2.9). They offer advantages such as rapid analysis, sensitivity, and compatibility with flow systems, making them suitable for applications requiring continuous analysis and high sample throughput (Marshall & Gibson, 1992).
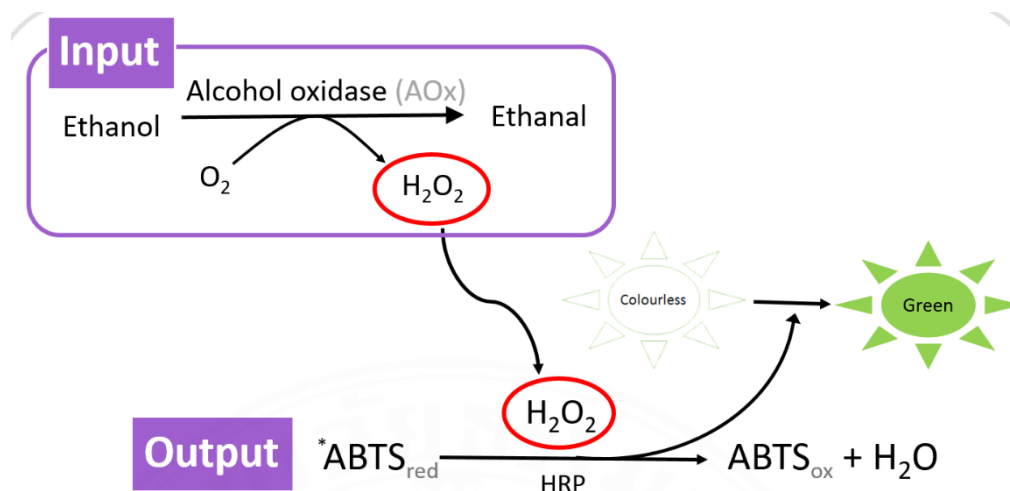
**Figure 2.8** AOX/ABTS/HRP system for ethanol detection (Ukeda *et al.*, 1999).
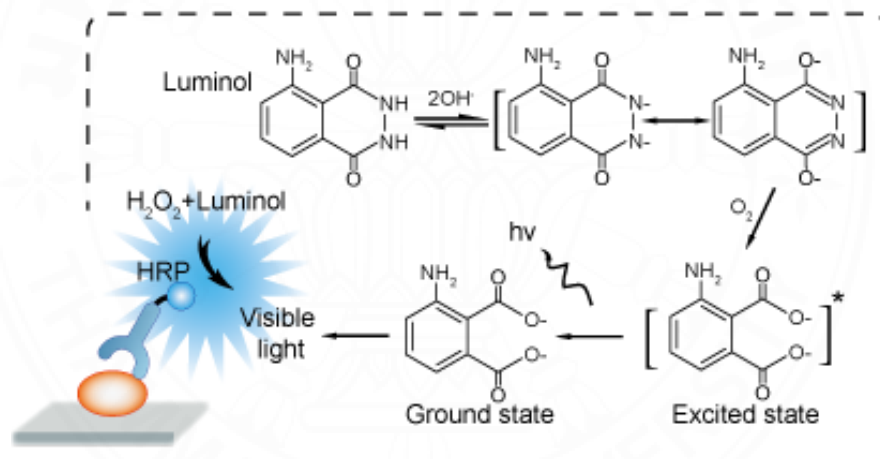


**Figure 2.9** Mechanism of luminol-HRP chemiluminescence system (Marshall & Gibson, 1992)

Several commercial alcohol sensors utilizing the bienzymatic system have been developed for the estimation of blood ethanol levels. These sensors employ colorimetric detection methods and are designed to detect alcohol in breath or saliva samples (Barzana *et al.*, 1989; Janssen & Ruelius, 1968; Gonchar *et al.*, 2001; Adams, 1988). These spectroscopic and electrochemical detection methods provide reliable and sensitive means for alcohol determination using AOX-based biosensors. Various chromogenic, fluorigenic, and luminogenic substrates have been employed in

these sensors. Commonly used chromogens include ABTS and TMB as mentioned below.

### (1) ABTS

ABTS is a frequently employed substrate either alongside hydrogen peroxide in conjunction with peroxidase enzymes like horseradish peroxidase, or independently with blue multicopper oxidase enzymes such as laccase or bilirubin oxidase. This versatile compound enables the tracking of peroxidase enzyme kinetics. Moreover, it serves as an indirect means to monitor the kinetics of any enzyme that produces hydrogen peroxide, or to quantify hydrogen peroxide levels in a given sample ("ABTS," n.d.). Figure 2.10 illustrated the structure of ABTS. This compound is selected due to the enzyme's ability to catalyze the reaction with hydrogen peroxide, resulting in the formation of a green and soluble end product (with an extinction coefficient, $\varepsilon$, of $3.6 \times 10^4 \, M^{-1}cm^{-1}$ (Shin & Lee, 2000). Tracking this spectral change can be conveniently accomplished using a spectrophotometer a widely used laboratory device.
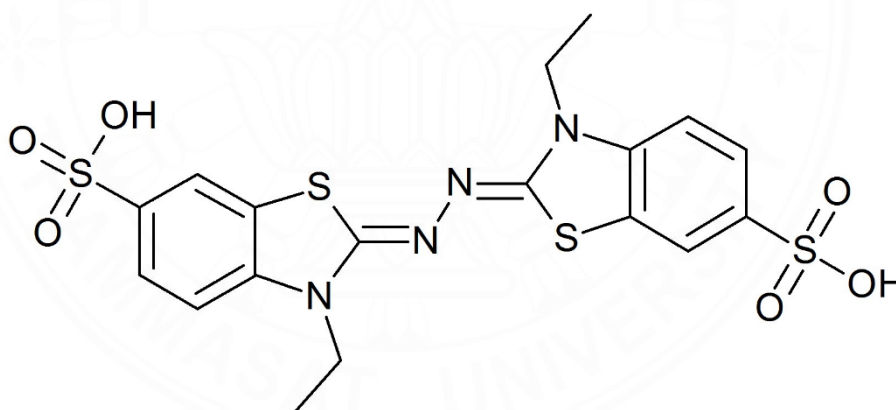


**Figure 2.10** The structure of 2,2'-azino-bis(3-ethylbenzothiazoline-6-sulfonic acid (ABTS)

### (2) TMB

The substrate TMB is commonly used in assays involving HRP and undergoes oxidation during the enzymatic degradation of hydrogen peroxide ($H_2O_2$). Figure 2.11 illustrates the chemical structure of TMB. Upon oxidation, TMB produces a deep, blue-colored product. TMB, an aromatic amine, functions as a co-substrate for reduction, undergoing oxidation by the elevated oxidation states of heme

peroxidases, including compounds I and II. The oxidation of TMB proceeds through a one-electron transfer mechanism, leading to the generation of a radical cation. This radical cation then forms a charge transfer complex with the unoxidized form of TMB. This charge transfer complex exhibits a peak absorption at 652 nm ($\varepsilon = 59,000$) and is formed through two consecutive one-electron oxidations of TMB. The oxidation reaction involving TMB and peroxidase follows a stoichiometry where either 0.5 mole of charge transfer complex (with a maximum absorbance at 652 nm) or 1 mole of dimine (with a maximum absorbance at 450 nm) is formed per mole of hydroperoxide reduced by the peroxidase enzyme. TMB has demonstrated superior sensitivity to HRP compared to other chromogenic substrates like o-phenylenediamine (OPD), ABTS, and 5-aminosalicylic acid (5-AS) ("3,3',5,5'-Tetramethylbenzidin", 2023). This makes TMB a preferred choice for assays requiring high sensitivity in peroxidase-based applications.
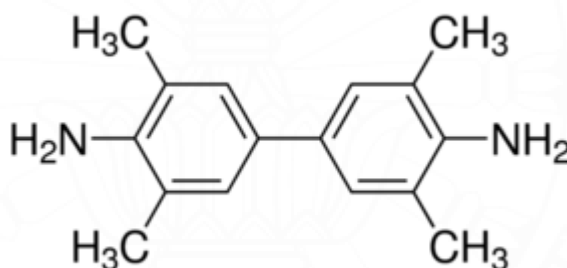
**Figure 2.11** The structure of 3,3',5,5'-Tetramethylbenzidine (TMB)

**2.3 Biosensor**

A biosensor is an innovative device that combines biological components with transducers to accurately detect and measure specific analytes in a given sample. Typically, biosensors consist of three key components, as illustrated in Figure 2.12. These components include a biological recognition element, a transducer or detector, and a signal processing system (Reisner *et al.*, 2014). It harnesses the power of bioreceptors, such as enzymes, antibodies, or nucleic acids, to selectively interact with the target analyte (Otles, 2023). These recognition elements are engineered to demonstrate exceptional specificity and binding affinity towards the desired molecule,

thereby enabling precise and accurate detection. The transducer element of the biosensor translates the biological interaction into a detectable signal, allowing for quantification and analysis. The nature of the signal generated by the biosensor can vary depending on its design, including optical, electrochemical, piezoelectric, or thermal signals (Tetyana & Shumbula, 2021). The signal output is directly proportional to the concentration of the target analyte present in the sample, allowing for quantitative analysis. Biosensors have gained significant attention and found applications in various fields, including healthcare, environmental monitoring, food safety, and biotechnology. They offer numerous advantages, such as rapid response, sensitivity, selectivity, and the potential for real-time monitoring. Biosensors have revolutionized the field of diagnostics by enabling on-site and point-of-care testing, reducing the need for laboratory-based analysis.
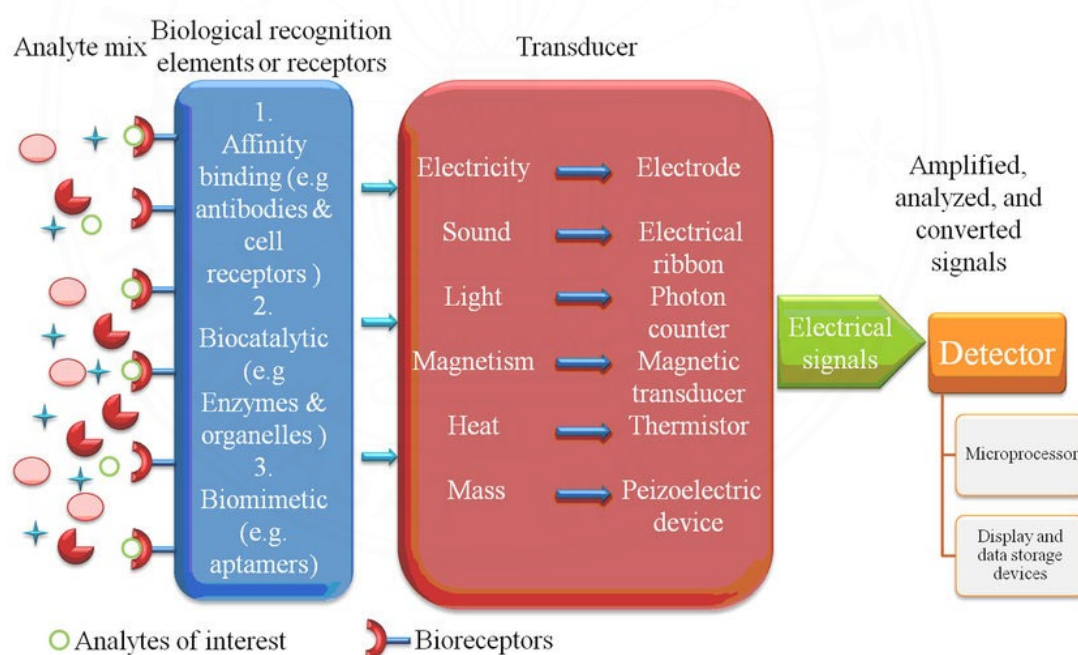


**Figure 2.12** Illustration of essential elements in a biosensor: examples of biological recognition elements, transducers, and signal display (Reisner *et al.*, 2014)

The effectiveness of biosensors that employ immobilized molecules is dependent on several factors, including the prevailing chemical and physical conditions, such as pH level, temperature, and the presence of contaminants.

Additionally, the thickness and stability of the materials utilized for immobilization significantly impact the overall performance of the biosensors. These considerations are crucial in ensuring optimal functioning and accurate detection in biosensing applications (Kissinger, 2005). The importance components of biosensor that in charge of analytical applications were mentioned below:

### 2.3.1 Biological recognition elements

The sensor or detector element is the essential component in biosensors that facilitates the sensing and detection of the target analyte. It acts as a biological recognition element, specifically engineered to recognize, and engage with the target analyte in a selective manner (Chaubey & Malhotra, 2002). Upon binding of the biological recognition element to the target analyte, a signal is generated, which can induce diverse changes, including modifications in light emission, heat generation, pH level, electrical charge, or mass (Bhalla *et al.*, 2016). The sensitivity of the biosensor relies on the capability of the biological recognition element to generate the appropriate physiochemical signal, which is then sensed and measured by the transducer.

The detection and sensing of the target analyte can utilize a wide range of biological entities, such as tissues, microorganisms, organelles, cell receptors, enzymes, antibodies, or nucleic acids (Castillo *et al.*, 2004). These biological entities have a critical role in selectively recognizing and interacting with the target analyte, facilitating its sensing and quantification in biosensor systems. Based on the biorecognition principle, biosensors can be categorized into two main types: catalytic biosensors and affinity or non-catalytic biosensors (Nguyen *et al*., 2019). Catalytic biosensors involve an analyte-bioreceptor interaction that leads to the generation of a novel biochemical reaction product. Bioreceptors in this category encompass enzymes, microorganisms, tissues, and whole cells. Conversely, affinity (non-catalytic) biosensors operate by binding the analyte irreversibly to the receptor, with no formation of new biochemical reaction products during the interaction. This class of biosensors includes antibodies, cell receptors, and nucleic acids as the target for detection (Shukla, *et al.*, 2016). There are several types of biosensor sensors according to biological recognition elements as depicted below:

### 2.3.1.1 Enzymes-based biosensor

Enzymes are commonly utilized as biomaterials in the fabrication of biosensors (Castillo *et al.*, 2004). Specific category of enzymes is utilized in biosensors (as shown in Table 2.2) that exhibit selectivity towards the target molecules and enable the production of a product through catalytic reactions. The resulting product can then be directly measured using any of the transducers.

**Table 2.2** Enzyme categories and their functions for selective detection of substrates by biosensors (Otles, 2023)

| Enzyme category | Function | Analytes |
|---|---|---|
| Oxidoreductases | oxidation/reduction reactions | lactate, malate, ascorbate, alcohol, cholesterol, amino acid, glucose fructose, glycerol |
| Transferase | transfer of molecular groups from one molecule to another | acetic acid, xenobiotics (captan or artazine) |
| Hydrolases | hydrolytic cleavage | sucrose |
| Lyases | cleavage of C-C, C-O, C-N bonds by other means than oxidation or hydrolysis | citric acid |
| Isomerase | intramolecular rearrangement | DNA point mutation detection |
| Ligases | joining of two molecules | 19-norandrostenedione |

Biosensors that have achieved significant commercial success are primarily designed for the measurement of glucose levels in blood samples, making up around 90% of the worldwide biosensor market. These biosensors employ enzymes such as glucose oxidase or glucose dehydrogenase (Monosik *et al.*, 2012). Several factors can impact the performance of enzyme-based biosensors, including the enzyme

loading on the sensor, optimization of pH and temperature conditions, and the potential utilization of a cofactor to sustain enzyme activity. In addition, the choice of a suitable immobilization method for enzyme immobilization and the thickness of the enzyme layer on the sensor surface are crucial factors that significantly impact the performance of the biosensor.

### 2.3.1.2 Antibodies-based biosensor

Antibodies, composed of unique sequences of amino acids, possess the ability to selectively bind to specific antigens, making them valuable components in immunosensors (Vo-Dinh *et al.*, 2000). Immunosensors utilize this specific binding interaction to detect and quantify target analytes. Two formats of biomolecular interactions are commonly employed in immunosensors: direct and indirect. In the direct format, the target molecule is immobilized and directly interacts with a ligand molecule. For fluorescent analytes, the naturally fluorescent analyte is measured after *in situ* incubation (Vo-Dinh *et al.*, 1987). Non-fluorescent analytes, however, require the use of a fluorophore-labeled second antibody following *in situ* incubation. In contrast, indirect format utilizes a separate labeled species that binds to the target molecule, and the presence of this labeled species is detected through fluorescence or luminescence, providing a signal for the existence and concentration of analyte of interest. This approach involves competition between the target analyte and a labeled analyte for the limited binding sites on the receptor. The degree of competition and subsequent binding of the labeled analyte can be quantified to determine the concentration of the target analyte. The change in signal from the label indicates the formation of an immunocomplex between the analyte-label conjugate and the antibody. The sensitivity of the assay increases with a decrease in the amount of immobilized reagent (Tromberg *et al.*, 1987). Immunosensors find application in various fields, including cancer cell monitoring, cancer marker detection, bacteria and virus identification, and toxin detection, among others (Ehrhart *et al.*, 2008; Malhorta *et al.*, 2010; Liu *et al.*, 2008; Mani *et al.*, 2009; Carnes & Eikins, 2005; Konig & Gratzel, 1993; Kadir & Tothill, 2010; Labib *et al.*, 2009). They provide a flexible platform suiTable for a diverse array of applications in biomedical research and diagnostics.

### 2.3.1.3 Nucleic-acid based biosensor

Nucleic acid is biopolymers or macro molecule that are composed of nucleotide. Nucleic acid biosensors are innovative analytical devices that exploit the unique properties of nucleic acids for the detection and analysis of target molecules. These biosensors utilize nucleic acids, such as DNA or RNA, as the sensing element, taking advantage of their ability to specifically bind to complementary sequences. The binding event triggers a signal, which is then transduced into a measurable output, offering valuable insights into the existence and concentration of the target molecule, this process provides significant information. In addition to DNA and RNA, peptide nucleic acid (PNA) has also emerged as a promising component in nucleic acid biosensors (Borgmann *et al.*, 2011). PNA exhibits enhanced stability and hybridization properties, making it an attractive alternative for biosensing applications. Nucleic acid biosensors offer several advantages, including high sensitivity, selectivity, and specificity. Their strong affinity for complementary nucleotide sequences enables the detection of target molecules with exceptional accuracy. Furthermore, nucleic acid biosensors can be designed to detect a wide range of targets, including pathogens, genetic mutations, and environmental contaminants (Lucarelli *et al.*, 2011; Wang *et al.*, 2004). The specificity of biorecognition in DNA biosensors relies on the complementary pairing of adenine (A) – thymine (T) and cytosine (C) – guanine (G) in DNA. The general mechanism scheme of DNA biosensor is described in Figure 2.13. DNA-based biosensors have demonstrated their efficacy in various applications, such as drug determination in serum sample matrices (Vanickova *et al.*, 2005), assessment of DNA damage and identification of DNA-protective antioxidants (Galandova *et al.*, 2009; Buckova *et al.*, 2002), measurement of 1-aminopyrene and 1-hydroxypyrene by voltammetry (Ferancova *et al.*, 2005), and the evaluation of berberine's effect on DNA in cancer cells (Ovadekova *et al.*, 2006). These examples underscore the versatility and potential of DNA-based biosensors in a wide range of research and analysis fields.
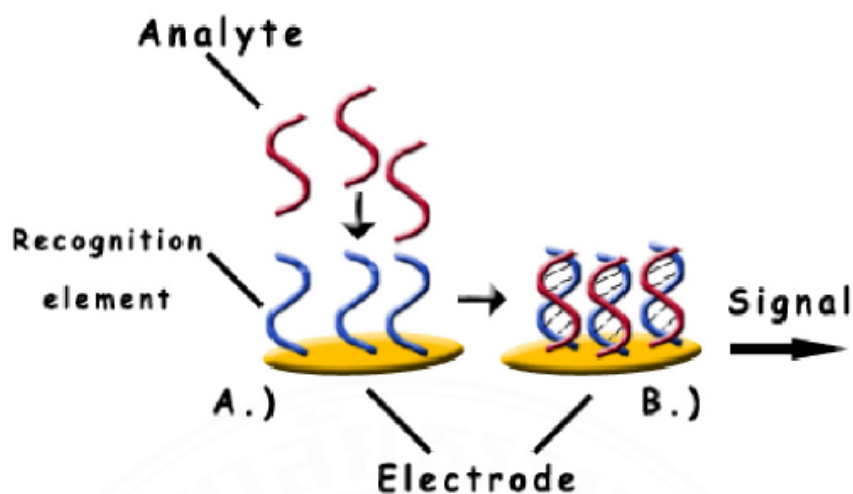
**Figure 2.13** Schematic representation of a DNA biosensor: capture of target DNA at the recognition layer (A) and transduction of hybridization into an electronic signal (B) (Lucarelli *et al.*, 2004)

### 2.3.1.4 Cells-based biosensor

Biological recognition element in biosensors can be categorized into two primary groups.: whole cells/microorganisms and specific cellular components that possess the capability to selectively bind to certain target species (Figure 2.14). Utilizing these bioreceptors offers a significant advantage of achieving low detection limits due to signal amplification. Numerous biosensors utilizing these bioreceptors have been developed, harnessing their catalytic or pseudocatalytic properties (Vo-Dinh, 2000). For instance, in microbial biosensors, viable or non-viable microbial cells are commonly employed. Non-viable cells obtained after permeabilization or whole cells containing periplasmic enzymes serve as cost-effective alternatives to enzymes. Living cells efficiently utilize their respiratory and metabolic functions, enabling the monitoring of the analyte as either a substrate or an inhibitor of these processes (D'Souza, 2001).
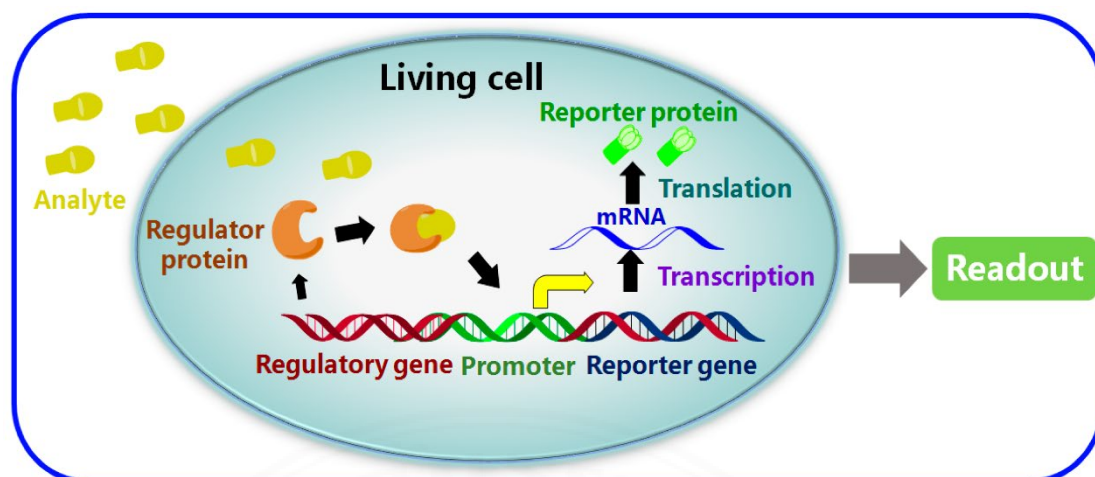
**Figure 2.14** Scheme of cell-based biosensor (Gui *et al.*, 2017)

### 2.3.2 Transducers

The transducer plays a crucial role in biosensors as it converts the input quantity, such as the presence or concentration of an analyte, into an output signal that exhibits a defined relationship with the input. Biosensors can be categorized based on the specific transduction methods they employ. There are five main classes of transduction commonly used in biosensors: electrochemical, electrical, optical, piezoelectric (mass detection methods), and thermal detection. Each class of transduction method offers unique advantages and is suitable for different types of analytes and applications. By selecting the appropriate transduction method, biosensors can effectively convert the biochemical or biophysical interactions into measurable signals, enabling accurate detection and quantification of target analytes. For those five main classes of transducers are described for the following topics (McNaught & Wilkinson, 1997).

#### 2.3.2.1 Electrochemical biosensor

Electrochemical biosensors utilize the interaction between a target analyte and an immobilized biomolecule to induce chemical reactions that generate or consume ions or electrons. These reactions result in detectable alterations in the electrical characteristics of the solution, including changes in electric current or potential. Through the detection and quantification of these alterations in electrical signals, electrochemical biosensors facilitate the measurement of the target analyte's presence or concentration. They offer several notable advantages, including high

sensitivity, rapid response, and the potential for miniaturization. These features make biosensors valuable tools in various fields, including clinical diagnostics, environmental monitoring, and food safety applications (Thevenot *et al.*, 1999). Based on the classification of the transduction principle and on the corresponding electrochemical technique, the electrochemical biosensors are categorized as potentiometric, amperometric, conductometric, and ion sensitive as described below (Curulli, 2021).

### (1) Amperometric biosensor

Amperometric biosensors are widely used and versatile in detecting and quantifying biochemicals. This transducer is able to respond to and transform a bio-chemical and/or physico-chemical property into a measurable signal (Figure 2.15) (Vorþáková *et. al.*, 2012). These biosensors can also employ enzymatic reactions involving hydrolysis or phosphorylation, followed by electro-oxidation or electro-reduction, as well as participate in bioaffinity reactions that result in electro-oxidation or electro-reduction. With high sensitivity, selectivity, and rapid response times, amperometric biosensors have become valuable tools in medical diagnostics, environmental monitoring, and food analysis. Their ability to provide real-time and accurate measurements of target analytes makes them highly applicable in various fields (Heller, 1996).
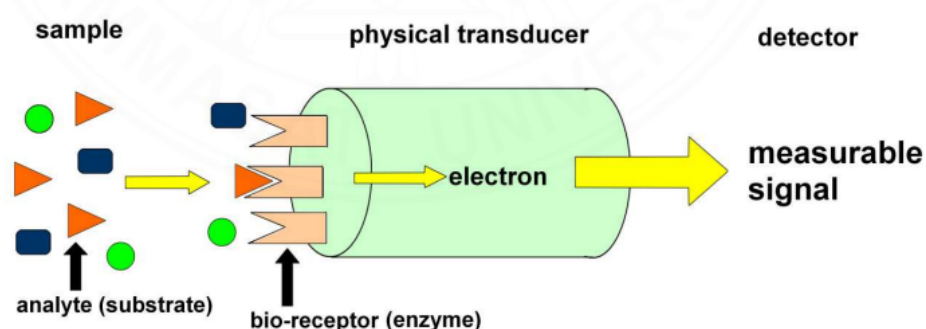


**Figure 2.15** Scheme of amperometric biosensor (Vorþáková *et al*., 2012)

### (2) Potentiometric biosensor

The potentiometric transducer serves as a sensing element specifically designed to measure the potential difference generated across an ion-

selective membrane when two solutions are separated, allowing for minimal current flow. The working principle of bioelectric sensors is summarized in a Figure 2.16 (Tan & Xu, 2020). Various potentiometric sensors, such as glass electrodes, metal oxide-based sensors, and ion-selective electrodes, are readily accessible in the market. These sensors can be easily manufactured on a large scale using advanced technologies like silicon or thick-film fabrication techniques, enabling their miniaturization and integration into various devices and systems. Potentiometric transducers offer several advantages, including simplicity, versatility, and compatibility with different analytes and applications. They have demonstrated their value as valuable tools in various fields, such as biomedical diagnostics, environmental monitoring, and industrial process control (Mohanty & Kougianos, 2006).
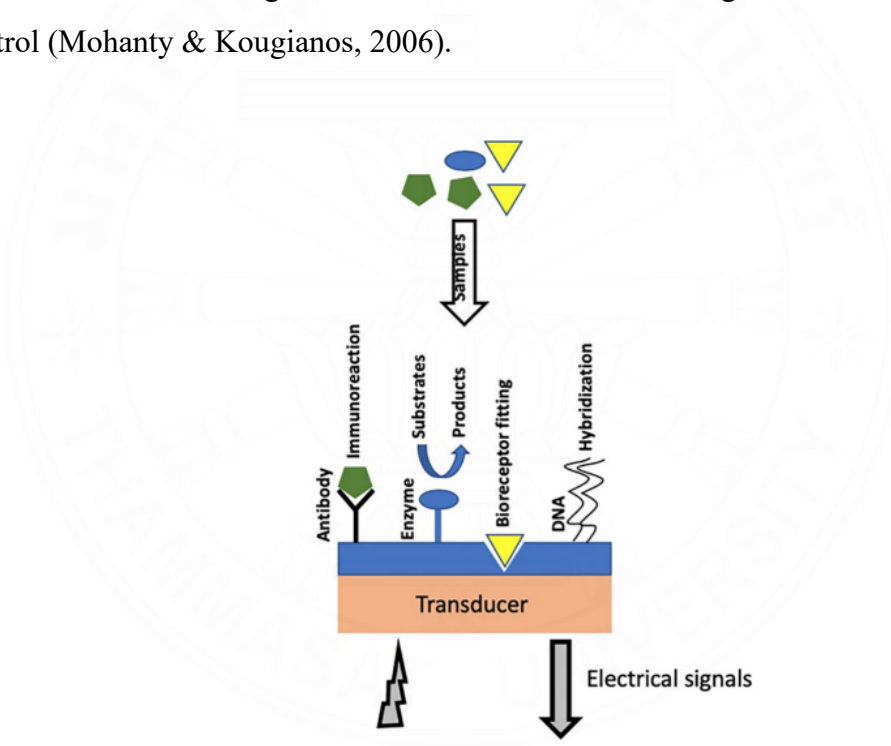


**Figure 2.16** An example of a potentiometric biosensor (Tan & Xu, 2020)

### (3) Conductometric (Impedimetric) biosensor

When ions or electrons are generated during a biochemical reaction, they can alter the overall conductivity or resistivity of the solution. The parameter measured in conductometric biosensors is the electrical conductance or resistance of the solution. Conductometric biosensors quantify the change in the conductance between the pair of electrode due to an electrochemical reaction (change

in conductivity properties of the analyte) as showed in Figure 2.17 (Curulli, 2021). To address potential issues such as Faradaic processes, double layer charging, and concentration polarization, a sinusoidal voltage (AC) is often applied to generate an electric field. This helps minimize these undesired effects, leading to more accurate measurements in conductometric biosensors (Mohanty & Kougianos, 2006). Despite its lower sensitivity compared to other techniques, conductometric biosensors offer simplicity, cost-effectiveness, and versatility in measuring a wide range of analytes (Dzyadevych *et al.*, 2006).
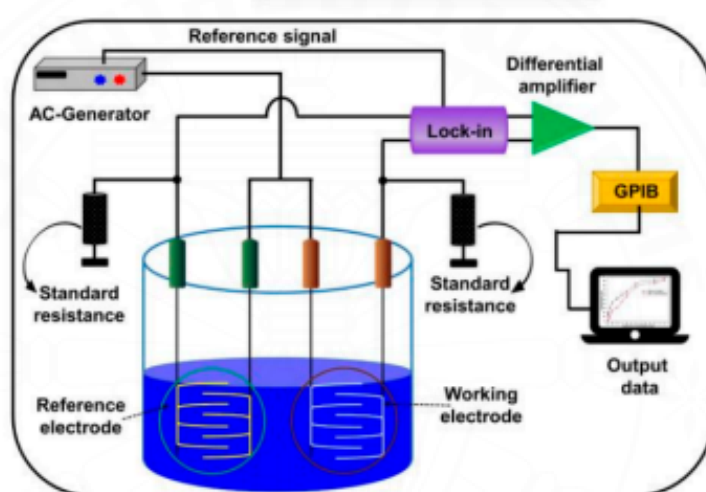


**Figure 2.17** Scheme of conductometric biosensor (Curulli, 2021)

### (3) Ion-sensitive biosensor

The ion-sensitive filed-effect transistor (ISFET) is widely recognized as a prominent electrical biosensor and was pioneering as the inaugural miniaturized silicon-based chemical sensor. Originally recognized as a pH sensor, the ISFET serves the purpose of quantifying ion concentrations, especially $H^+$ or $OH^-$, within a solution, inducing an interface potential across the gate insulator. Operating on potentiometric principles, the ISFET functions akin to the Metal Oxide Semiconductor Field-Effect Transistor (MOSFET) (Lee *et al.*, 2009). The ISFET bears a resemblance to a MOSFET but distinguishes itself by incorporating a distinct gate terminal, recognized as the reference electrode. This reference electrode makes direct contact with the solution, delivering the voltage necessary for channel current modulation. The gate oxide layer assumes the role of a sensing film, engaging with the target analyte to

generate charges at the interface between the electrolyte and insulator. The quantity of charge produced varies depending on the specific sensing film employed and the pH level of the solution. The electrical schematic of ISFET is demonstrated in Figure 2.18 (Bhardwaj *et al*., 2017).
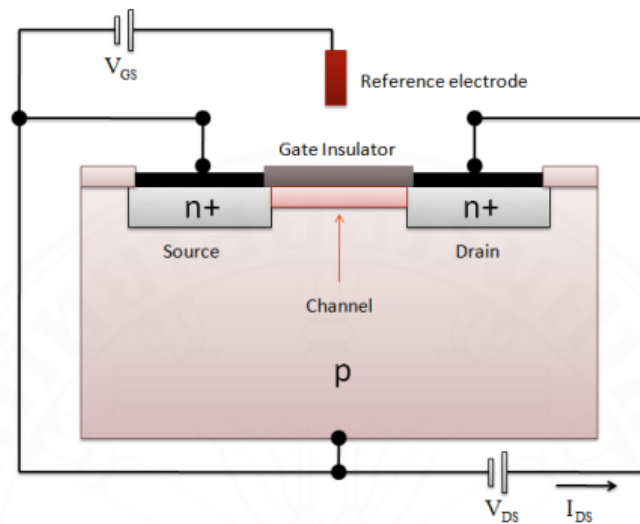


**Figure 2.18** Scheme of ISFET (Bhardwaj *et al*., 2017).

### 2.3.2.2 Optical biosensor

Optical biosensors are analytical devices that utilize the principles of light-matter interactions to detect and quantify analytes in a sample. Optical biosensors operate by leveraging the interaction between an analyte and a sensing element to detect alterations in optical properties, including light intensity, wavelength, polarization, and more. This interaction leads to measurable changes that enable the accurate identification and quantification of the target molecule. The sensing element in an optical biosensor can be based on various mechanisms, such as absorbance, fluorescence, bioluminescence, surface plasmon resonance (SPR), or interferometry. Each mechanism offers unique advantages and can be tailored for specific applications (Velasco-Garcia, 2009). In an optical biosensor, the interaction between the analyte of interest and the sensing element results in a detectable alteration in the optical signal. This change is then detected by a transducer, which converts it into an electrical signal for further analysis and quantification. The transducer can be a

photodetector, a spectrometer, or other optical measurement devices (Figure 2.19) (Damborsk´y, 2016).
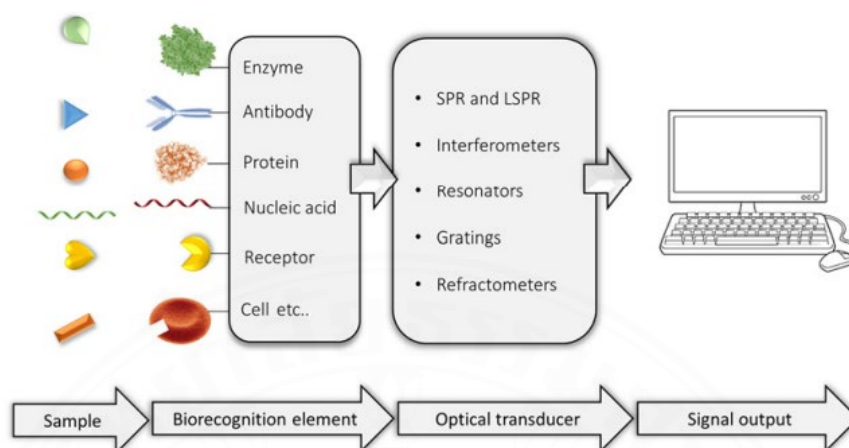


**Figure 2.19** Scheme of optical biosensor (Damborsk´y et. al., 2016)

### 2.3.2.3 Piezoelectric (or Mass-sensitive) biosensor

Piezoelectric biosensors, also known as mass-sensitive biosensors, are a type of biosensor that utilizes the piezoelectric effect to detect and quantify analytes. The piezoelectric effect refers to the generation of an electric charge in certain materials, such as quartz or ceramics, in response to mechanical stress or pressure. In a piezoelectric biosensor, a thin film or coating containing the bioreceptor (such as antibodies, enzymes, or nucleic acids (Janshoff *et al.*, 2000) is deposited onto the surface of a piezoelectric crystal, typically quartz (Figure 2.20). When the target analyte binds to the bioreceptor, it causes a change in mass on the crystal surface, resulting in a shift in the resonant frequency of the crystal (Vo-Dinh *et al.*, 1987). This frequency change is detected by an electronic circuit connected to the crystal, which converts it into a measurable electrical signal. The magnitude of the frequency shift is proportional to the mass change on the crystal surface, providing a quantitative indication of the analyte concentration. Piezoelectric biosensors offer several advantages, including high sensitivity, real-time detection, label-free analysis, and the ability to operate in complex sample matrices. They have been widely used in various applications, such as medical diagnostics, environmental monitoring, food safety, and drug discovery (Tombelli *et al.*, 2005).
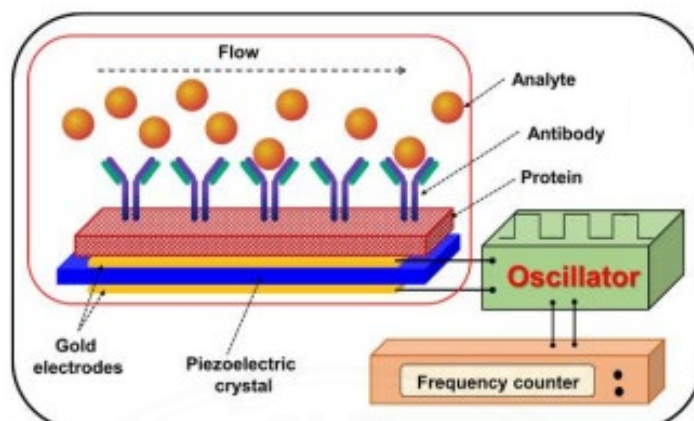
**Figure 2.20** Schematic diagrams of piezoelectric biosensor (Naresh & Lee, 2021)

### 2.3.2.4 Calorimetric (or Thermometric) biosensor

Calorimetric biosensors, also known as thermometric biosensors, are a type of biosensor that operate based on the principle of heat generation or absorption upon specific biochemical reactions. These biosensors utilize the change in temperature associated with the biochemical reaction to detect and quantify analytes (Mohanty & Kougianos, 2006). In a calorimetric biosensor, the sensing element is typically coated with a bioreceptor, such as antibodies, enzymes, or DNA probes, which selectively interacts with the target analyte. When the analyte binds to the bioreceptor, it initiates a biochemical reaction that generates or absorbs heat, resulting in a temperature change in the system. The temperature change is then detected and measured using various techniques, such as thermistors, thermocouples, or infrared sensors. The magnitude of the temperature change is directly proportional to the concentration of the analyte, allowing for quantitative analysis (Figure 2.21). These biosensors have been widely employed in various fields, including medical diagnostics, environmental monitoring, food safety, and drug discovery. Furthermore, in drug discovery, calorimetric biosensors have facilitated the study of molecular interactions and the screening of potential drug candidates (Antonelli *et al.*, 2008; Bhand *et al.*, 2010).
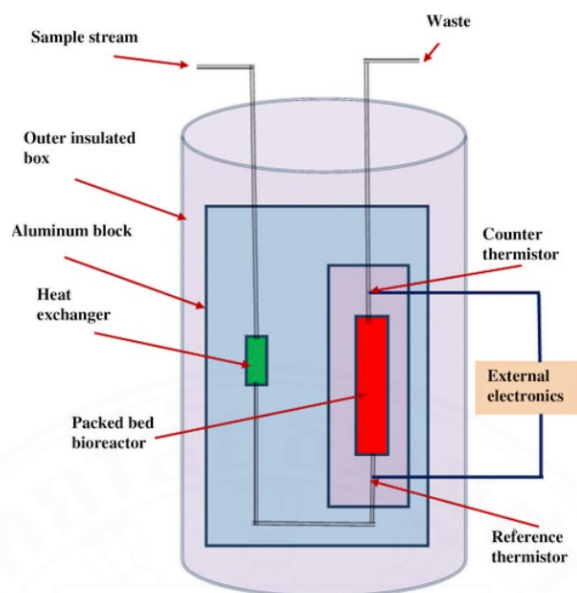
**Figure 2.21** Diagram of a calorimetric biosensor (Kaur *et al.*, 2019)

### 2.3.3 characteristics of biosensors

When developing a biosensor, it is essential to consider several characteristics or parameters that define its performance and utility based on the intended application. These attributes are essential in ensuring the efficacy of the biosensor as described in the following 7 topics.

### 2.3.3.1 Sensitivity

Sensitivity is a fundamental characteristic of biosensors that determines their ability to detect and quantify analytes with precision. It refers to the responsiveness of a biosensor towards changes in analyte concentration. A highly sensitive biosensor exhibits a significant change in the output signal in response to even small variations in analyte concentration (Wilkins & Atanasov, 1996). Sensitivity is typically quantified by the slope of the calibration curve, which represents the relationship between the analyte concentration and the corresponding signal intensity. A biosensor with high sensitivity enables the detection and measurement of low analyte concentrations, making it invaluable in various fields such as medical diagnostics, environmental monitoring, and food safety. Achieving optimal sensitivity in biosensors often involves careful selection of biorecognition elements, appropriate transduction mechanisms, and optimization of experimental conditions (Bhalla *et al.*, 2016).

Biosensor sensitivity is quantified as the response signal elicited per unit concentration of the target sample. The typical standard curve illustrating the biosensing response to target detection, fitted using a dose-response model, is presented in Figure 2.22. The sensitivity within the fitting curve is determined by the slope of the linear region, denoting the magnitude of the signal (y) divided by the unit concentration (x) of the response slope. A higher y value at a given x value signifies superior sensitivity in the biosensor's performance (Prabowo *et al.*, 2019).
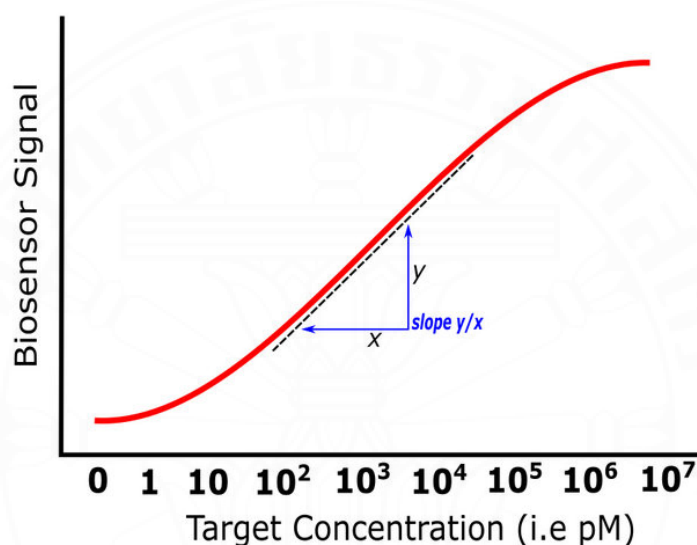


**Figure 2.22** Sensitivity performance of biosensor (Prabowo *et al.*, 2019)

### 2.3.3.2 Selectivity

Selectivity is an essential characteristic of a biosensor, referring to its ability to specifically bind and respond to the desired analyte while disregarding interference from other molecules or substances present in the sample. Achieving selectivity is crucial for accurate and reliable detection, as it ensures that the biosensor's response is attributed solely to the target analyte of interest. When designing a biosensor, careful consideration is given to selectivity by choosing appropriate bioreceptors that exhibit high affinity and specificity towards the target analyte (Bhalla *et. al*., 2016). By incorporating highly selective bioreceptors, the biosensor can effectively discriminate against potential interferents, enabling precise and reliable analysis of the desired analyte in complex sample matrices. The ability to selectively detect and quantify target analytes is of utmost importance in optimizing the

performance and broadening the applicability of biosensors in diverse fields including medical diagnostics, environmental monitoring, and food safety (Tayler-Smith, 2017). Azmi *et. al.* (2012) studied the response of an optical based ammonium biosensor to the potential interferents and found that one of the interferents appear to cause interference to the biosensor leaded to less in selectivity (Azmi *et al.*, 2012).

### 2.3.3.3 Stability

The stability of biosensors is a critical attribute, especially in applications that require continuous monitoring. It pertains to the capability of a biosensor device to retain its performance consistently over time, even when subjected to external influences like temperature variations, humidity changes, or other environmental conditions. These external factors have the potential to impact the precision and accuracy of the biosensor, emphasizing the significance of stability in ensuring reliable and dependable measurements (Bhalla *et al.*, 2016). Temperature sensitivity is a factor that can influence biosensor stability as changes in temperature can impact the response of transducers and electronics. It is crucial to account for temperature variations and implement measures to mitigate their effects on biosensor performance. Another significant factor is the affinity of the bioreceptor, which determines the strength of the bond between the analyte and the receptor. Bioreceptors with high affinities promote strong electrostatic bonding or covalent linkage with the analyte, enhancing the stability of the biosensor. Furthermore, the degradation of the bioreceptor over time can affect stability, as it can impair the binding capability and overall performance of the biosensor (Wikins & Atanasov, 1996). Therefore, selecting stable bioreceptor materials and optimizing their longevity is essential to ensure the stability of the biosensor over an extended period.

In summary, stability is a critical feature of biosensors, particularly in scenarios involving continuous monitoring or prolonged incubation. By addressing temperature sensitivity, optimizing bioreceptor affinity, and selecting stable bioreceptor materials, biosensors can maintain their performance and provide accurate measurements over time, ensuring their reliability in various environmental conditions.

### 2.3.3.4 Range or linearity

The range of linearity is a fundamental characteristic of a biosensor that defines the concentration range over which the sensor can provide

accurate and reliable measurements. It represents the linear relationship between the concentration of the target analyte and the corresponding signal response generated by the biosensor. In the range of linearity, the biosensor's response is directly proportional to the analyte concentration, allowing for precise quantification of the target analyte. This linear relationship ensures that the biosensor produces consistent and predictable results, enabling users to obtain reliable data within the specified concentration range (Tayler-Smith, 2017).

The range of linearity is determined during the calibration process of the biosensor, where known concentrations of the analyte are measured, and the corresponding signals are recorded. By plotting a calibration curve, the linear range can be identified as the concentration range over which the biosensor's response remains linear and predictable. It is crucial to consider that beyond the linear range, the biosensor's response may exhibit deviations from linearity, which can lead to inaccurate measurements and a potential decrease in sensitivity. Therefore, it is crucial to select a biosensor with a range of linearity that encompasses the expected concentration range of the target analyte. Linearity represents the reliability of the biosensor's response when subjected to diverse analyte concentrations, often described by a linear equation $y = mc$, where y represents the output signal, c represents the analyte concentration, and m denotes the biosensor's sensitivity (Bhalla *et al.*, 2016; Wikins & Atanasov, 1996). The range of linearity is a critical parameter for assessing the performance and suitability of a biosensor for specific applications. A wider range of linearity allows for the analysis of a broader concentration range, increasing the versatility and applicability of the biosensor.

### **2.3.3.5 Low detection limit** (LOD)

The detection limit of a biosensor is a fundamental characteristic that defines its ability to detect and quantify target analytes accurately. The detection limit refers to the minimum concentration of the analyte that can be accurately detected and differentiated from background noise by the biosensor. The detection limit is a critical parameter in various fields, including medical diagnostics, environmental monitoring, and food safety, where the presence of analytes at extremely low concentrations may be of significant importance. A lower detection limit indicates higher sensitivity, enabling the biosensor to detect and measure trace amounts of the

analyte with precision and accuracy. Achieving a low detection limit is a key objective in biosensor development, as it allows for the detection and quantification of analytes even at very low levels, enhancing the diagnostic capabilities and reliability of the biosensor in practical applications (Wikins & Atanasov, 1996).

The LOD is determined by calculating the lowest response signal, which is typically set at three times the standard deviation (3SD) from the mean value of a blank measurement ($y_0$). For simplicity in Figure 2.23, a confidence level of 3 is employed. The distance of 3SD from the reference signal can be used to determine the concentration value corresponding to the LOD (Prabowo $et\ al.$, 2019).
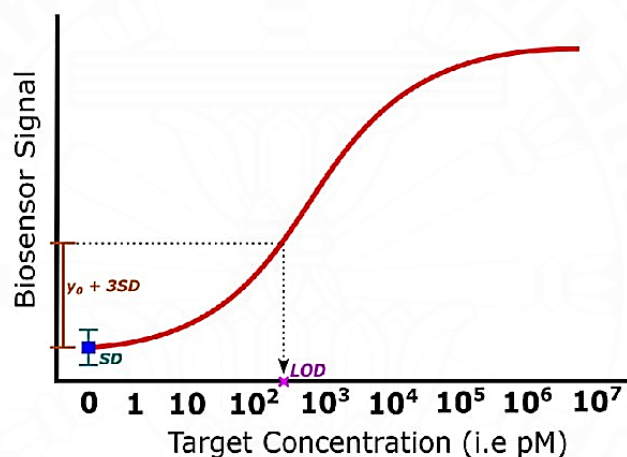


**Figure 2.23** Biosensor LOD determination concept (Prabowo $et\ al.$, 2019)

### 2.3.3.6 Response time

The response time of a biosensor is an important characteristic that directly impacts its performance and usability in various applications. The response time of a biosensor refers to the duration it takes for the biosensor to generate a detectable signal following the interaction between the biological recognition element and the target analyte. A shorter response time is desirable as it enables rapid detection and monitoring of the analyte, facilitating real-time analysis and timely decision-making. It allows for faster and more accurate measurements, which is crucial in fields such as medical diagnostics, environmental monitoring, and food safety (Wikins & Atanasov, 1996).

### 2.3.3.7 Reproducibility

The reproducibility of a biosensor is a critical aspect that ensures consistent and reliable performance. It is influenced by the precision and accuracy of the transducer and electronics employed in the biosensor. Precision refers to the ability of the biosensor to produce consistent results when measuring the same analyte under similar conditions. It quantifies the degree of agreement between repeated measurements and reflects the instrument's reliability in reproducing the same results. Accuracy, on the other hand, measures the closeness of the biosensor's measurement to the true value or a reference value. It indicates the absence of systematic errors and the reliability of the biosensor in providing accurate measurements. Both precision and accuracy are essential for ensuring the reproducibility of the biosensor, enabling consistent and dependable analysis of the target analyte. By optimizing the transducer and electronics, biosensor developers strive to enhance the reproducibility, leading to more reliable and trustworthy results in various applications (Bhalla *et al.*, 2016).

In recent years, there has been a notable emphasis on harnessing the potential of porphyrins and their derivatives for sensor applications., particularly for detecting substances such as glucose, metal ions, pesticides, and more. Extensive exploration has been carried out on porphyrin-based composites and hybrids, showcasing their capabilities as biomimetic catalysts and intrinsic peroxidases. In a previous study, porphyrin functionalization with $NiO$, $Fe_3O_4$, and $Co_3O_4$ (Liu *et al.*, 2015(a); Liu *et al.*, 2015(b); Liu *et al.*, 2014) has been demonstrated to enhance peroxidase activity. These functionalized porphyrins act as catalysts for the reaction between dye substrates and $H_2O_2$, leading to a noticeable color change that can be easily observed without the need for specialized equipment. Furthermore, Wu L. and colleagues (2008) developed an ethanol biosensor by immobilizing AOX on a carbon nanofiber - iron(III) meso-tetrakis(N-methylpyridinum-4-yl) porphyrin (CNF-FeTMPyP) modified electrode (Wu *et al.*, 2008). The consumption of $O_2$ resulting from the oxidation of ethanol by AOX was monitored by the electrochemical signal of oxygen reduction at the CNF-FeTMPyP modified sensor surface. The biosensor demonstrated a linear decrease in response corresponding to ethanol concentration in the range of 2.0 μM to 112 mM. It achieved a detection limit of 1.2 μM, indicating its high sensitivity for ethanol detection.

**2.4 Porphyrins**

Porphyrins are a diverse group of aromatic organic compounds, both naturally occurring and synthetically derived. They belong to the class of heterocyclic macrocycles and are composed of four pyrrole rings linked by four methine bridges. The correct structure of porphyrin was first proposed by Kuster in 1912 and later confirmed by Hans Fischer, a prominent Figure in porphyrin chemistry, who successfully synthesized the first porphyrin protoheme in 1929 (Harrison *et al.*, 1971). The term "porphyrin" originates from the Greek word "porphura," which means purple, alluding to their characteristic deep purple color ("Porphyrin," 2017). The porphyrin skeleton consists of twenty carbon atoms, with each carbon atom in the porphyrin system labeled 1-20 according to the IUPAC numbering system, and the integral nitrogen atoms designated as 21-24, as illustrated in Figure 2.24.



**Figure 2.24** The structure and the numbering system for porphyrins.

The central cavity of porphyrin macrocycles possesses a size that allows for the accommodation of diverse metal ions ($Mn^+$), involving Cu, Fe, Co, Ni, and others. The two nitrogen atoms at opposite corners of the porphyrin ring are deprotonated and form dianionic ligands by binding with the transition metal ion. The presence of the metal ion in the porphyrin structure can lead to a distortion of the molecule from its flat conformation (see Figure 2.25). While the color of porphyrins primarily arises from the π*-π electron transition within the porphyrin ring orbitals, the presence of the bound metal ion introduces interactions between its d orbitals and the π

orbitals. These interactions influence the energy levels of the orbitals, leading to variations in the color exhibited by metalloporphyrins (Milgrom, 1979).
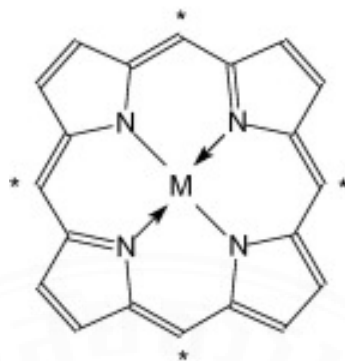


**Figure 2.25** Structure of metalloporphyrin cycle; M is the incorporated metal ion.

### 2.4.1 Natural Porphyrins

Porphyrin derivatives, particularly metal complexes, are of significant importance in natural biological systems, where they fulfill crucial roles in processes such as respiration, photosynthesis, and transportation within living organisms (Battersby *et al.*, 1980; Messerschmidt *et al.*, 2001). These compounds are abundant in nature and encompass a diverse range of essential biological entities, such as heme, chlorophyll, vitamin B12, and coenzyme B12 as in Figure 2.26 and described in following topics.
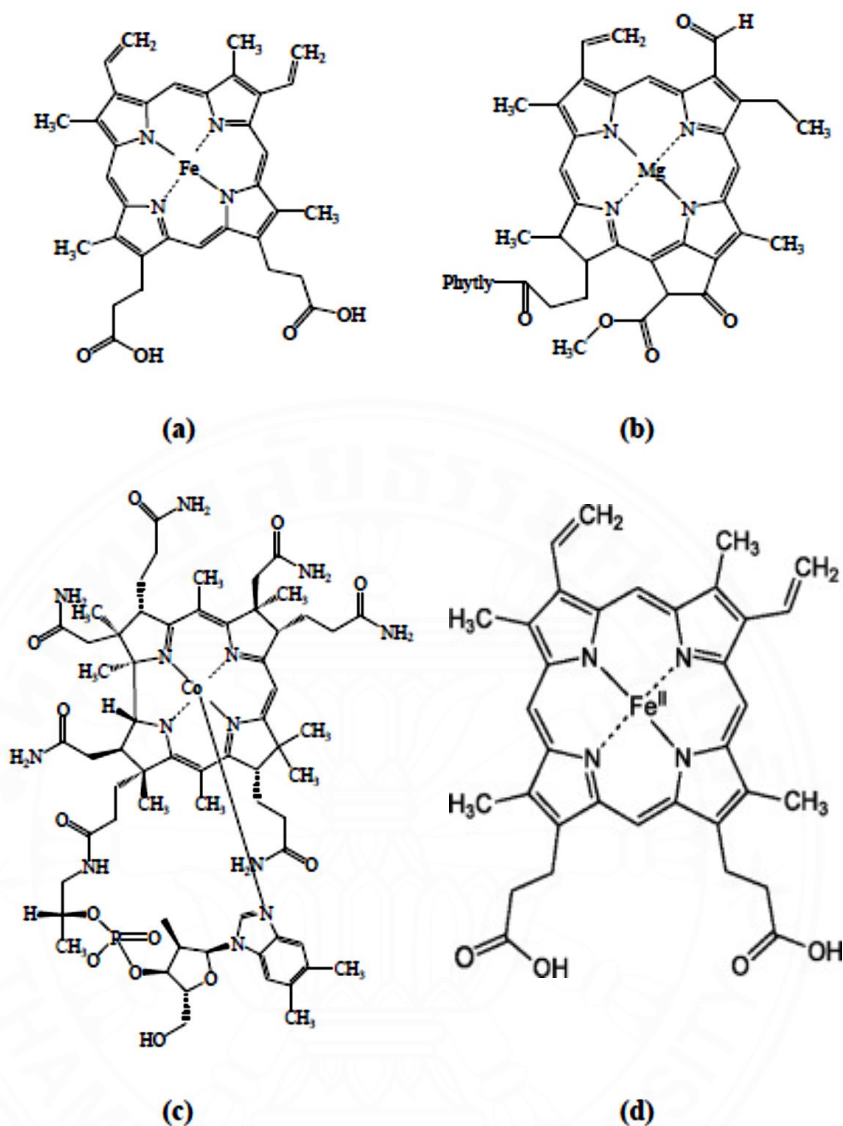
**Figure 2.26** Structure of (a) heme ("Heme." n.d.), (b) chlorophyll, ("Chlorophyll," n.d.), (c) vitamin B12 ("Vitamin B12," n.d.) and (d) Cytochrome P450 (Cook *et. al.*, 2016).

### 2.4.1.1 Heme

Heme is a vital biomolecule that plays a critical role in various biological processes. It is an iron-containing compound found in the prosthetic group of many proteins, including hemoglobin, myoglobin, and cytochromes. The structure of heme consists of a porphyrin ring coordinated to an iron ion in the center (Figure 2.26a). This unique arrangement allows heme to participate in reversible binding and transport of oxygen, as well as electron transfer reactions. In addition to its oxygen-carrying capabilities, heme is involved in a range of enzymatic reactions, such as the

catalysis of redox reactions and the metabolism of drugs and toxins. It serves as a cofactor for various enzymes, including peroxidases, catalases, and cytochrome P450 enzymes, enabling them to carry out their specific biochemical functions. The presence of heme in these proteins contributes to their distinctive spectral properties, particularly their characteristic absorption bands in the visible and ultraviolet regions. This property has been extensively utilized in spectroscopic techniques to study heme-containing proteins and investigate their structural and functional properties. Overall, heme is a remarkable molecule with diverse biological functions, ranging from oxygen transport to enzymatic catalysis. Its structural and functional versatility makes it a key component in numerous biological processes, making it an essential molecule to study in the field of biochemistry and biomedical research ("Heme." n.d.).

### 2.4.1.2 Chlorophyll

Chlorophyll, the green pigment present in leaves and green stems, is an essential component for photosynthesis. The term "chlorophyll" is originating from the Greek words "chloros," definition green, and "phyllon," definition leaf. Chlorophyll is a vital biomolecule that plays a crucial role in capturing light energy during photosynthesis. It is a derivative of porphyrin containing magnesium (refer to Figure 2.26b). The porphyrin moiety containing a magnesium ion adopts a square planar conformation. It is linked to a hydrocarbon chain that exhibits insolubility and interacts with proteins within the thylakoid membrane, effectively tethering the molecule within the internal membranes of the chloroplast. Chlorophyll molecules exhibit strong light absorption, especially in the longer wavelength regions. When light is absorbed by a chlorophyll molecule, the energy is distributed and propagated across the entire electronic structure of the excited molecule ("Chlorophyll," n.d.).

### 2.4.1.3 Vitamin B12

Vitamin B12, also known as cobalamin, is a water-soluble vitamin that plays a vital role in supporting brain function, maintaining a healthy nervous system, and aiding in the formation of blood cells. Its molecular structure is composed of four interconnected pyrrole rings joined by methane bridges, with two of the pyrrole rings being directly linked together. It has a resemblance to porphyrin, although one of the bridging methylene groups is absent. At the center of the structure, there is a corrin ring containing a cobalt atom as depicted in Figure 2.26c (Marsh, 1999).

Bacteria and archaea are exclusively responsible for the synthesis of the fundamental structure of vitamin B12, whereas the human body has the capability to convert between different forms of the vitamin ("Vitamin B12," n.d.).

### 2.4.1.4 Cytochrome P450

Enzymes are vital biological catalysts that play a crucial role in governing, initiating, and regulating essential biological reactions necessary for life processes. While enzymes are predominantly composed of proteins, some enzymes incorporate non-protein components known as prosthetic groups, which are essential for their catalytic activities ("Enzyme," n.d.). One prominent type of prosthetic group found in various enzymes is metalloporphyrins. Examples of enzymes that utilize metalloporphyrins as prosthetic groups include oxygenases and peroxidases, among others. Among these, cytochrome P-450 is a particularly important oxygenase found in the microsomes of liver cells (Cook *et al*., 2016).

### 2.4.2 Synthetic porphyrins

Recent years have witnessed extensive research efforts dedicated to the synthesis of porphyrins across various scientific disciplines. A critical factor in porphyrin synthesis involves the meticulous organization of diverse substituents in predetermined patterns around the macrocycle. Two notable patterns that have garnered attention are β-substituted porphyrins and meso-substituted porphyrins (Baiju *et. al*., 2014). β Extensive research has been conducted on β-substituted porphyrins due to their striking resemblance to naturally occurring porphyrins. Meanwhile, meso-substituted porphyrins, despite not being naturally present, have demonstrated diverse applications as biomimetic models and valuable constituents in material chemistry (Dehghani & Fathi, 2008). Meso-substituted porphyrins exhibit a wide range of properties and potential applications due to the incorporation of various substituents at the meso-positions, such as alkyl, aryl heterocyclic, organometallic groups, and even other porphyrins.

The chemistry of meso-substituted porphyrins traces its roots back to the work of Rothemund in 1935. The Rothemund reaction, introduced by Paul Rothemund in 1936, is a chemical process that involves the condensation and oxidation of four pyrroles and four aldehydes to produce a porphyrin as show in Figure 2.27. To prevent the loss of volatile acetaldehyde, sealed vessels were used. Upon meticulous

analysis of the reaction products, it was observed that approximately 10-25% of the reaction mixture consisted of another porphyrinic substance. This contaminant was subsequently isolated using chromatography and identified as various chlorins. The chlorins could be easily converted to the corresponding porphyrin through oxidation. Rothemund made several modifications to the synthetic conditions in order to optimize the reaction, ultimately determining that high concentration and high temperature in sealed vessels, without the addition of an external oxidant, were the most favorable conditions for the synthesis (Rothemund, 1935; Rothemund, 1936).
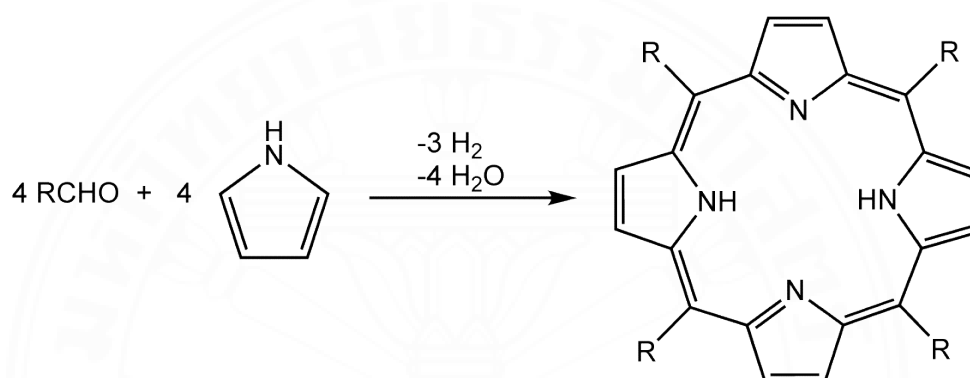


**Figure 2.27** Rothemund reaction of porphyrin synthesis ("Rothemund reaction," n.d.)

### 2.4.3 Application of porphyrins

The captivating spectroscopic and chemical attributes of porphyrins and their metal complexes have garnered significant attention. Extensive research has been conducted on their applications in diverse fields, including dye-sensitized solar cells (DSSCs) (Zhou *et al.*, 2012; Mathew *et al.*, 2014; Arteaga *et al.*, 2015), as well as organic photoelectronics (Waltera *et al.*, 2010), such as organic light-emitting diodes (OLEDs) and organic field-effect transistors (OFETs). The distinctive electronic properties of porphyrins, resulting from their extensive electron conjugation within the macrocycle, make them highly adaptable through chemical modification. This tunability allows for the precise control and manipulation of their electronic and optical properties, opening up new possibilities for their utilization in various technological applications.

The application of porphyrins in DSSCs has received continuous attention due to their favorable properties for low-cost, relatively high-efficiency, and simplified production processes. Moreover, porphyrins have found utility in an

extensive array of applications, encompassing catalysis (Groves & Kruper, 1985), anticancer therapy (Lammer *et al.*, 2015), antimicrobial agents (Stojiljkovic *et al.*, 2001), molecular sensing (Kondo, 2011), and their use as photosensitizing drugs in photodynamic therapy (PDT) (Sternberg & Dolphin, 1998). In the context of PDT, porphyrins offer a valuable approach to selectively destroy tumor tissues using light. The photosensitizing ability of porphyrins and metalloporphyrins, stemming from their rich electron conjugation within the heterocyclic rings, has made them subjects of intense investigation (Yoon & Shim, 2013).

Porphyrins also demonstrate suitability for the optical detection of volatile organic compounds, offering a promising avenue for their application. The distinctive electrical and optical properties of metalloporphyrins, arising from the interaction between the metal center of the porphyrin and the target gas, combined with their extensive conjugated system, make them ideal candidates for gas sensing applications (Dunbar *et al.*, 2010).

### 2.4.4 Porphyrins as sensor device

Porphyrins, as versatile tetrapyrrole derivatives, have attracted significant research interest across multiple disciplines, including physics, chemistry, medicine, and biology (Harrison *et al.*, 1971). In recent years, there has been significant interest in investigating the potential of porphyrins and their derivatives as sensors for the detection of diverse substances, including glucose, metal ions, pesticides, and other analytes. By modifying the spectrophotometric properties of porphyrins through bonding or interactions with other molecules and ions, it is possible to induce spectral changes that depend on the strength of association energy and association constant (Rahman & Harmon, 2006). The properties required for the development of optical sensor elements are of significant importance. In a research study led by Fei Q. *et al.*, (2016), a new water-soluble sulfonated porphyrin named 5,10,15,20-tetra(3-ethoxy-4-hydroxy-5-sulfonate)-phenyl porphyrin ($H_2TEHPPS$) was synthesized with the purpose of serving as a UV-visible sensor to detect $Cu^{2+}$ ions. The suggested mechanism entails the progressive dissociation of the J-aggregation structure of $H_2TEHPPS$ as the concentration of $Cu^{2+}$ increases. This process results in a noticeable color change in the solution, shifting from green to colorless. The utilization of $H_2TEHPPS$ for the quantification of $Cu^{2+}$ ions exhibited a reliable linear response range spanning from

0.05 to 2.5 µmol/L, accompanied by an impressive detection limit of 15 nmol/L (Fei, *et al.*, 2016).

Porphyrins and metalloporphyrins possess recognition sites due to the presence of cationic central metal ions and functional groups at the meso- and β-positions of the pyrrole rings. A spectrophotometric detection method was developed by Awawdeh A.M. and Harmon J.H. (Awaadeh & Harmon, 2005) utilizing various porphyrin derivatives, namely meso-tetra(4-sulfonatophenyl)porphyrin (TPPS), zinc meso-tetra(4-sulfonatophenyl)porphyrin (Zn-TPPS), monosulfonate-tetraphenylporphyrin (TPPS1), meso-tri(4-sulfonatophenyl)mono(4-carboxyphenyl)porphyrin (C1TPP), meso-tetra(4-carboxyphenyl)porphyrin (C4TPP), and copper meso-tetra(4-carboxyphenyl)porphyrin (Cu-C4TPP) (Figure 2.28). A solution-based spectrophotometric method employing these porphyrins was employed for the detection of pentachlorophenol (PCP) in water. Remarkably, the method achieved detection limits as low as 1, 0.5, 1.16, 1, 0.5, and 0.5 parts per billion (ppb) for TPPS, Zn-TPPS, TPPS1, C1TPP, C4TPP, and Cu-C4TPP, respectively.
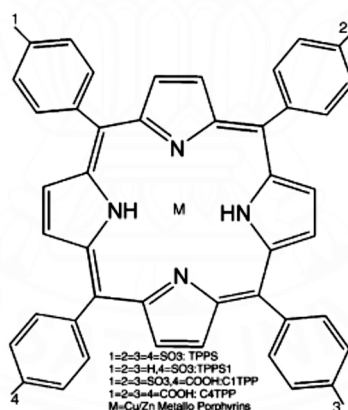


**Figure 2.28** Molecular structures of various porphyrins utilized for the detection of PCP.

Natural enzymes are highly efficient catalysts for chemical reactions but can be limited in harsh chemical environments. To overcome this limitation, researchers have focused on developing efficient enzyme mimetics. Peroxidase enzymes, including HRP and enzyme mimetics, often contain iron ions in their active sites. Corgié *et al.* demonstrated enhanced enzymatic activity by self-assembling HRP with magnetic nanoparticles (MNPs) (Kruse, 1992). They used porphyrin-

functionalized $Fe_3O_4$ nanoparticles ($H_2TCPP$-$Fe_3O_4$ nanocomposites), Among the mentioned porphyrins, Cu-C4TPP exhibited remarkable intrinsic peroxidase-like activity, efficiently catalyzing the reaction between TMB and $H_2O_2$. This catalytic process led to a rapid blue color reaction that was easily observable to the naked eye (Kruse, 1992). A glucose biosensor was developed by combining the catalytic reactions of glucose oxidase (GOx) and 5,10,15,20-Tetrakis(4-carboxyphenyl) porphyrin-functionalized $Fe_3O_4$ nanocomposites ($H_2TCPP$-$Fe_3O_4$). The biosensor effectively utilizes the catalytic properties of both components to detect glucose levels. The functionalized $Fe_3O_4$ nanocomposites, integrated with glucose oxidase, enable the selective and sensitive detection of glucose. This colorimetric method enabled the determination of glucose content. The linear range for glucose concentration was found to be 5 µM to 25 µM, with a detection limit of $2.21 \times 10^{-6}$ M. Additionally, peroxidase-like activity was reported for $H_2TCPP$-$Co_3O_4$ nanocomposites (Liu *et al.*, 2014) and $H_2TCPP$-NiO nanocomposites (Liu *et al.*, 2015), which were successfully utilized for visual and colorimetric glucose detection. These advancements show promise for the development of efficient enzyme mimetics and biosensors in various applications.

In a previous investigation conducted by Carlos-Alonso *et al*. in 2015, the anti-inflammatory characteristics of several porphyrins, including TPP, were examined. The researchers observed that TPP exhibited remarkable effectiveness in mitigating inflammation caused by oxidative stress (Alonso-Castro *et al*., 2015). FeTOMPP, on the other hand, is a porphyrin complex containing Fe(III), similar to hemin, which is a protoporphyrin IX derivative with a ferric ion. Given its structural similarity to hemin, it is plausible to assume that FeTOMPP may possess peroxidase-like activity. Based on these findings, both TPP and FeTOMPP were selected for further investigation due to their potential peroxidase activity.

HRP is a commonly used enzyme for $H_2O_2$ sensing, but its preparation and purification can be time-consuming, and it is susceptible to denaturation under extreme conditions. In recent years, porphyrins, known for their biological functions, have been explored as biomimetic catalysts with intrinsic peroxidase activity (Dehghani & Fathi, 2008). Wu L. and colleagues (2008) developed an ethanol biosensor by immobilizing alcohol oxidase (AOX) on a CNF-FeTMPyP modified electrode (Wu *et al.*, 2008). The electrochemical signal of oxygen reduction

at the CNF-FeTMPyP modified sensor surface was utilized to monitor the consumption of $O_2$ resulting from the oxidation of ethanol by $O_2$ in AOX. Furthermore, porphyrins functionalized with metal oxides such as NiO, $Fe_3O_4$, and $Co_3O_4$ (Liu *et al.*, 2015(a); Liu *et al.*, 2015(b); Liu *et al.*, 2014) have demonstrated enhanced peroxidase activity and catalytic ability in the reaction between the substrate TMB and $H_2O_2$, leading to a visible blue color reaction. By combining the catalytic reactions of alcohol with AOX and the catalytic reactions of porphyrin-functionalized metal oxides, a biosensor for alcohol detection can be developed.

# CHAPTER 3
# RESEARCH METHODOLOGY

## 3.1 Materials

### 3.1.1 Reagents

- Porphyrins (Analytical chemistry laboratory, Science and technology faculty, Thammasat University)

- metalloporphyrin (Analytical chemistry laboratory, Science and technology faculty, Thammasat University)

- Sodium acetate ($C_2H_3O_2Na$, ACS reagent, $\geq$99.0%, Sigma-aldrich, USA)

- 3,3′,5,5′-tetramethylbenzidine (TMB) (Peroxidase substrate, Sigma-aldrich, USA)

- Hydrogen peroxide solution 30% ($H_2O_2$, Sigma-aldrich, USA)

- Alcohol oxidase solution from *Pichia pastoris* (AOx) (10-40 units/µg protein (biuret), Sigma-aldrich, USA)

- Sodium phosphate dibasic heptahydrate ($Na_2HPO_4.7H_2O$, ACS reagent, 98.0-102.0%, Sigma-aldrich, USA)

- Sodium phosphate monobasic monohydrate ($NaH_2PO_4.H_2O$, ACS reagent, $\geq$98%, Sigma-aldrich, USA)

- Hydrochloric acid (HCl, ACS reagent, 37%, Sigma-aldrich, USA)

- Sodium Hydroxide (NaOH, ACS reagent, $\geq$97.0%, pellets, Sigma-aldrich, USA)

- Malic acid ($C_4H_6O_5$, Supelco)

- Tartalic acid ($C_4O_6H_6$, Supelco)

- Acetic acid ($C_2H_4O_2$, glacial, ACS reagent, $\geq$99.7%, Sigma-aldrich, USA)

- Lactic acid ($C_3H_6O_3$, Natural $\geq$85%, Sigma-aldrich, USA)

• Citric acid anhydrous ($C_6H_2O_7$, 99-100%, Chemipan corporation, Thailand)

• Oxalic acid ($C_2H_2O_4$, 98%, Sigma-aldrich, USA)

• Ascorbic acid ($C_6H_8O_6$, Sigma-aldrich, USA)

• Sodium sulphite ($Na_2SO_3$, ACS reagent, ≥98%, Sigma-aldrich, USA)

• Ethanol ($C_2H_6O$, Sigma-aldrich, USA)

• DMSO ($C_2H_6SO$)

• Distill water ($H_2O$)

• Local and commercial alcoholic beverage samples collected from local market and mall in Pakkred, Nonthaburi area.

### 3.1.2 Apparatus

The following analytical techniques were employed for data acquisition and analysis: UV-Vis absorption measurements were conducted on a Biochrom Libra S80 model UV-Visible spectrophotometer. Gas chromatography (GC) analysis was performed using a Shimadzu GCMS-TQ series instrument.

### 3.1.2.1 UV-vis spectrophotometry

To evaluate the peroxidase-like activity of porphyrin and metalloporphyrin compounds, a catalytic oxidation reaction was performed utilizing the peroxidase substrate TMB and $H_2O_2$. The progress of the reaction was monitored by observing the development of blue solutions, indicating the reduced form of TMB. The advancement of the reaction was quantified at a wavelength of 652 nm utilizing a spectrophotometer. The absorption at this specific wavelength corresponds to the development of a charge transfer complex, which arises from the oxidation of TMB in the presence of the porphyrin or metalloporphyrin catalysts.

### 3.1.2.2 Gas chromatography

To determine the ethanol content in alcoholic beverage samples, gas chromatography techniques with flame ionization detection were employed. A capillary column filled with dimethyl polysiloxane (DB-1) measuring 30 m in length and 0.25 mm in diameter was utilized for the separation of the ethanol compound.

**3.2 Methods**

**3.2.1 Synthesis of free base porphyrins and metalloporphyrin**

The porphyrins and metalloporphyrin used in this study were obtained from analytical chemistry laboratory, Thammasat University and synthesized by Mr.Thossapon Phromsatit. The synthesis of porphyrin and metalloporphyrin were illustrated in Figure 3.1 – 3.3 (Thossapon, 2015).



Pyrrole

Aldehyde
R=H
R=OCH₃
R=O(CH₂)₃CH₃

Porphyrin
TPP, R=H
TOMPP, R=OCH₃
TOBPP, R=O(CH₂)₃CH₃
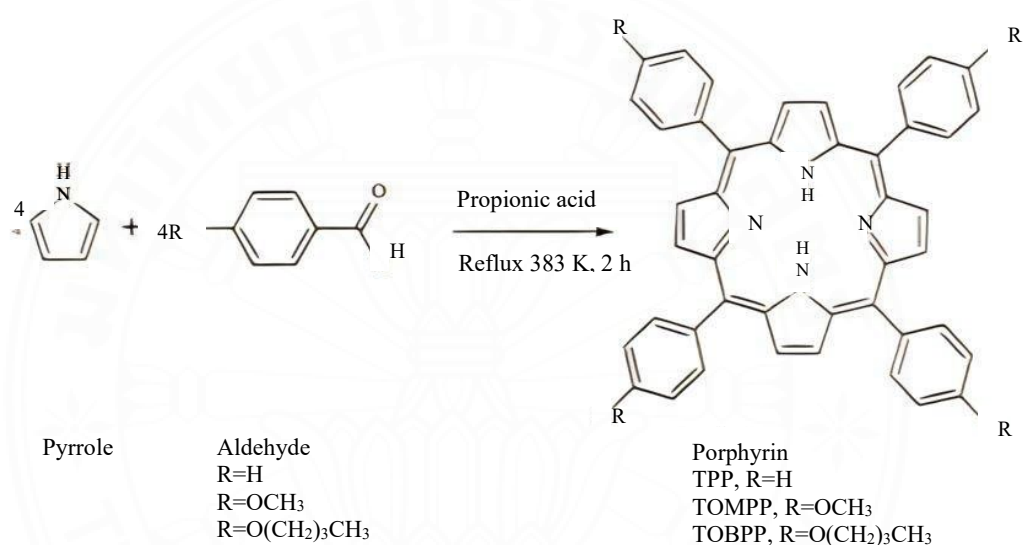
**Figure 3.1** Synthesis of porphyrins (Thossapon, 2015)



TPP, R=H
TOMPP, R=OCH₃
TOBPP, R=O(CH₂)₃CH₃

CuTPP, R=H
CuTOMPP, R=CH₃
CuTOBPP, R=O(CH₂)₃CH₃
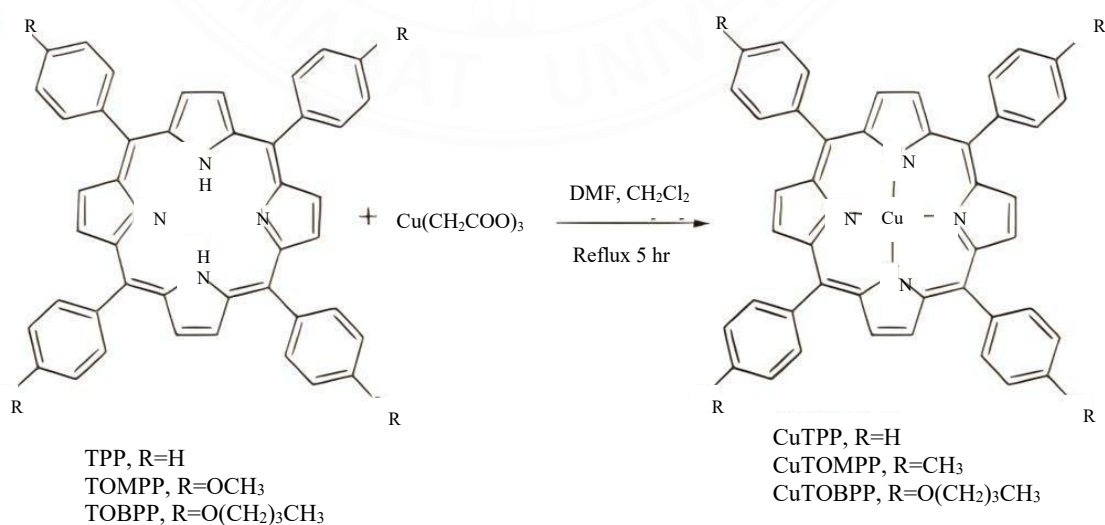
**Figure 3.2** Synthesis of copper(II) porphyrins
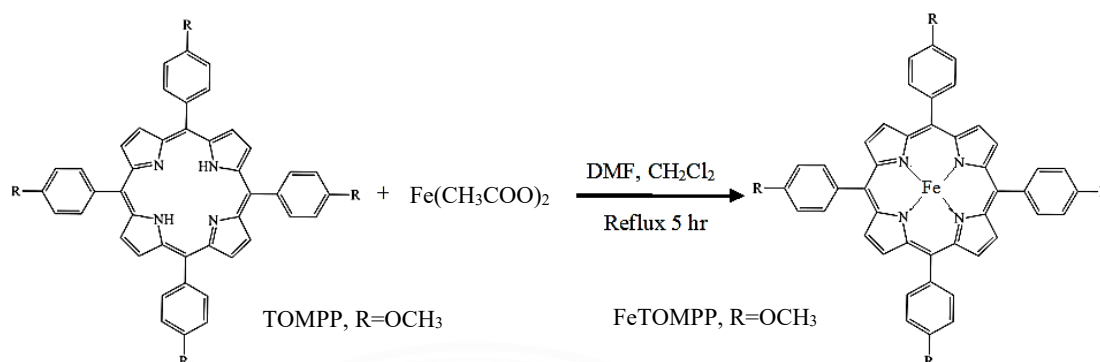
**Figure 3.3** Synthesis of Iron(III) porphyrins

### 3.2.2 The design of biosensor for ethanol analysis

The biosensor designed for ethanol analysis utilizes a bi-enzyme system comprising AOX and HRP. AOX plays a crucial role in catalyzing the oxidation of small alcohols to their corresponding aldehydes, with molecular oxygen ($O_2$) acting as the electron acceptor. This oxidation process is irreversible due to the inherent strong oxidizing nature of $O_2$. The enzymatic reactions facilitated by AOX can be quantified by observing either the reduction in $O_2$ tension or the elevation in $H_2O_2$ concentration. In this reaction scheme, AOX oxidizes alcohols, leading to the generation of $H_2O_2$. Subsequently, HRP acts as a catalyst to convert $H_2O_2$ to $H_2O$, as depicted in Figure 2.4.

In this particular study, the design of the ethanol biosensor relies on the catalytic conversion of alcohol to hydrogen peroxide through the action of the enzyme AOX, as described by Equation (1).

$$CH_3CH_2OH + O_2 \xrightarrow{\text{AOX}} CH_3CHO + H_2O_2 \qquad (1)$$

The $H_2O_2$ generated in the previous step is subsequently subjected to catalysis by peroxidase mimetics, such as porphyrin and metalloporphyrin. When $H_2O_2$ is present alongside porphyrin peroxidase mimetics, it facilitates the oxidation of TMB, which serves as a substrate for peroxidase. This oxidation process involves the transfer of electrons from the reduced form of TMB (colorless) to $H_2O_2$, resulting in

the production of the oxidized form of TMB (dark blue) as the end product (Equation (2)).

$$H_2O_2 + \text{reduced TMB} \xrightarrow{\text{porphyrin}} \text{oxidized TMB} + H_2O \quad (2)$$
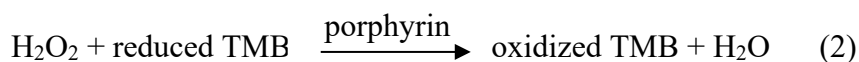
Consequently, the enzymatic reaction can be optically monitored through the visual observation of the color change of TMB, transitioning from colorless to a deep blue hue, as illustrated in Figure 3.4.
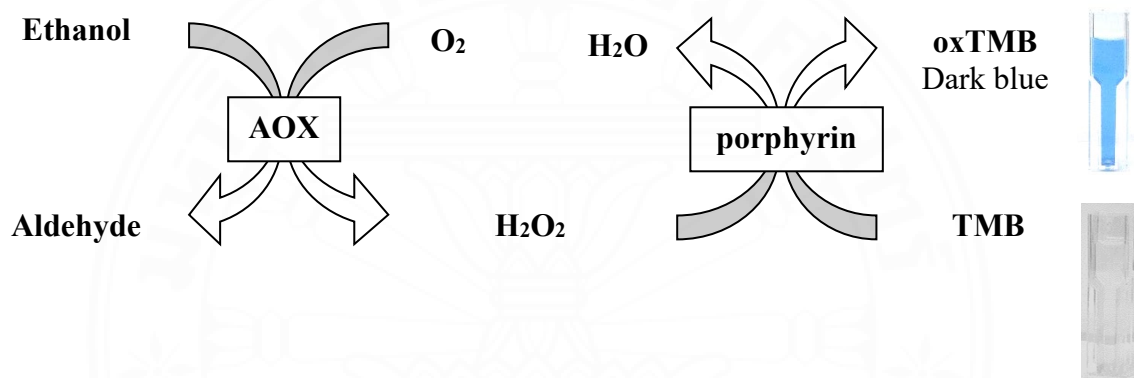


**Figure 3.4** Schematic illustration detection mechanism for $H_2O_2$ and ethanol sensing using Porphyrins and AOX.

### 3.2.2.1 UV-visible absorbance measurements

UV-Vis spectroscopy, also referred to as UV-visible spectroscopy or UV/Vis spectroscopy, is an analytical technique employed to measure the absorption of ultraviolet (UV) and visible light by a sample. Its primary applications include determining substance concentrations in solutions and identifying the functional groups present within molecules. During UV-Vis spectroscopy, the sample's absorption of light is measured at various wavelengths, and the collected data is plotted as a spectrum. This absorption spectrum serves as a tool to identify specific functional groups and quantify substance concentrations in solutions. By analyzing the characteristic absorption bands exhibited in the spectrum, the presence of distinct functional groups can be identified, while the magnitude of absorption can be correlated with the concentration of a substance. UV-Vis spectroscopy finds broad utility across

disciplines such as chemistry, biochemistry, pharmaceuticals, environmental analysis, and materials science.

The peroxidase-like activity of porphyrin and metalloporphyrin can be assessed by observing the oxidation of TMB in the presence of $H_2O_2$. TMB, initially colorless, undergoes oxidation in the presence of peroxidase enzymes or compounds possessing peroxidase-like activity, along with $H_2O_2$. This oxidation process leads to the formation of oxidized TMB (oxTMB), which is distinguished by its characteristic blue color. The oxidation process can be detected and quantified using UV-Vis absorption spectroscopy. The molecular structure of TMB is depicted in Figure 2.7. TMB, an aromatic amine, functions as a co-substrate for reduction and undergoes one-electron oxidation by the higher oxidation states of heme peroxidases, including compound I and compound II. This enzymatic process leads to the transformation of TMB, facilitating its conversion into an oxidized form. Consequently, a radical cation is generated, which subsequently forms a charge transfer complex when interacting with unoxidized TMB. The charge transfer complex exhibits an absorption peak at a wavelength of 652 nm, with a molar absorptivity ($\varepsilon$) of 39,000. Further oxidation of TMB results in the formation of the fully oxidized product, known as diimine, which absorbs light at 450 nm, with a molar absorptivity ($\varepsilon$) of 59,000. The stoichiometry of the oxidation reaction reveals that either 0.5 mole of the charge transfer complex, characterized by a maximum absorption wavelength ($\lambda$max) of 652 nm, or 1 mole of diimine, exhibiting a maximum absorption wavelength ($\lambda$max) of 450 nm, is formed (or TMB is oxidized) for each mole of hydrogen peroxide reduced by the peroxidase enzyme.

To prepare porphyrin and metalloporphyrin solutions, each respective compound was dissolved in dimethylsulfoxide (DMSO) at a concentration of 0.5 mg/ml. These stock solutions were then diluted with sodium acetate to attain a final DMSO concentration of 1% (v/v) and a final concentration of 50 µg/ml for each compound.

The proficiency of porphyrins and metalloporphyrins in emulating peroxidase activity was determined by monitoring the enzymatic oxidation of the peroxidase substrate TMB in the presence of $H_2O_2$. The experiments were conducted in a reaction volume of 2.0 ml, with 500 µM TMB and 100 µM $H_2O_2$ as the

substrates. The colorimetric analysis was prepared by combining 200 µl of a 500 µM TMB, 200 µl of the porphyrins and metalloporphyrin stock solution (at a concentration of 50 µg/ml), and 200 µl of a 1 mM $H_2O_2$ solution in 1.4 ml of a sodium acetate (NaOAc) buffer (0.1 mM, pH 6). After the completion of the reaction mixture preparation, it was allowed to incubate for 10 minutes. The concentration of the TMB species in its oxidized form was then assessed by measuring the UV-Vis absorption at 652 nm using a Biochrom Libra S80 model UV-Visible spectrophotometer. A blank sample, containing the reaction mixture without any porphyrin or metalloporphyrin, was used as a reference for all analyses.

### 3.2.2.2 Optimization of the reaction conditions

For further analysis of the optimal reaction conditions, solutions of porphyrin and metalloporphyrin were prepared by dissolving each compound in DMSO. The concentration used varied between 0.1 and 0.8 mg/ml. The stock solutions were subsequently diluted with sodium acetate, resulting in a final concentration of 1% (v/v) DMSO, with varying concentrations of each compound ranging from 10 to 80 µg/ml. These prepared solutions were used to explore the peroxidase-like activity of the porphyrins and metalloporphyrin under different reaction conditions.

To establish the optimal conditions for the peroxidase-like activity of porphyrins and metalloporphyrins, the following parameters were systematically altered:

- Amount of porphyrin and metalloporphyrin: Different amounts ranging from 0 to 80 µg (200 µl from stock solution) were added to a mixture of reactants comprising 1.4 ml of NaOAc buffer (0.1 mM, pH 2-10), 1 mM $H_2O_2$ as the substrate, and a TMB concentration of 500 µM. The total reaction volume was 2 ml.

- pH: To examine the impact of pH on the peroxidase-like activity, the sodium acetate buffer's pH was adjusted within the range of 2 to 10 in the reaction mixture.

- Temperature: The peroxidase-like activity was assessed by incubating the reaction mixture at temperatures varying from 25 to 50 °C to examine its temperature dependence.

Following a 10 minute incubation period, the concentration of the oxidized TMB was determined by measuring the absorbance at 652 nm using UV-Vis absorption spectroscopy. By analyzing the results obtained under different conditions, the optimal amount of porphyrin and metalloporphyrin, pH, and temperature for maximizing the peroxidase-like activity can be determined.

The each of optimum conditions were then used to compare the peroxidase-like activity among porphyrin and metalloporphyrin. For comparing the peroxidase-like activity, a reaction mixture was prepared by combining 200 µl of $H_2O_2$ solution at various concentrations (0, 0.5, 1, 1.5, and 2 mM), 200 µl of TMB (500 µM), and the optimum concentration of either porphyrin or metalloporphyrin (as determined in step 3.2.2.2). The mixture was added to 1.4 ml of NaOAc buffer (0.1 mM, pH 6). The resulting solution was incubated at the determined optimum temperature for 10 minutes to allow the peroxidase-like activity to occur. Upon completion of the incubation period, the concentration of the oxidized TMB was determined by conducting UV-Vis spectroscopy and measuring the absorbance at 652 nm. The assessment of the peroxidase-like activity of both porphyrin and metalloporphyrin compounds can be conducted by comparing the absorbance values obtained for varying concentrations of $H_2O_2$. The compound exhibiting higher peroxidase-like activity, as indicated by a greater increase in absorbance with increasing $H_2O_2$ concentration, can be selected for further experiments.

### 3.2.2.3 Detection of $H_2O_2$

The peroxidase-like activity of the chosen porphyrin and the optimal reaction conditions identified in step 3.2.2.2 demonstrated a reliance on the $H_2O_2$ concentration, as evident from the experimental findings. Hence, the quantitative detection of $H_2O_2$ can be achieved by monitoring the alteration in absorbance intensity at 652 nm. To create a 2 ml reaction mixture, 200 µl of $H_2O_2$ solution with varying concentrations (ranging from 0 to 10 mM) was added to a 0.1 mM NaOAc buffer (pH 6.0) containing 500 µM TMB and the optimal concentration of the chosen porphyrin as determined in step 3.2.2.2. The reaction mixture was incubated for 10 minutes to allow the peroxidase-like activity to occur. After incubation, the absorbance of the solution was measured at 652 nm using UV-Vis spectroscopy. The absorbance values obtained

from the experiment were utilized to establish a calibration curve that correlates the absorbance with the corresponding concentration of $H_2O_2$.

The limit of detection (LOD) is typically determined by performing multiple measurements of the blank sample and calculating the standard deviation of these measurements. The LOD is then calculated as a multiple of the standard deviation, usually defined as a signal-to-noise ratio (SNR) of 3:1 or 10:1. In other words, the LOD is the concentration at which the signal is significantly higher than the noise level, allowing for reliable detection and quantification of the analyte. The LOD can be calculated using the following formula:

$$LOD = 3.3 * \sigma / S$$

where $\sigma$ represents the standard deviation of the response and S denotes the slope of the calibration curve.

The slope (S) of the calibration curve can be determined by analyzing the linear relationship between the absorbance and the concentration of $H_2O_2$. The LOD can then be calculated to quantify the sensitivity and detection limit of the selected porphyrin for $H_2O_2$ detection.

### 3.2.2.4 Steady-state kinetic assays

In order to investigate the catalytic mechanism and determine the kinetic parameters of the porphyrin-catalyzed reaction involving $H_2O_2$ and TMB as substrates, enzyme kinetics theory and methods were utilized. The Michaelis-Menten equation ($v = V_{max}S/(K_m + S)$) was employed to characterize the enzymatic activity, where v represents the initial rate of the reaction and S corresponds to the substrate concentration. The Michaelis constant ($K_m$) is a parameter that reflects the affinity between the catalyst and the substrate in an enzymatic reaction. A lower $K_m$ value indicates a higher affinity between the catalyst and the substrate. To determine the kinetic data for the porphyrin-catalyzed reaction, a series of experiments were performed. The concentration of one substrate was varied while keeping the concentration of the other substrate constant.

For the experiments with TMB as the substrate, a reaction mixture containing 200 μl of the optimized concentration of the selected porphyrin (from Section 3.2.3.2), 1.4 ml of NaOAc buffer solution (pH 6), and 25 mM $H_2O_2$ was prepared. The progress of the reaction was tracked by monitoring the changes in

absorbance at 652 nm as a function of time. Conversely, when $H_2O_2$ was used as the substrate, the reaction mixture consisted of 200 µl of the optimized concentration of the selected porphyrin, 200 µl of a TMB solution (500 µM), and varying concentrations of $H_2O_2$ in a 1.4 ml NaOAc buffer solution (pH 6), resulting in a total reaction volume of 2 ml. The concentrations of $H_2O_2$ ranged from 10 to 125 mM. The kinetic data obtained from the experiments were analyzed using Lineweaver-Burk plots (Sansuk *et al.*, 2020) to determine the maximum initial velocity (Vmax) and the Michaelis-Menten constant (Km). In the Lineweaver-Burk plots, the reciprocal of the double reciprocal of the Michaelis-Menten equation was plotted against the reciprocal of the substrate concentration. By analyzing the slope and intercept of the Lineweaver-Burk plot, the values of Vmax and Km could be determined, respectively. The Michaelis-Menten equation is represented as follows:

$$\frac{1}{v} = \frac{Km}{Vm} \times \left( c + \frac{1}{km} \right)$$

In the context of the reaction kinetics, the Michaelis-Menten equation relates the initial velocity (v) to the substrate concentration (C). In this equation, Vm represents the maximal reaction velocity, while Km is known as the Michaelis constant. These parameters provide insights into the enzyme-substrate interaction.

### 3.2.2.5 Stability test of the TMB/FeTOMPP system

The stability of a biosensor is a critical aspect that determines its capability to maintain consistent performance over time despite external factors. Several factors can influence the performance of the biosensor device, including environmental conditions such as temperature, humidity, and other variables. These factors have the potential to affect the precision and accuracy of the device (Bhalla et. al., 2016). The stability of a biosensor refers to its capacity to withstand and adapt to changes in its performance throughout a specified duration. This characteristic is crucial for ensuring reliable and dependable measurements, as it guarantees that the biosensor's responses remain unaffected by external interruptions.

The test system was prepared by combining a stock solution containing dissolved porphyrin, 0.1 mM NaOAc buffer (pH 6.0), and 500 µM TMB. The solution was stored at room temperature, shielded from light to maintain its

stability. Daily monitoring of the pH was conducted, ensuring its consistency and reliability before each test.

To evaluate the stability of the system, TMB-$H_2O_2$ reactions were performed using the stock solution stored for different durations ranging from 0 to 15 days. The stock solution served as the catalyst, while the concentration of $H_2O_2$ remained constant at 1 mM. The resulting solution was subjected to UV-Vis absorption spectroscopy at 652 nm to quantify the concentration of the oxidized TMB. By measuring the concentration of oxidized TMB, any variations or changes in the system's stability could be observed and analyzed.

### 3.2.2.6 Detection of ethanol

A colorimetric detection system was developed for ethanol, leveraging the intrinsic peroxidase-like catalytic activity of porphyrins and metalloporphyrins. The catalytic activity of these compounds was determined to be directly proportional to the concentration of hydrogen peroxide ($H_2O_2$), as indicated by the observed change in absorbance at 652 nm. To create a specific ethanol sensor, AOX was combined with the porphyrins and metalloporphyrins, enabling the detection of ethanol through the colorimetric response.

The ethanol detection process involved several steps. Initially, 10 µl of AOX (Gvozdev *et al*., 2010) and 100 µl of ethanol at varying concentrations (ranging from 0-15% v/v) were combined in a 0.1 M phosphate buffer (pH 7.0) to achieve a total volume of 600 µl. The incubation of the mixture was carried out at a temperature of 37°C for a duration of 20 minutes. Following this, 200 µl of TMB solution with a concentration of 500 µM, 200 µl of a porphyrin stock solution, and 1 ml of a NaOAc buffer with a pH of 6 were added to the ethanol reaction solution. The resulting solution was subjected to UV-Vis measurement, and a standard curve was constructed using the obtained data. The linear range of detection and LOD were determined accordingly. The LOD was determined as described above (3.2.2.3.)

### 3.2.2.7 Stability and reproducibility test of the
### AOX/TMB/FeTOMPP system

The test system was studied by preparing a stock solution I containing AOX and phosphate buffer (pH 7.0) and stock solution II containing dissolved porphyrin, 0.1 mM NaOAc buffer (pH 6.0), and 500 µM TMB. The solution

I was stored at 4 º C and solution II stored at room temperature, shielded from light to maintain its stability.

To evaluate the stability of the system, AOX/TMB/FeTOMPP reactions were performed using the stock solution I and II stored for different durations ranging from 0 to 15 days. The stock solution served as the catalyst, while the concentration of ethanol remained constant at 5% v/v. The resulting solution was subjected to UV-Vis absorption spectroscopy at 652 nm to quantify the concentration of the oxidized TMB. By measuring the concentration of oxidized TMB, any variations or changes in the system's stability could be observed and analyzed.

Reproducibility was assessed by conducting tests on eight parallel samples under identical conditions. To evaluate reproducibility, UV-Vis absorption spectroscopy at 652 nm was employed after introducing 5% v/v of ethanol into the AOX/TMB/FeTOMPP reactions.

### 3.2.2.8 Interferences Measurement

In order to assess potential interferences that could affect the accuracy of ethanol determination in fermented beverage samples, and interference test was performed to assess the potential impact of common ingredients commonly present in real samples. This test aimed to identify any substances that may interfere with the biosensor response used for ethanol determination. The tested substances included antioxidants such as L-ascorbic acid and lactic acid, as well as flavorings like citric acid and acetic acid that are commonly used in certain beers. Furthermore, organic acids that could be present during the fermentation process were also examined, including succinic acid, malic acid, oxalic acid, citric acid, tartaric acid, and sodium sulfite, which is commonly used as a preservative agent. By screening these substances, their potential interference with the biosensor response could be determined.

For the interference test, the reaction solution was prepared by adding the interferent and ethanol in a 2:1 ratio (2% v/v interferent and 1% v/v ethanol) in a total volume of 100 µl. For the measurement of interferences, a 0.1 M phosphate buffer (pH 7.0) was prepared, and 10 µl of AOX and 100 µl of different reaction solutions were added to achieve a total volume of 600 µl. The mixture was incubated at 37°C for 20 minutes. Afterward, 200 µl of a TMB solution (500 µM), 200 µl of the

porphyrin stock solution, and 1 ml of a NaOAc buffer (pH 6) were added to the reaction solution. The resulting solution was then quantified using UV-Vis spectroscopy.

To evaluate the applicability of ethanol detection in colored solutions, various color interference tests were conducted. These tests involved examining red wine (12% v/v, contributing a red color), orange juice (imparting a yellow color), apple juice (resulting in a brown color), and grape juice (with a purple/dark color). In each case, 1% ethanol was introduced into the samples. To facilitate sample treatment and analysis, all of these solutions required an appropriate dilution (1:10) using a phosphate buffer with a pH of 7. For the measurement of interferences, a 0.1 M phosphate buffer (pH 7.0) was prepared, and 10 µl of AOX and 100 µl of different reaction solutions were added to achieve a total volume of 600 µl. The mixture was incubated at 37°C for 20 minutes. Afterward, 200 µl of a TMB solution (500 µM), 200 µl of the porphyrin stock solution, and 1 ml of a NaOAc buffer (pH 6) were added to the reaction solution. The resulting solution was then quantified using UV-Vis spectroscopy.

### 3.2.2.9 Real sample measurement

The analysis of ethanol samples from alcoholic beverages was conducted as follows: Initially, 10 µl of AOX and 100 µl of alcoholic beverage samples with concentrations ranging from 0% to 15% v/v were mixed in a 0.1 M phosphate buffer at pH 7.0, resulting in a total volume of 600 µl. The mixture was then incubated at 37°C for a duration of 20 minutes. Following that, 200 µl of a 500 µM solution of TMB, 200 µl of the porphyrin stock solution, and 1 ml of a NaOAc buffer at pH 6 were added to the 600 µl ethanol reaction solution. The resulting solution was then measured using UV-Vis spectroscopy. The obtained data were compared to a standard curve to determine the concentration of alcohol.

### 3.2.2.10 Gas chromatographic measurement

In order to compare the ethanol concentration determined by the biosensor with a reference method, gas chromatography was employed using a Shimadzu GCMS-TQ series instrument. A capillary column filled with dimethyl polysiloxane (DB-1, 30m × 0.25 mm) was utilized for the analysis. To determine the ethanol concentration, an internal standard of isopropanol was employed. To prepare working solutions, ethanol was mixed with 1 cm$^3$ of isopropanol, resulting in ethanol

concentrations ranging from 1.0% to 10.0% v/v. These solutions were then injected into the GC system for analysis. A calibration curve was constructed by determining the peak area ratio of ethanol to isopropanol at each concentration level (the calibration curve was showed in Appendix C). To analyze actual samples, they were first diluted, and then 2 cm$^3$ of each diluted sample was mixed with isopropanol before undergoing GC analysis. The ethanol content was determined by calculating the ratio of the peak area to the dilution factor of each sample. Table 3.1 expressed detailed information about the GC conditions employed in the experiment (Sansuk *et al.*, 2020; Somboon & Sansuk, 2018).

The alcoholic beverage samples were collected from market and mall in Pakkred, Nonthaburi area. The samples were 4 brands of Beer, 2 brands of Soju, 3 brands of Sato, 1 type of Krachae, 3 brands of Wine and 2 brands of liquor.

**Table. 3.1** Optimum conditions for ethanol analysis using gas chromatography – flame ionization (FID) technique.

| Parameters | Analytical conditions |
|---|---|
| Carrier gas | $N_2$ |
| Flowrate (ml/min) | 72 |
| Column temperature (°C) | 37-50 |
| Injector temperature (°C) | 180 |
| Detector temperature (°C) | 250 |
| Injection volume (μl) | 0.5 |

# CHAPTER 4
# RESULTS

## 4.1 Synthesis and Characterization of Porphyrins, Copper(II) Porphyrins, and Iron(III) Porphyrin Complexes

The porphyrin and metalloporphyrin in this study were synthesized and characterized by Mr. Thossapon Phromasatit (Thossapon, 2015). The characteristics data of porphyrins and metalloporphyrin such as structure, CHN elemental analysis, mass spectrometry, NMR spectroscopy, Infrared spectroscopy, UV-vis spectroscopy, fluorescence spectroscopy and thermal gravimetric analysis were showed in Appendix B.

## 4.2 Biosensor development

In the colorimetric sensor system, the presence of AOX enables the oxidation of ethanol in the presence of oxygen. During this enzymatic reaction, ethanol is converted to aldehyde, and $H_2O_2$ is generated as a byproduct. The generated $H_2O_2$ is then utilized to oxidize a compound acted upon by peroxidase enzyme called TMB. This oxidation process results in the formation of oxidized TMB (oxTMB), a chromogenic product that displays a characteristic color. Porphyrins, which possess intrinsic peroxidase-like activity, are introduced into the system. They function as catalysts, facilitating the oxidation of TMB by $H_2O_2$. As a result, the concentration of $H_2O_2$ produced in the ethanol oxidation reaction is indirectly determined by the color intensity of the formed oxTMB as show in Figure 3.4. As the concentration of ethanol increases in the sample, a corresponding increase in the generation of $H_2O_2$ occurs, resulting greater noticeable color change from clear to blue (redTMB). By quantifying the absorbance or the product color strength, the ethanol concentration in the sample can be estimated.

The ability of porphyrins and metalloporphyrins to mimic peroxidase activity was examined by quantifying the oxidation of TMB in the presence of $H_2O_2$. Initially, TMB is in a colorless state. However, in the presence of peroxidase or substances exhibiting peroxidase-like activity, along $H_2O_2$, TMB undergoes oxidation and turns into a blue-colored oxidized form known as oxTMB (as shown in Figure 4.1). The oxidation of TMB to oxTMB can be confirmed by analyzing the UV-Vis absorption spectrum (Tan *et al*., 2014).

### 4.2.1 The peroxidase-like activity of porphyrin and metalloporphyrin

To assess the peroxidase-like activity, a study was conducted utilizing porphyrins and metalloporphyrins. In this experimental setup, 200 µl of a stock solution containing porphyrins and metalloporphyrins at a concentration of 50 µg/ml was combined with 1.4 ml of sodium acetate (NaOAc) buffer (0.1 mM, pH 6). To serve as the substrate, the reaction mixture was supplemented with 200 µl of a 5 mM solution of TMB and 200 µl of a 1 mM solution of $H_2O_2$, bringing the total volume to 2 ml. The reaction mixture was then incubated for a duration of 10 minutes. The UV-Vis absorption of the oxidized TMB was measured at a wavelength of 652 nm using a Biochrom Libra S80 UV-Visible spectrophotometer. In order to establish a reference, a blank sample was prepared without the addition of porphyrins and metalloporphyrins in the reaction mixture.
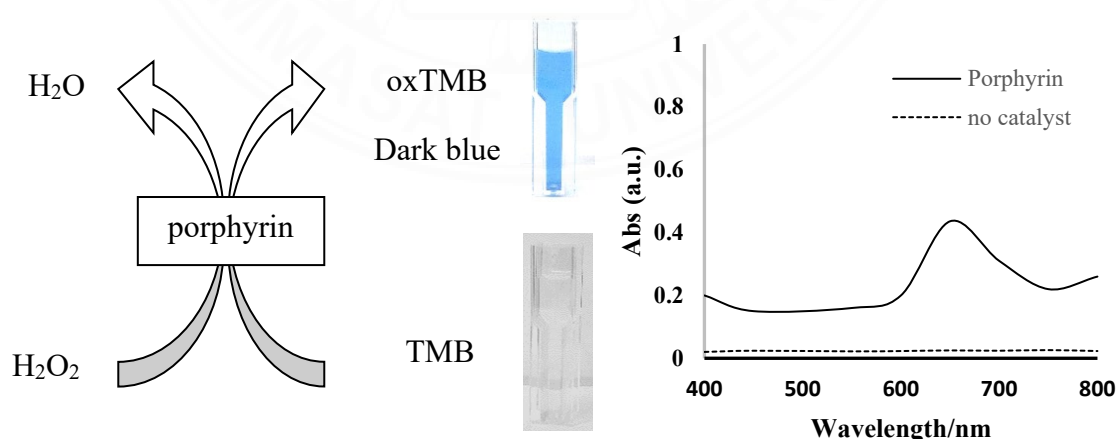


**Figure 4.1** Schematic representation of TMB Oxidation color reaction catalyzed by porphyrin mimetic peroxidase in the presence of $H_2O_2$

The resulting solution from the reaction exhibited distinct absorption peaks at 375 nm and 652 nm, which are well-known characteristic peaks associated with the absorption of oxidized TMB (oxTMB) (Nirala *et al*., 2015; Zhao *et al*., 2015; Lin *et al.*, 2015). These specific absorption peaks at 375 nm and 652 nm are widely used indicators for the presence of oxTMB and can be utilized to assess the peroxidase or substances exhibiting peroxidase-like activity. The absorbance values of oxTMB, reflecting the catalytic activity of porphyrin and metalloporphyrins, are compiled and presented in Table 4.1.

**Table 4.1** The absorbances of oxTMB from peroxidase-like activity of porphyrin and metalloporphyrins.

| Samples | Abs (652 nm) |
|---|---|
| TPP | 0.42 |
| FeTOMPP | 0.58 |
| CuTPP | NA |
| TOMPP | 0.0111 |
| TOBPP | 0.0008 |
| CuTOMPP | 0.0014 |
| CuTOBPP | 0.0182 |

NA = Not detect

Upon examination of the data presented in Table 4.1, it is evident that both TPP and FeTOMPP exhibited considerable catalytic activity in the oxidation reaction of TMB and $H_2O_2$, resulting in the formation of $H_2O$ and a blue color due to oxidized form of TMB. As a result of this reaction, a distinctive blue intermediate product is formed, characterized by a prominent absorption peak at 652 nm. The accurate measurement of this absorption peak can be achieved through the use of UV-Vis spectroscopy. The absorbance results from Table 4.1 clearly indicate that TPP and FeTOMPP were able to effectively oxidize TMB in the presence of $H_2O_2$, as evidenced by their measurable absorbance values. In contrast, the other metalloporphyrins tested did not exhibit noticeable catalytic activity in this reaction. Based on these findings, TPP and FeTOMPP were selected for further investigation and analysis.

To explore the detection capability of $H_2O_2$, a set of experimental investigations were carried out using TPP and FeTOMPP as catalysts. The detection process by adding varying concentration of $H_2O_2$ (ranging from 50 to 200 µM) to a solution containing 200 µl of TMB (500 µM), 50 µg/ml of TPP and FeTOMPP stock solution, and 1.4 ml of NaOAc buffer (0.1 mM, pH 6). After incubating the reaction mixture at 30 °C for 10 minutes, the extent of oxidation was determined by measuring the absorbance of the solution at a wavelength of 652 nm using UV-Vis spectroscopy.

The experimental results depicted in Figures 4.2 clearly demonstrate the peroxidase-like activity of both TPP and FeTOMPP. The oxidation of TMB by these compounds resulted in the generation of a distinct blue-colored solution, indicating their ability to catalyze the typical peroxidase reaction. The strength of the resulting blue color directly correlated with the concentration of $H_2O_2$, with higher concentrations leading to a more prominent color development. These results highlight the effectiveness of TPP and FeTOMPP as catalysts for $H_2O_2$ detection, offering a sensitive and dependable method for assessing peroxidase activity.
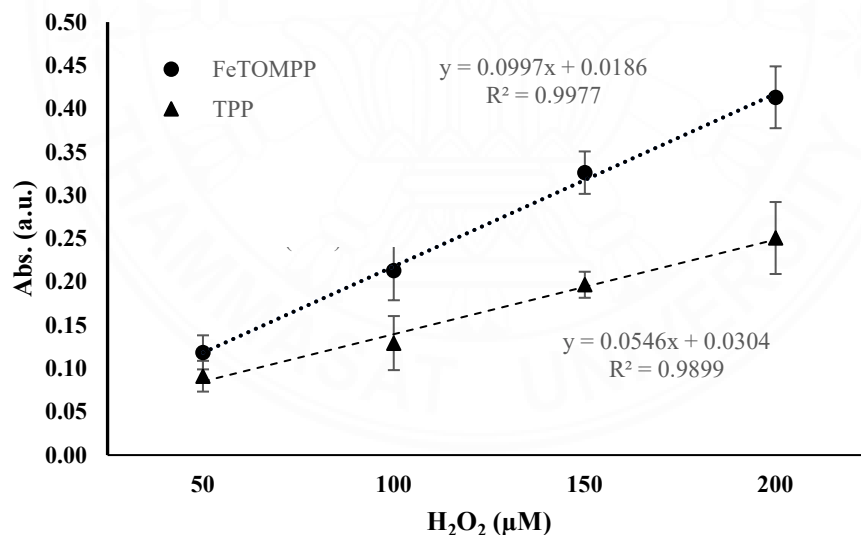


**Figure 4.2** Peroxidase-like activity of TPP at varying concentrations of $H_2O_2$ (50-200 µM) determined by the absorption of oxidized TMB at 652 nm

TPP and FeTOMPP exhibited a unique property of being oxidized by $H_2O_2$, resulting in the reduction of $H_2O_2$ to $H_2O$. The oxidation of TMB by TPP and FeTOMPP resulted in the formation of an oxidized state of these compounds. The oxidized TPP and FeTOMPP then acted as catalysts to further oxidize TMB, generating the blue-colored product, oxTMB. This blue oxTMB species was utilized to assess the peroxidase-like activity of TPP and FeTOMPP. The UV-Vis absorption spectra shown in Figures 4.2 illustrate the correlation between the concentration of $H_2O_2$ and the absorption intensity at 652 nm, which corresponds to the presence of the oxTMB species. As the concentration of $H_2O_2$ increases, the absorbance at 652 nm also increases, indicating a greater formation of the oxTMB species. The observed sensitivity of the detection system in accurately measuring different $H_2O_2$ concentrations confirms the effectiveness of TPP and FeTOMPP as catalysts for the detection and quantification of $H_2O_2$ in the presence of TMB. The measurement of absorbance at 652 nm provides a reliable method for determining the concentration of $H_2O_2$ using TPP and FeTOMPP as catalysts. These findings highlight the significant contribution of TPP and FeTOMPP as valuable assets in achieving the sensitive and selective detection of $H_2O_2$. The exceptional capability of these compounds to generate a discernible response through the oxidation of TMB represents a promising avenue for the advancement of peroxidase-mimicking sensors and analytical methodologies.

### 4.2.2 Optimization of the reaction conditions

This study was focused on the factors that influence the catalytic activity such as pH, temperature, and porphyrin concentration as showed in Figure 4.3 – 4.5.

The optimum amount of TPP and FeTOMPP for the catalytic reaction was determined by performing experiments with different concentrations of these compounds. By systematically varying the catalyst concentration while keeping other factors constant. Moreover, the peroxidase-like activity of TPP and FeTOMPP was evaluated under different pH and temperature conditions to assess their catalytic performance. Different pH values and temperature were tested to determine the optimal pH range and temperature that favored their catalytic efficiency.

### 4.2.2.1 Optimum amount of TPP and FeTOMPP

The catalytic activity of TPP and FeTOMPP was evaluated by examining the effect of varying amounts of these compounds, as shown in Figure 4.3. By comparing the absorbance or any other relevant parameter at 652 nm, the optimal amount of TPP and FeTOMPP can be determined. This optimal concentration would correspond to the highest catalytic activity and can be used as a reference for subsequent studies or applications. As showed in Figure 4.3, the optimal concentration of TPP and FeTOMPP were 50 µg/ml and and 35 µg/ml respectively.
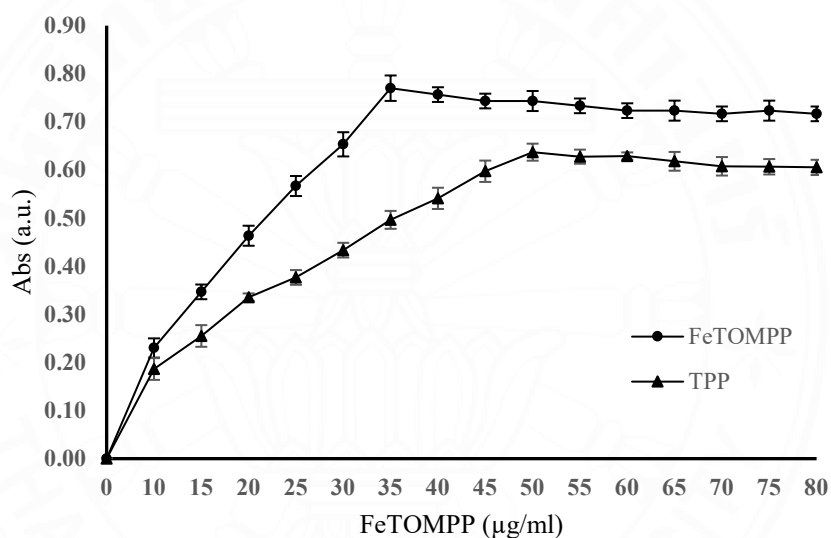


**Figure 4.3** Effect of optimum amount on the absorbance of oxTMB at 652 nm

### 4.2.2.2 Optimum pH of TPP and FeTOMPP

To identify the pH range that optimizes the catalytic activity of TPP and FeTOMPP, the experiment was carried out using the previously determined optimal amounts of TPP (35µg/ml) and FeTOMPP (50µg/ml) in NaOAc buffer. The catalytic activity was investigated by varying the pH of the buffer solution in the range of 2 to 10 to assess its impact on the reaction. The concentration of the substrate, $H_2O_2$, was maintained at 1 mM throughout the experiment, while the concentration of the peroxidase substrate, TMB, was kept constant at 500 µM. The total volume of the reaction mixture was 2 ml, and the mixture was incubated at a temperature of 30°C for

10 minutes. The influence of different pH levels on the catalytic activity of TPP and FeTOMPP was investigated, and the results are illustrated in Figure 4.4.
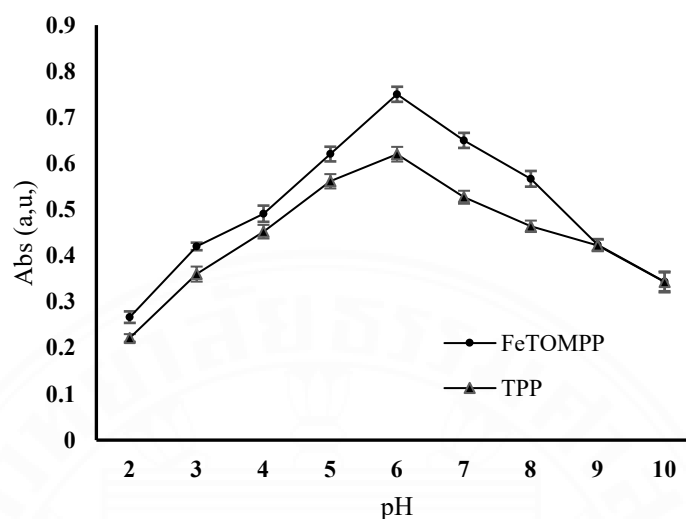


**Figure 4.4** Effect of optimum pH on the absorbance of oxTMB at 652 nm

Figure 4.4 demonstrates the influence of pH (ranging from 2.0 to 10.0). The data obtained from the experiment demonstrated a gradual increase in absorbance as the pH value increased, reaching a maximum at pH 6.0. Beyond this optimal pH, the absorbance begins to decrease. These results suggest that TPP and FeTOMPP may experience deactivation under extremely low or high pH conditions. The experimental data demonstrates that the catalytic activity of TPP and FeTOMPP is more pronounced in slightly acidic conditions as compared to neutral and alkaline environments. This observation can be attributed to the lower solubility of TMB in alkaline conditions (Mu *et al.*, 2012). Following these findings, a pH of 6.0 was identified as the optimal pH for conducting further experiments.

### 4.2.2.3 Optimum Temperature of TPP and FeTOMPP

Figure 4.6 illustrates the impact of temperature (ranging from 25 to 50 °C) on the catalytic activity of TPP and FeTOMPP, using the previously determined optimal amounts of these compounds in NaOAc buffer (0.1 mM, pH 6) with $H_2O_2$ (1 mM) as the substrate. TMB concentration was maintained at 500 µM, and the total reaction volume was 2 ml. The absorbance values in Figure 4.5 display variations in response to different temperatures, indicating the temperature-dependent nature of

the catalytic activity of TPP and FeTOMPP. The catalytic activity of TPP and FeTOMPP is temperature-dependent, and their peroxidase-like activity is maximized within a specific temperature range, leading to the highest absorbance. Determining the optimal temperature is crucial as it ensures the maximum catalytic activity and reliability of TPP and FeTOMPP in the presence of $H_2O_2$.
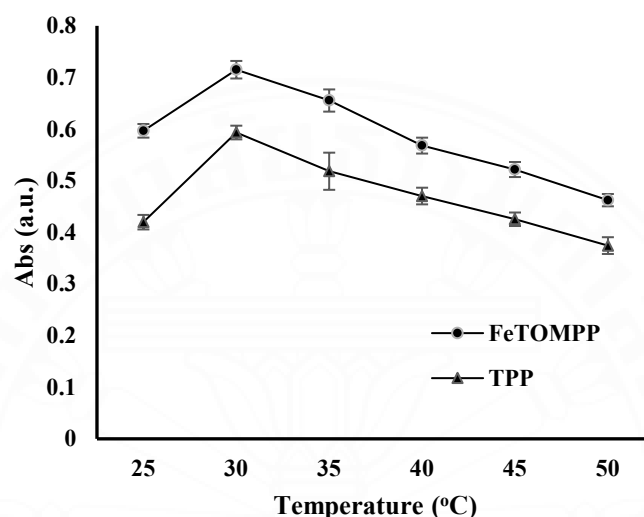


**Figure 4.5** Effect of optimum temperature on the absorbance of oxTMB at 652 nm

Figure 4.5 demonstrate a positive correlation between temperature and absorbance, indicating an increase in catalytic activity with rising temperatures until reaching the maximum point at 30 °C. However, beyond 30 °C, there is a noticeable decrease in absorbance, which can be attributed to the denaturation or degradation of TPP and FeTOMPP. It is important to note that the optimum temperature of TPP and FeTOMPP, determined to be 30 °C, is lower than the reported optimum temperature of HRP, which was found to be 40 °C (Chattopadhyay & Mazumdar, 2000). This result suggests that TPP and FeTOMPP exhibit their highest catalytic efficiency at a relatively lower temperature compared to HRP. These findings highlight the unique characteristics and thermal properties of TPP and FeTOMPP compared to HRP. The differences in their structures and chemical compositions may contribute to the variation in their optimum temperatures for catalytic activity.

**Table 4.2** The optimum conditions of FeTOMPP and TPP

|  | FeTOMPP | TPP |
|---|---|---|
| Amount | 35 µg/ml | 50 µg/ml |
| pH | 6 | 6 |
| Temperature | 30 ºC | 30 ºC |

Figure 4.3-4.5 present the experimental outcomes for TPP and FeTOMPP, illustrating the ideal concentrations, pH levels, and temperatures that yield the highest catalytic activity in the reaction. The highest absorbance values were observed at concentrations of 35 µg/ml for FeTOMPP and 50 µg/ml for TPP, pH 6, and a temperature of 30 °C. These optimal conditions are summarized in Table 4.2. Hence, for subsequent analysis of TPP and FeTOMPP catalytic activity, the standard conditions of pH 6 and 30 °C were adopted. Notably, the catalytic activity of both TPP and FeTOMPP was markedly enhanced in slightly acidic conditions compared to neutral conditions. This indicates that the oxidation reaction of TMB is more favorable under slightly acidic conditions, as observed in other synthesized porphyrins (Fenefen *et al.*, 2016; Liu *et al.*, 2014; Liu *et al.*, 2015) and the enzyme HRP (Josephy *et al.*, 1982).

### 4.2.3 Comparison of the peroxidase-like activity between TPP and FeTOMPP

To assess and contrast the peroxidase-like activity of TPP and FeTOMPP, varying concentrations of $H_2O_2$ were introduced to the reaction mixture containing optimal amounts of TPP (50 µg/ml) and FeTOMPP (35 µg/ml). The oxidation of TMB was then monitored to assess the catalytic performance of the compounds (ranging from 100 to 1000 µM). As depicted in Figure 4.6, the TPP-TMB-$H_2O_2$ and FeTOMPP-TMB-$H_2O_2$ solutions demonstrated a concentration-dependent increase in the oxidation state, indicating the conversion of TMB into oxTMB with the increasing $H_2O_2$ concentration. This progression was accompanied by a corresponding rise in UV-Vis absorbance at 652 nm
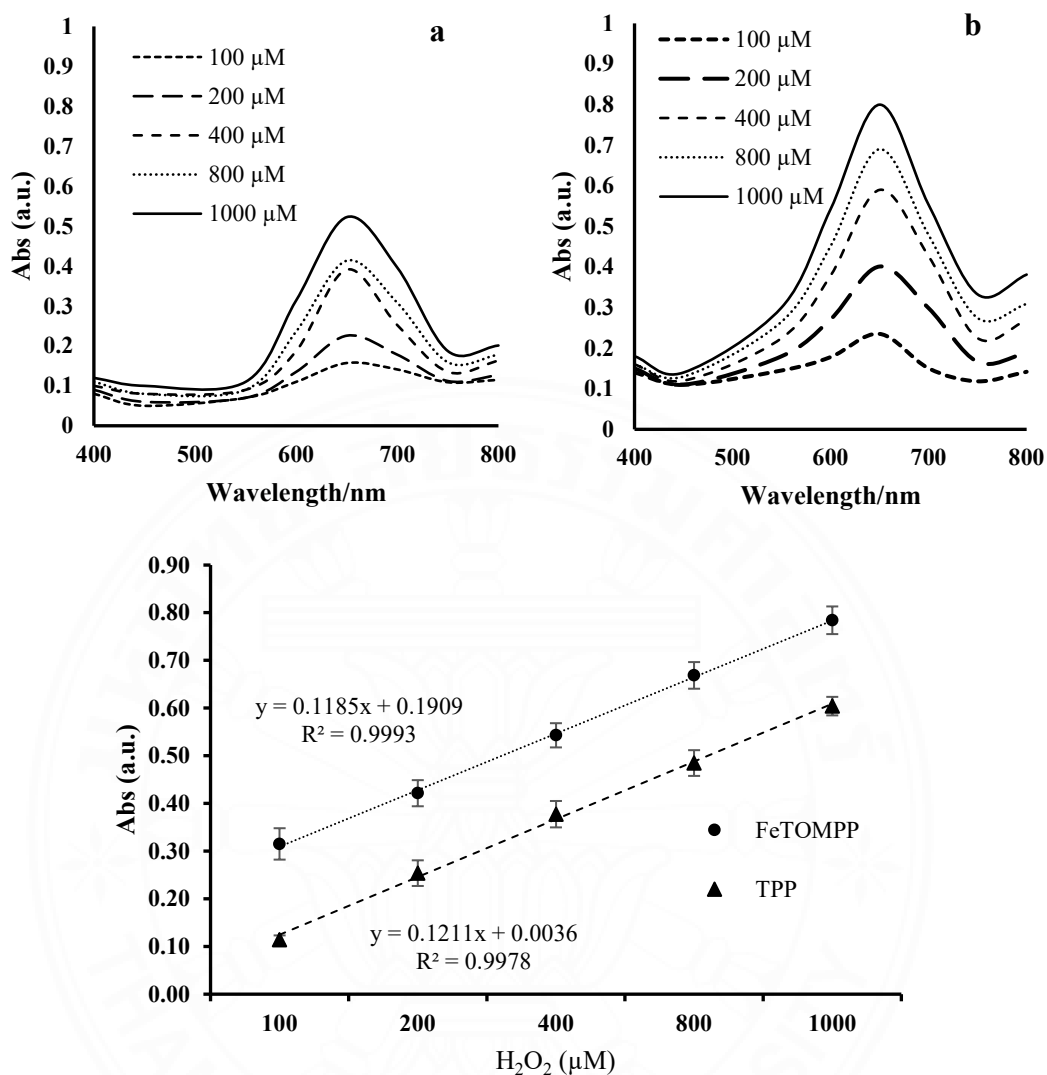
**Figure 4.6** UV-Vis spectra (a) TPP-TMB-$H_2O_2$ (b) FeTOMPP-TMB-$H_2O_2$ and (c) Peroxidase-like activity of TPP and FeTOMPP at varying $H_2O_2$ concentrations detected by absorption of oxTMB at 652 nm

Interestingly, it was observed that the UV-Vis absorbance in the TPP-TMB-$H_2O_2$ solution was consistently lower than that in the FeTOMPP-TMB-$H_2O_2$ solution, even with the increasing concentration of $H_2O_2$. This difference in absorbance suggests that FeTOMPP exhibited higher peroxidase-like activity compared to TPP, resulting in a more efficient oxidation of TMB into oxTMB. In Figure 4.6, a regression equation is depicted as $y = aX + b$, where 'a' represents the slope of the straight line, and 'b' represents the point of intersection with the vertical axis. The

sensitivity of the biosensor is determined by the slope of this linear region. A higher 'a' value indicates superior sensitivity performance of the biosensor (Prabowo *et al.*, 2021). Interestingly, based on the regression equation, FeTOMPP exhibited a higher sensitivity at 0.118 µM compared to TPP at 0.1211 µM.

These findings highlight the enhanced catalytic performance of FeTOMPP and its potential as a peroxidase mimic in oxidative reactions. The results clearly demonstrated that FeTOMPP exhibited a higher peroxidase-like activity compared with TPP. Based on this finding, FeTOMPP was selected for further investigation and analysis in subsequent studies.

## 4.3 Detection of $H_2O_2$

As shown in Figure 4.7, the UV-Vis absorbance at 652 nm exhibited a linear increase with the increasing concentration of $H_2O_2$ in the presence of FeTOMPP. With the increasing concentration of $H_2O_2$, a noticeable change in color was observed as the solution gradually transitioned to a blue color. The Figure 4.7 illustrates the calibration curve, which shows the relationship between the UV-Vis absorbance at 652 nm and $H_2O_2$ concentrations ranging from 1 to 100 µM. The color changes observed during the TMB oxidation catalyzed by FeTOMPP were found to be dependent on the concentration of $H_2O_2$. The absorbance at 652 nm exhibited a linear relationship with $H_2O_2$ concentrations ranging from 1 to 100 µM. The detection limit of the assay was determined to be 2.4 µM. The absorbance at 652 nm (Y) displayed a linear correlation with the concentration of $H_2O_2$ (X) in µM, as depicted by the calibration curve (Figure 4.7). The equation describing this relationship was determined to be Y = 0.0013 + 0.0022X, with a high linear correlation coefficient (R) of 0.997. Notably, the detection limit of 2.4 µM was lower than that reported in many other $H_2O_2$ sensors (Lu *et al.*, 2011; Li *et al.*, 2015; Zhang *et al.*, 2015). Moreover, the linear range of the FeTOMPP sensor demonstrated a wider range compared to the limited ranges reported in certain previous studies (Zhang *et al.*, 2015; Dong *et al.*, 2012; Hao *et al.*, 2013; Zhang *et al.*, 2014; Kuswandi *et al.*, 2014). These findings emphasize the significant promise of FeTOMPP as a highly sensitive and efficient sensor for $H_2O_2$ detection. With its

exceptional detection limit and wide dynamic range, demonstrate that the FeTOMPP reveals sensor $H_2O_2$ potential candidate for various applications.
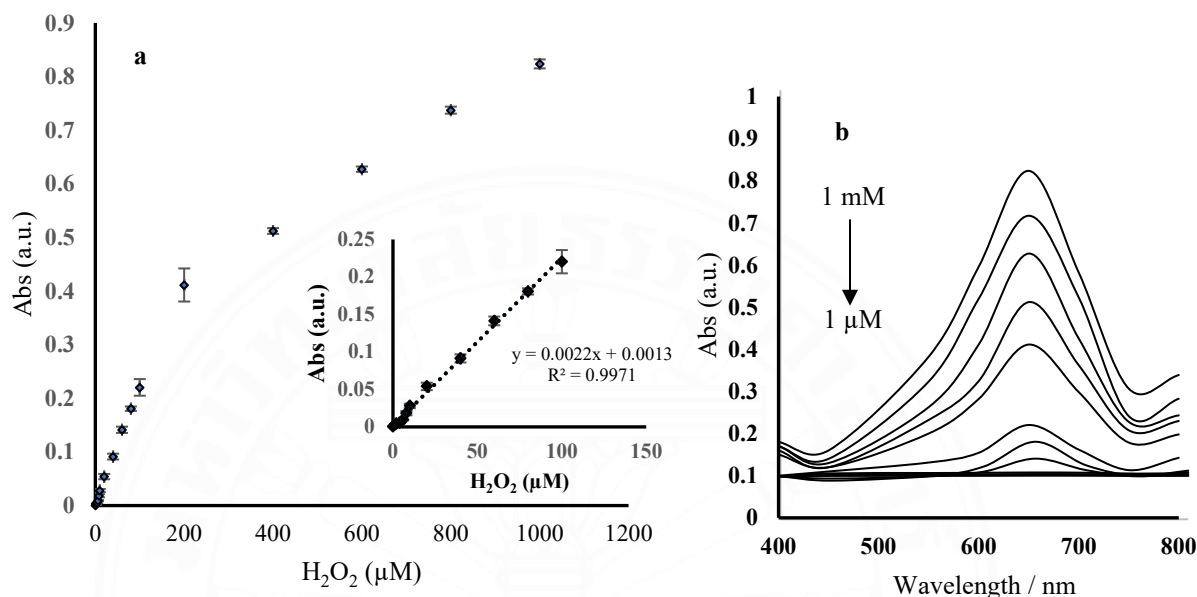


**Figure 4.7 a**) Linear calibration plot and the linear range **b)** UV-Vis absorption spectra of oxTMB in the presence of FeTOMPP at various concentrations of $H_2O_2$ (1.0 µM to 1.0 mM) detected by absorption of oxTMB at 652 nm

### 4.3.1 Steady-state kinetic assays

The catalytic behavior of FeTOMPP was investigated using enzyme kinetics theory and experimental methods. This analysis focused on studying its ability to catalyze the oxidation reaction of TMB by $H_2O_2$, providing valuable insights into the reaction kinetics and catalytic properties of FeTOMPP. The Michaelis-Menten equation ($v = VmaxS/(Km + S)$) was employed to establish the relationship between the initial rate of the catalytic reaction (v) and the substrate concentration (S) (Akins & Paula, 2006). The Michaelis constant (Km) characterizes the binding affinity between the enzyme and its substrate. A comprehensive set of experiments was performed to investigate the kinetic parameters and elucidate the catalytic mechanism. In these experiments, the concentration of one substrate was systematically varied while maintaining a constant concentration of the other substrate. The Lineweaver-Burk plots

were utilized to analyze the catalytic efficiency and substrate affinity of FeTOMPP for $H_2O_2$ and TMB as showed in Figure 4.8. By determining the values of the maximum initial velocity (Vmax) and the Michaelis-Menten constant (Km), valuable insights into the enzymatic activity and substrate binding characteristics of FeTOMPP could be obtained. The results, presented in Table 4.3, provide comprehensive information on the kinetic parameters of FeTOMPP and its interactions with $H_2O_2$ and TMB. This analysis contributes to a better understanding of the enzyme's kinetic behavior.
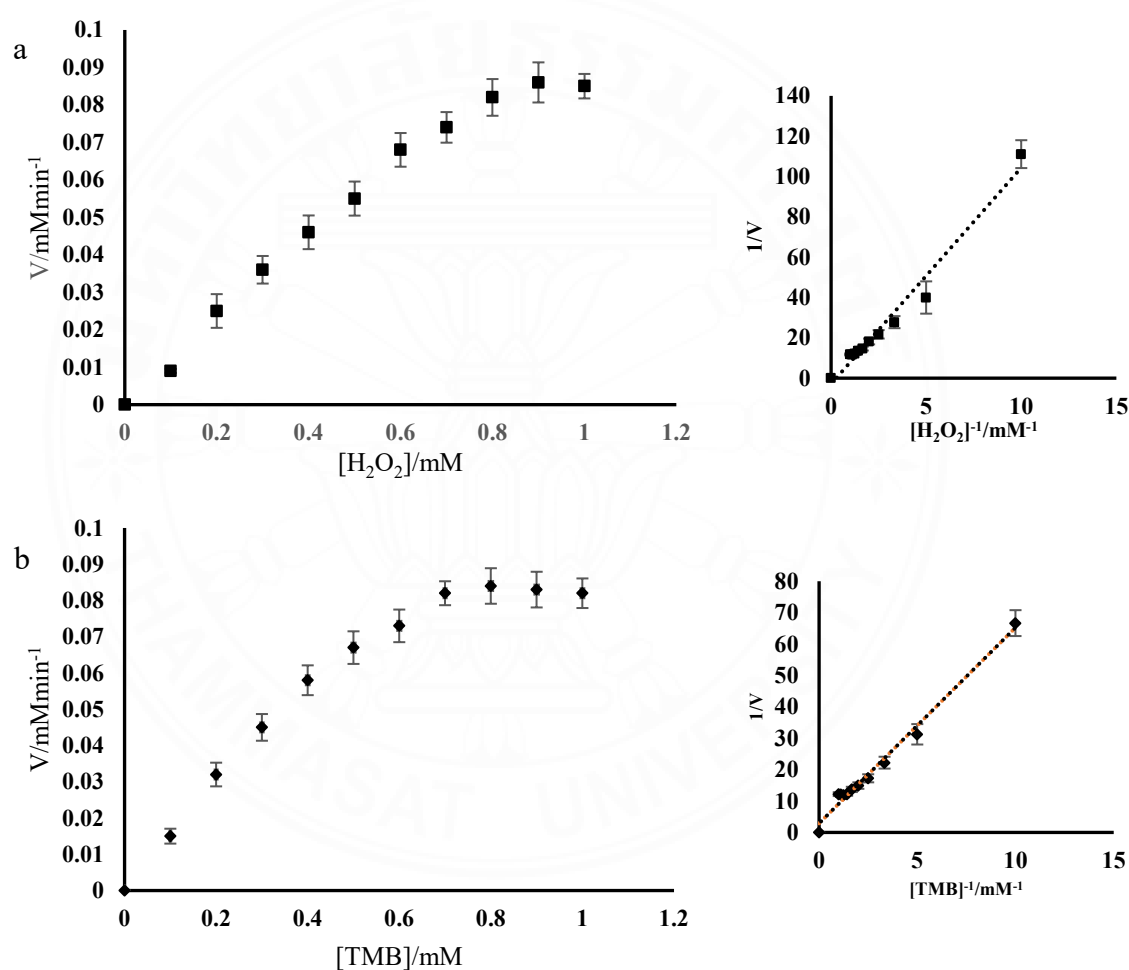


**Figure 4.8** Steady-state kinetic analysis of FeTOMPP. a) Variation of TMB concentration at a fixed $H_2O_2$ concentration of 400 μM. b) Variation of $H_2O_2$ concentration at a fixed TMB concentration of 500 μM

**Table 4.3** Kinetic Parameters for FeTOMPP Catalysis

| Catalyst | $Vm[10^{-8}Ms^{-1}]$ | | $Km[mM]$ | |
|---|---|---|---|---|
| | TMB | $H_2O_2$ | TMB | $H_2O_2$ |
| FeTOMPP | 0.278 | 8.54 | 3.74 | 2.15 |
| HRP | 0.434 | 3.70 | 13.08 | 5.31 |

The Michaelis constant (Km) serves as an indication of the enzyme's affinity for substrates, with a smaller Km value indicating a stronger affinity. In Table 4.3, the data reveals that FeTOMPP exhibited a smaller Km value (2.15 mM) for $H_2O_2$ and a larger Km value (3.74 mM) for TMB compared to HRP (Zhao *et al.*, 2015). These findings suggest that FeTOMPP has a higher affinity for $H_2O_2$, indicating a strong binding between the enzyme and $H_2O_2$. Conversely, the larger Km value for TMB suggests a weaker affinity between FeTOMPP and TMB in comparison to HRP. The smaller Km value for $H_2O_2$ also suggests that FeTOMPP exhibits a more efficient catalytic activity towards $H_2O_2$ compared to HRP. Furthermore, the maximum initial velocity (Vm) of FeTOMPP for both $H_2O_2$ and TMB, as shown in Table 4.3, is larger than that of HRP for the same substrates. These results further support the notion of an enhanced catalytic activity of FeTOMPP in comparison to HRP.

### 4.3.2 Stability test of the FeTOMPP/TMB system

The long-term stability of the biosensor is a critical aspect for its practical application. Therefore, the storage stability of the system was carefully assessed for a duration of 15 days in this study. The stock solution, comprising of FeTOMPP, 0.1 mM NaOAc buffer (pH 6.0), and 500 μM TMB, was stored at room temperature under light-free conditions. The pH of the solution was monitored daily and before each test to ensure consistency.

To assess the stability of the FeTOMPP/TMB system, TMB-$H_2O_2$ reactions were performed using the stock solution stored for different durations (0-15 days) as the catalyst, with a constant $H_2O_2$ concentration of 1 mM. The concentration of the oxidized TMB was determined by measuring the UV-Vis absorption at 652 nm.

The decrease in absorbance from day 1 to day 15 was calculated to be 3.57%. The results indicated that the absorbance at 652 nm showed minimal variation during the 15-day storage period, with variations of less than 5% as depicted

in Figure 4.9. Moreover, the pH of the stock solution was assessed and found to exhibit minimal changes from day 1 to day 15, as shown in Figure 4.10. These findings indicate that the FeTOMPP-TMB system maintained its stability over the testing period, suggesting its potential for reliable and long-term applications. The stability test of the colorimetric sensor in the Cu-hemin metal-organic framework (MOFs)-TMB-H2O2 system, which was stored for 15 days, revealed that the response of the system remained nearly constant (Liu *et al*., 2016).
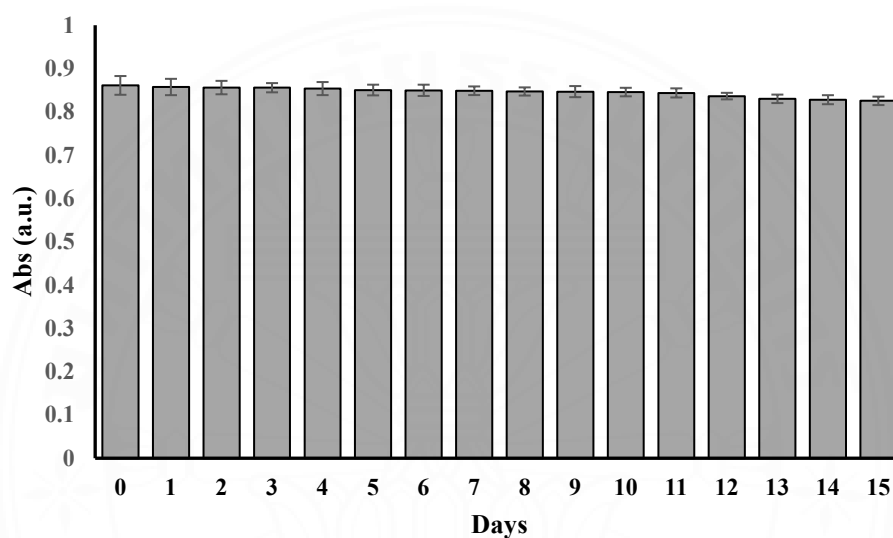


**Figure 4.9** Absorbance at 652 nm of FeTOMPP-TMB stored for different days as a catalyst ($H_2O_2$ concentration: 1 mM)
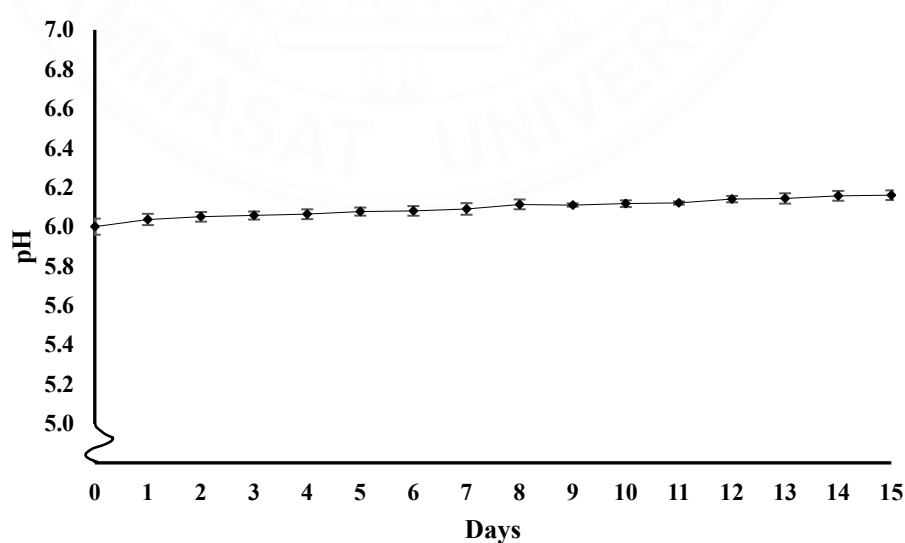


**Figure 4.10** The pH of FeTOMPP-TMB stock solution stored for different days

The oxidation reaction of TMB is known to be more favorable under slightly acidic conditions, and it has been observed that FeTOMPP exhibits enhanced catalytic activity in this pH range. Therefore, the pH of the system is an important factor to consider. Figure 4.11 displays the pH variations during the stability test, and it can be observed that the pH of the solution remains relatively stable, with minimal changes of less than 5% throughout the duration of the test. Over time, there is a slight increase in pH, which may have a small impact on the optimum conditions for the system and result in a slight decrease in the absorbance values. However, considering the overall stability of the FeTOMPP-TMB system, these changes are minimal and do not significantly affect its performance. The results demonstrate the good stability of the colorimetric sensor, indicating its reliability for practical applications.

## 4.4 Detection of ethanol

By combining the catalytic reaction of AOX with the TMB-$H_2O_2$ colorimetric reaction, a reliable method for ethanol detection can be established. Ethanol is oxidized by AOX to produce $H_2O_2$ as the main product. This $H_2O_2$ can then participate in the TMB-$H_2O_2$ catalytic color reaction, resulting in a color change. The concentration of ethanol can be quantified by analyzing the absorbance of the reaction mixture. This colorimetric method provides a simple and efficient way to detect ethanol, utilizing the same chromogenic substrate TMB and the catalytic activity of AOX and $H_2O_2$.

The enzyme AOX facilitates the conversion of ethanol to aldehyde while simultaneously reducing molecular $O_2$ to $H_2O_2$. To quantify the ethanol concentration, 10 µl of AOX was added to 0.1 M phosphate buffer solutions (PBS, pH 7.0) containing various ethanol concentrations. The mixture was incubated at 30 °C for 20 minutes. Following the incubation period, the solution obtained from the ethanol reaction was combined with a 0.1 mM NaOAc buffer with a pH of 6.0. To this solution, 500 µM of TMB and a stock solution of FeTOMPP were added, resulting in a final volume of 2 ml. The resulting solution was further incubated at 30 oC before UV-Vis measurements. As depicted in Figure 4.11, the absorbance at 652 nm exhibited a linear increase within a certain range of ethanol concentrations (0-15% v/v). The correlation between the

absorbance and ethanol concentration was found to be linear, demonstrating a direct relationship. From the linear equation, this biosensor exhibited a detection limit of 0.0524% (v/v) and sensitivity at 0.0535% (v/v).
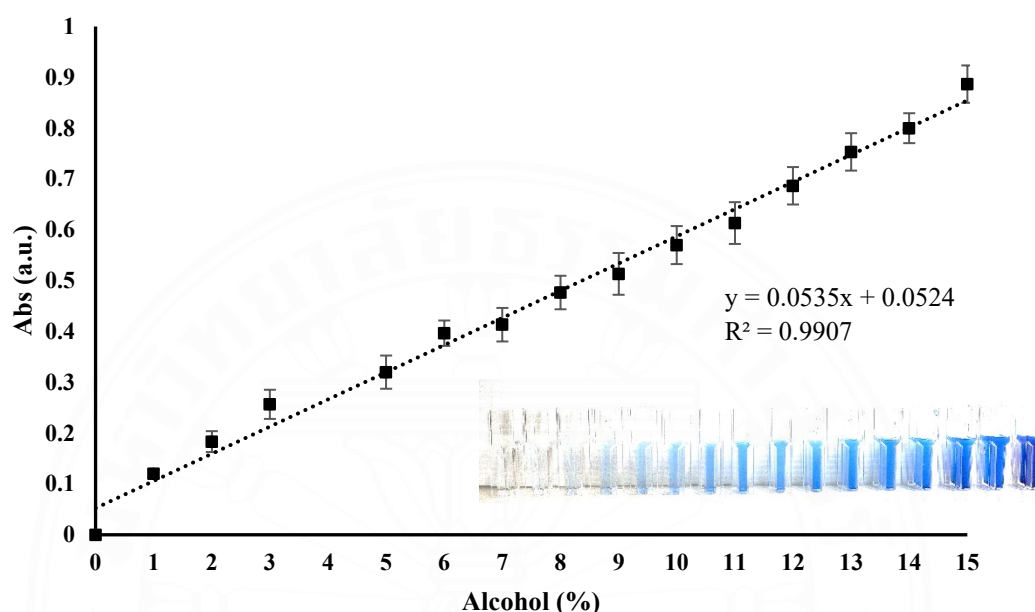


**Figure 4.11** Linear relationship between absorbance (652 nm) and ethanol concentration (0-15% v/v) in the presence of AOX/TMB/FeTOMPP

### 4.4.1 Stability and reproducibility test of the AOX/TMB/FeTOMPP system

The storage stability of the system was tested for a duration of 15 days. The stock solution I, comprising of AOX in 0.1 M PBS was stored at 4 °C. The stock solution II, comprising of FeTOMPP, 0.1 mM NaOAc buffer (pH 6.0), and 500 μM TMB, was stored at room temperature under light-free conditions. The pH of the stock solution 2 was monitored daily and before each test to ensure consistency.

To assess the stability of the biosensor, the reactions were performed using the stock solution I and II stored for different durations (0-15 days), with a constant ethanol concentration of 5% (v/v). The concentration of the oxidized TMB was determined by measuring the UV-Vis absorption at 652 nm. After 15 days, the biosensor response decrease by only 1.23% and could retain 98.77% of the original

value. The results indicated that the absorbance at 652 nm showed minimal variation during the 15-day storage period, with variations of less than 5% as depicted in Figure 4.12.
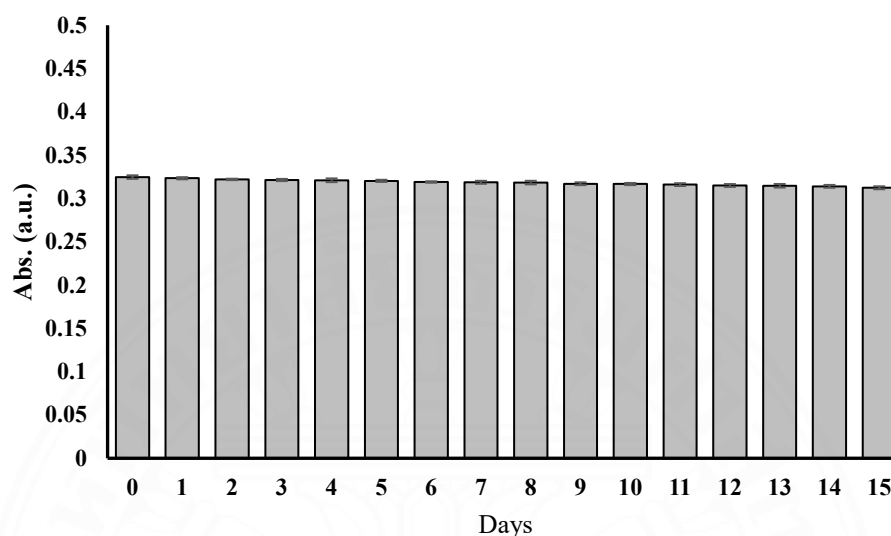


**Figure 4.12** Absorbance at 652 nm of AOX/TMB/FeTOMPP stored for different days

The system's reproducibility was assessed with the introduction of 5% v/v ethanol. Eight separate AOX/TMB/FeTOMPP systems were prepared for the evaluation. The measurements of the differences in absorbance at 652 nm from these eight systems resulted in a reproducibility RSD (Relative Standard Deviation) value of 2.43% (Figure 4.13). This low RSD value indicates a high level of reproducibility and reliability in the system.
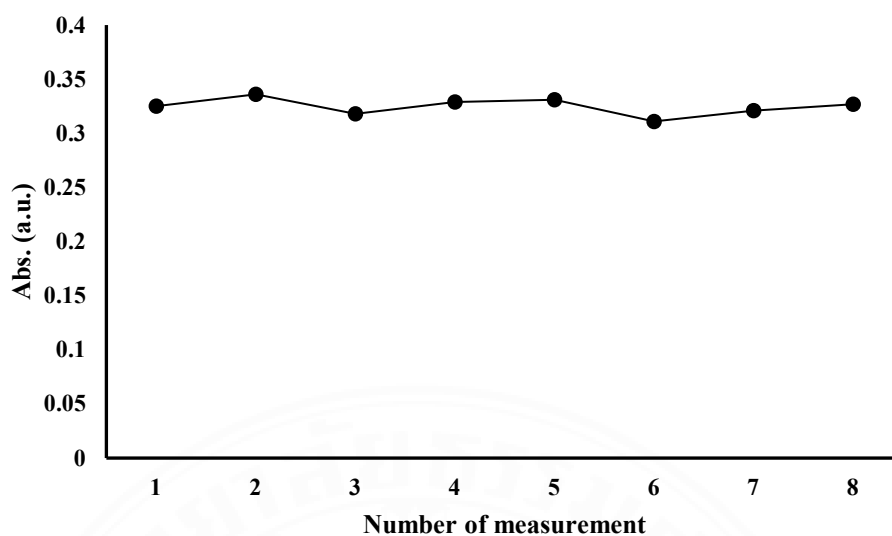
**Figure 4.13** The reproducibility of AOX/TMB/FeTOMPP system toward 5% v/v of ethanol (absorbance at 652 nm)

### 4.4.2 Interferences measurement

In their study, Luangkhlapho *et al.* (2013) analyzed Sato, a traditional alcoholic beverage, and identified several organic acids including citric acid, succinic acid, lactic acid, acetic acid, and glycerol. The presence of these organic acids is a result of the fermentation process using different sources of Loogpang (Luangkhlayoho *et al.*, 2014). Likewise, wine products are known to contain various organic acids such as tartaric acid, malic acid, citric acid, succinic acid, lactic acid, and acetic acid (Chidi *et al.*, 2018). Tartaric acid and malic acid are naturally present in fruits like apples and grapes (Volschenk *et al.*, 2006; Krueger, 2012). Citric acid, which serves as an important intermediate in the tricarboxylic acid (TCA) cycle, is naturally found and widely distributed in various sources. In contrast, succinic acid, lactic acid, and acetic acid are organic acids that are typically produced as byproducts during the fermentation process (Chidi *et al.*, 2018). The colorimetric system's response was evaluated for potential interferences by examining various organic acids, including succinic acid, ascorbic acid, acetic acid, lactic acid, malic acid, oxalic acid, citric acid, tartaric acid, and sodium sulfite. The effects of these organic acids on the color change of the system were assessed, and the results are summarized in Table 4.4. This analysis provides

important information regarding the potential influence of these organic acids on the colorimetric response of the system.

**Table 4.4** Interference of selected compounds on ethanol response of biosensors at a 2:1 interference ratio (2% v/v) to ethanol (1% v/v)

| Compounds | Abs. of 1% (v/v) ethanol | Abs. of the mixture | Response of Biosensor (%) |
|---|---|---|---|
| Succinic acid | 0.106 | 0.1033 | 97.5±0.408 |
| Ascorbic acid | 0.105 | 0.1050 | 99±0.624 |
| Acetic acid | 0.105 | 0.1044 | 98.5±0.408 |
| Lactic acid | 0.106 | 0.1049 | 99±0.408 |
| Malic acid | 0.105 | 0.1028 | 97±0.816 |
| Oxalic acid | 0.106 | 0.1049 | 99±0.624 |
| Citric acid | 0.106 | 0.1017 | 96±0.624 |
| Tartaric acid | 0.106 | 0.1023 | 96.5±0.408 |
| Sodium sulphite | 0.105 | 0.1043 | 98.5±0.408 |

According to the data provided in Table 4.4, it was noted that the presence of organic acids and sodium sulfite caused a slight decrease in the sensor response to ethanol. The small interference can be attributed to the oxidation of these interferents, which may affect the activity of alcohol oxidase (AOX), the enzyme responsible for catalyzing the oxidation of ethanol. However, the level of interference was found to be minimal, with the sensor response being reduced by less than 5%. These findings suggest that the presence of organic acids and sodium sulfite may have a minor impact on the accuracy of ethanol detection using the sensor.

Organic acids, being easily oxidizable compounds, can potentially interfere with the performance of biosensors designed for ethanol detection. The reaction between these organic acids and oxygen can lead to a decrease in the current of amperometric biosensors (Fumio *et al.*, 2001). In a study conducted by Wen *et al.* (2013), the interference of organic acids on ethanol biosensors based on bacteria was investigated. The researchers examined the decrease in oxygen levels and calculated its equivalence to ethanol concentration. The findings of the study indicated that the tested

interferents exhibited negligible or minimal interference on the performance of the ethanol biosensor (Wen *et al.*, 2013).

The results for ethanol detection in colored solutions have been summarized in Table 4.5. There was a slight interference observed in the biosensor response, which can be attributed to the presence of colored compounds in the samples. To mitigate this interference, a dilution step (1:10) in a phosphate buffer with a pH of 7 (0.1 M) was included as part of the sample treatment process. As a result, the impact of colored sample effects could be reduced to a level well within the acceptable range of interferences, specifically less than 5%.

**Table 4.5** Interference of colored solution; in the presence of 1% (v/v) ethanol, on the response to ethanol of biosensor.

| Compound | Response of the Biosensor (%) |
|---|---|
| Orange Juice | 98 |
| Grape Juice | 104 |
| Apple Juice | 99 |
| Red Wine | 103.5 |

### 4.4.3 Ethanol analysis in beverage samples

The biosensor that was developed in this study was utilized to accurately quantify the concentration of ethanol in various types of alcoholic beverages. The samples obtained from the market were subjected to a simple pretreatment step, which involved diluting each sample with a 0.1 M phosphate buffer at pH 7. This dilution step served two purposes: it ensured that the samples fell within the optimal range for the biosensor's detection capability and minimized any potential interference from other components present in the samples. The ethanol content of each fermented beverage sample was then measured using the biosensor, and the results were compiled and presented in Table 4.5. To assess the accuracy of the biosensor, the obtained ethanol values were compared with those provided by the beverage producers and other references using the gas chromatography method. This comparative analysis enabled the assessment of the biosensor's accuracy and reliability in measuring the concentration of ethanol across various alcoholic beverages.

The comparison of ethanol content in different alcoholic beverages using both gas chromatography (GC) and the developed biosensor revealed a strong agreement, with ethanol values differing by less than 5%. The high agreement between the results obtained from the biosensor and gas chromatography methods suggests that the biosensor is a reliable and accurate tool for analyzing ethanol in fermented beverages. The biosensor presents an attractive alternative to conventional analytical methods, offering the advantage of rapid and on-site analysis for determining ethanol content in different types of alcoholic beverages. Its convenience and accuracy make it a valuable tool in the field of beverage analysis and quality control.

**Table 4.6** Determination of ethanol in fermented beverage samples using porphyrin biosensor comparing with GC Analysis

| Beverage | Ethanol (%v/v) | | |
| Samples | Value declared by the producer | GC | Biosensor |
| --- | --- | --- | --- |
| Beer 1 | 6.4 | 6.33±0.03 | 6.09±0.09 |
| Beer 2 | 5.5 | 5.45±0.16 | 5.28±0.12 |
| Beer 3 | 5.0 | 5.10±0.10 | 4.90±0.09 |
| Beer 4 | 5.0 | 5.14±0.07 | 4.95±0.04 |
| Sato 1 | - | 11.03±0.45 | 10.47±0.12 |
| Sato 2 | - | 7.12±0.10 | 6.70±0.16 |
| Sato 3 | 6.5 | 6.47±0.25 | 6.27±0.21 |
| Krachae | - | 9.07±0.17 | 8.73±0.17 |
| Soju 1 | 13 | 12.77±0.21 | 12.20±0.16 |
| Soju 2 | 14 | 14.03±0.21 | 13.47±0.21 |
| Wine 1 | 5 | 4.87±0.12 | 4.67±0.12 |
| Wine 2 | 5 | 4.73±0.12 | 4.47±0.12 |
| Wine 3 | 11.5 | 11.43±0.17 | 11.03±0.17 |
| Liquor 1 | 40 | 41.49±0.11 | 39.97±0.37 |
| Liquor 2 | 40 | 39.28±0.16 | 38.97±0.21 |

Table 4.6 displays the analytical findings of different commercially available alcoholic beverages, showcasing a comparison between the results obtained using the biosensor method and those obtained using gas chromatography. The comparison revealed no substantial disparities between the two methods, underscoring the precision of the biosensor in measuring ethanol content. To further assess the reliability of the biosensor method, recovery studies were conducted by spiking ethanol samples with a known amount of ethanol (1.5%) and then measuring the ethanol content using the biosensor. The percentage of recovery was ranging from 96% to 98.66%. The results, as depicted in Table 4.7, clearly indicate the biosensor's precise detection of added ethanol, thereby establishing its reliability and accuracy. These results emphasize the excellent accuracy and precision of the biosensor in measuring ethanol concentrations in real samples, offering a reliable and robust alternative to traditional analytical methods.

**Table 4.7** Recovery studies of ethanol in real Samples using a porphyrin biosensor.

| Sample | Ethanol concentration determine by the biosensor (% v/v) | Concentration of ethanol (% v/v) | | Recovery (%) |
|--------|--------|--------|--------|--------|
| | | Added | Found | |
| Beer 1 | 6.10 | 1.5 | 7.56 | 97.33 |
| Sato 1 | 10.50 | 1.5 | 11.98 | 98.66 |
| Soju 1 | 12.2 | 1.5 | 13.64 | 96 |
| Wine 1 | 4.65 | 1.5 | 6.12 | 98 |

# CHAPTER 5
# CONCLUSIONS

The peroxidase-like activity of porphyrin and metalloporphyrins was assessed by studying their ability to catalyze the oxidation reaction of TMB in the presence of $H_2O_2$. This reaction resulted in the production of a blue intermediate product, characterized by a strong absorption peak at 652 nm. Notably, both TPP and FeTOMPP demonstrated peroxidase-like activity, effectively catalyzing the oxidation of TMB and leading to the formation of the blue colored product. The optimal experimental conditions for TPP and FeTOMPP were determined, including the optimal amounts, pH levels, and temperatures. TPP displayed optimal activity at an amount of 50 µg/ml, a pH of 6, and a temperature of 30 °C, while FeTOMPP demonstrated optimal activity 35 µg/ml, a pH of 6, and a temperature of 30°C. A comparison between TPP and FeTOMPP revealed that FeTOMPP exhibited higher peroxidase-like activity. The absorbance at 652 nm exhibited a direct correlation with the concentration of $H_2O_2$, indicating that FeTOMPP can be employed for the quantitative determination of $H_2O_2$ in the presence of TMB. The system exhibited a detection limit of 2.4 µM, indicating its sensitivity for the detection of $H_2O_2$. The kinetic analysis using Lineweaver-Burk plots demonstrated that FeTOMPP exhibited a higher affinity for $H_2O_2$ compared to TMB, as indicated by the values of maximum initial velocity (Vmax) and Michaelis-Menten constant (Km). The stability of the system was assessed by storing the FeTOMPP stock solution under controlled conditions for various durations (0-15 days). The results showed that the absorbance at 652 nm exhibited minimal changes (less than 5% variation) over the course of the study, indicating the excellent stability of the colorimetric sensor.

The combination of FeTOMPP and TMB can be employed to accurately quantify the concentration of $H_2O_2$. In the presence of oxygen, ethanol can undergo catalytic conversion by alcohol oxidase, resulting in the production of aldehyde and the reduction of oxygen to $H_2O_2$. The absorbance-concentration relationship for ethanol was found to be linear within the range of 0-15 % v/v, with a detection limit of 0.0524 % v/v. The interference study revealed minimal interference when organic acids and

sodium sulfite were present, resulting in a slight decrease in the sensor response to ethanol (less than 5 %). The decline in sensor response can be ascribed to the oxidation of interfering substances, which can influence the activity of alcohol oxidase.

The biosensor that was developed was utilized for the analysis of diverse alcoholic beverages, such as beer, wine, Sato, and Krachae. To assess the precision of the biosensor, its findings were compared with the data provided by the beverage manufacturers as well as the results obtained from the gas chromatography technique. The analysis demonstrated a high level of agreement between the ethanol values obtained from the biosensor and those obtained by gas chromatography data, with differences of less than 5 %. This indicates that the biosensor can be considered reliable for the analysis of ethanol in fermented beverage samples. Additionally, recovery tests were conducted by adding 1.5 % ethanol to selected samples, and the amount of added ethanol was determined using the proposed ethanol biosensor. The results of the analyses and recovery tests unequivocally support the biosensor's exceptional accuracy, precision, and reliability in the quantification of ethanol in real samples.
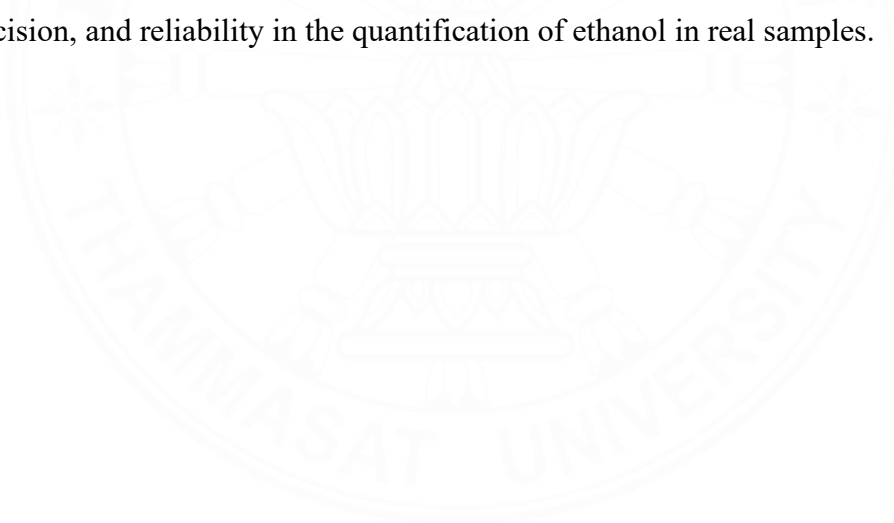
# REFERENCES

3,3',5,5'-Tetramethylbenzidin. (n.d.).
https://www.itwreagents.com/download_file/product_infos/A3840/en/A3840_en.pdf.

ABTS. (n.d.) In *Wikipedia.* http://en.wikipedia.org/wiki/ABTS.

Adams, E. C. (1988). Method of preparing a test strip for alcohol testing. Patent # 4 786 569, USA.

Adewale, I. O., & Adekunle, A. T. (2018). Biochemical properties of peroxidase from white and red cultivars of Kola nut (*Kola nitida). Biocatalysis and Agricultural Biotechnology, 14*, 1-9.

Akin, M., Yuksel, M., Geyik, C., Odaci, D., Bluma, A., Höpfner, T., Beutel, S., Scheper, T., & Timur, S. (2010). Alcohol biosensing by polyamidoamine (PAMAM)/cysteamine/alcohol oxidase-modified gold electrode. *Biotechnology progress*, *26*(3), 896–906.

Alonso-Castro, A. J., Zapata-Morales, J. R., Hernández-Munive, A., Campos-Xolalpa, N., Pérez-Gutiérrez, S., & Pérez-González, C. (2015). Synthesis, antinociceptive and anti-inflammatory effects of porphyrins. *Bioorganic & Medicinal Chemistry*, *23*(10), 2529-2537.

Azmi, N. E., Abdullah, J., Ahmad, M., Sidek, H., Heng, L. Y., & Rahman, S. A. (2012). An optical based biosensor for the determination of ammonium in aqueous environment. *American Journal of Analytical Chemistry. 3*(5), 364-370.

Antonelli, M. L., Spadaro, C., & Tornelli, R. F. (2008). A microcalorimetric sensor for food and cosmetic analyses: L-Malic acid determination. *Talanta, 74*(5), 1450-1454.

Arteaga, D., Cotta, R., Ortiz, A., Insuasty, B., Martin, N. & Echegoyen, L. (2015). Zn (II)-porphyrin dyes with several electron acceptor groups linked by vinyl-fluorene or vinyl-thiophene spacers for dye-sensitized solar cells. *Dyes Pigments, 112*, 127–137.

Atkins, P. & Paula, J. D. (2006). Elements of Physical Chemistry. Oxford University Press, Oxford, UK.

Awawdeh, A. M., & Harmon, H. J. (2005). Spectrophotometric detection of ~tachlorophenol (PCP) in water using immobilized water soluble porphyrins. *Biosensors & bioelectronics, 20*(80, 1595-1601.

Azevedo, A. M., Cabral, J. M. S., Gibson, T. D., & Fonseca, L. P. (2004). Operation and performance of analytical packed-bed reactors with an immobilised alcohol oxidase. *Journal of Molecular Catalysis B: Enzymatic*, *28*(2), 45-53.

Azevedo, A. M., Prazeres, D. M., Cabral, J. M., & Fonseca, L. P. (2005). Ethanol biosensors based on alcohol oxidase. *Biosensors & bioelectronics*, *21*(2), 235–247.

Bajju, G.D., Singh, N., & Deepmala (2014). Synthesis and characterization of new *Meso*-substituted and *β*-substituted unsymmetrical metalloporphyrins. *Journal of Chemical Sciences 120*(2), 259-266.

Bansal, N., & Kanwar, S.S. (2013). Peroxidase(s) in environment protection. *The scientific world journal, 2013*, 1-10.

Barman T. E. (1969). *Enzyme handbook*. Springer-Verlag New York.

Barzana, E., Klibanov, A. M., & Karel, M., (1989). A colorimetric method for the enzymatic analysis of gases: the determination of ethanol and formaldehyde vapors using solid alcohol oxidase. *Analytical Biochemistry, 182*(1), 109–115.

Battersby, A. R., Fookes, C. J., Matcham, G. W., & McDonald, E. (1980). Biosynthesis of the pigments of life: formation of the macrocycle. *Nature, 285*(5759), 17-21.

Beer (n.d.). In *Wikipedia.* http://en.wikipedia.org/wiki/Beer.

Beer (n.d.). In *Wikipedia.* http://en.wikipedia.org/wiki/Beer.

Bhalla, N., Jolly, P., Formisano, N., & Estrela, P. (2016). Introduction to biosensors. *Essays in Biochemistry, 60*(1), 1-8.

Bhand, S. G., Soundararajan, S., Surugiu-Wärnmark, I., Milea, JS., Dey, ES., Yakovleva, M., & Danielsson, B. (2010). Fructose-selective calorimetric biosensor in flow injection analysis. *Analytica chimica acta, 668*(1), 13-18.

Bhardwaj R., Majumder, S., Ajmera PK., Sinha, S., Sharma, R., Mukhiya, R. & Narang, P. (2017, August). Temperature compensation of ISFET based pH sensor using artificial neutral networks. IEEE Regional Symposium on Micro and Nanoelectronics (RSM), Malaysia.

Borgmann, S., Schulte, A., Neugebauer, S., & Schuhmann, W. (2011). *Advances in Electrochemical Science and Engineering*. WILEY-VCH Verlag GmbH & Co. KGaA, Weinheim ISBN: 978-3-527-32885-7.

Britanica, T. E. (2020). *Sake – Alcoholic Beverage*. Encyclopedia Britannica - https://www.britannica.com/topic/sake.

Britanica, T. E., (2023). *Alcoholic beverages*. http://www.britannica.com/topic/alcoholic-beverage.

Bucková, M., Labuda, J., Sandula, J., Krizková, L., Stepánek, I., & Duracková, Z. (2002). Detection of damage to DNA and antioxidative activity of yeast polysaccharides at the DNA-modified screen-printed electrode. *Talanta, 56*(5), 939-947.

Cabaleiro, N., de la Calle, I., Bendicho, C., & Lavilla, I. (2012). Enzymatic single-drop microextraction for the assay of ethanol in alcohol-free cosmetics using microvolume fluorospectrometry detection. *Analytica chemica acta, 733*, 28-33.

Carnes, E., & Wikins, E. (2005). The development of a new, rapid, amperometric immunosensor for the detection of low concentrations of bacteria part I: Design of the detection system and applications. *American Journal of Applied Sciences, 2*(3), 597-606.

Castillo, J., Gáspár, S., Leth, S., Niculescu, M., Mortari, A., Bontidean, I., Soukharev, V., Dorneanu, SA., Ryabov, AD., & Csöregi, E. (2004). Biosensors for life quality design, development, and applications. *Sensors & Actuators B. 102*(204), 179-194.

Cavinato, A. G., Mayes, D. M., Ge, Z. H., & Callis, J. B. (1990). Noninvasive method for monitoring ethanol in fermentation processes using fiber-optic near infrared spectroscopy. *Analytical chemistry, 62*(18), 1977-1982.

Chattopadhyay, K., & Mazumdar, S. (2000). Structural and conformational stability of horseradish peroxidase: effect of temperature and pH. *Biochemistry, 39*(1), 263-270.

Chaubey, A., & Malhotra, B. D. (2002). Mediated biosensors. *Biosensors & bioelectronics*, *17*(6-7), 441–456.

Chen, Y., Zhu, L., & Xiao, G. (2008). Ethanol sensing characteristics of ambient temperature sonochemically synthesized ZnO nanotubes. *Sensors & Actuators B: Chemical 129*(2), 639-642.

Chidi, B. S., Bauerr, F. F., & Rossouw, D. (2018). Organic acid metabolism and the impact of fermentation practices on wine acidity: A Review. *South African journal of enology and viticulture, 39*(2), 1-15.

Chlorophyll (n.d.). In *Wikipedia.* http://www.ch.ic.ac.uk/wiki/Chlorophyll.

Cook, D. J., Finnigan, J. D., Cook, K., Black, G. W. & Charnock, S. J. (2016). Cytochromes P450: History, classes, catalytic mechanism, and industrial application. *Advances in protein chemistry and structural biology, 105,* 105-126.

Cruulli A. (2021). Electrochemical biosensors in food safety: challenges and perspectives. *Molecules, 26*(2940).

Damborsk´y, P., Svitel, J. & Katrl´ık, J. (2017). Optical biosensors. *Essays in Biochemistry, 60,* 91-100.

D'Souza, S. F. (2001). Microbial biosensors. *Biosensors & bioelectronics, 16*(6), 337-353.

Dehghani, H. & Fathi, F. (2008). Molecular complexation of *meso*-tetraphenylporphyrins with $SO_2$. *Dyes and Pigments, 77*(2), 323–326.

Dong, Y., Zhang, H., Rahman, Z. U., Su, L., Chen, X., Hu, J., & Chen, X. (2012). Graphene oxide-$Fe_3O_4$ magnetic nanocomposites with peroxidase-like activity for colorimetric detection of glucose. *Nanoscale, 4*(130, 3969-3976.

Dragana, R., Nikola, G., Željko, D., Gordana, A., & Olgica, N. (2017). Separation of peroxidases from Miscanthus x giganteus, their partial characterisation and application for degradation of dyes. *Plant physiology and biochemistry : PPB*, *120*, 179–185.

Dunbar, A. D., Brittle, S., Richardson, T. H., Hutchinson, J. & Hunter, C. A. (2010). Detection of volatile organic compounds using porphyrin derivatives. *The journal of physical chemistry B, 114(*36), 11697–11702.

Dzyadevych, S. V., Soldatkin, A. P., El'skaya, A. V., Martelet, C., & Jaffrezic-Renauult, N. (2006). Enzyme biosensors based on ion-selective field-effect transistors. *Analytica chimica acta, 568*(1-2), 248-258.

Egea, T., Signorin M. A., Ongaro, L., Rivera, D., Obón de Castro, C., & Bruschi, P. (2016). Traditional alcoholic beverages and their value in the local culture of the Alta Valle del Reno, a mountain borderland between Tuscany and Emilia-Romagna (Italy). *Journal of ethnobiology and ethnomedicine, 12*(1), 1-20.

Ehrhart, J. C., Bennetau, B., Renaud, L., Madrange, J. P., Thomas, L., Morisot, J., Brosseau, A., Allano, S., Tauc, P., & Tran, PL. (2008). A new immunosensor for breast cancer cell detection using antibody-coated long alkylsilane self-assembled monolayers in a parallel plate flow chamber. *Biosensors & Bioelectronic, 24*(3), 467-474.

Enzyme (n.d.) In *Wikipedia.* http://en.wikipedia.org/wiki/Enzyme.

Fumio, M., Takahiro, S., & Seiichira, L. (2001). An interference-free, amperometric biosensor for acetic acid based on a tri-enzyme/polydimethylsiloxane-bilayer membrane. *Chemistry letters*, *30*(6), 556-557.

Fei, Q., Shan, H., Huan, Y., Zhang, Z., Mi, H., Xu, H., Li, G., Chen, F., & Feng, G. (2016). A novel copper (II) sensor based on a unique water-soluble porphyrin. *Analytical sciences, 32*(7), 745-749.

Ferancová, A., Bucková, M., Korgová, E., Korbut, O., Gründler, P., Wärnmark, I., Stepan, R., Barek, J., Zima, J., & Labuda, J. (2005). Association interaction and voltammetric determination of 1-aminopyrene and 1-hydroxypyrene at cyclodextrin and DNA based electrochemical sensors. *Bioelectrochemistry, 67*(2), 191-197.

Galandová, J., Ovádeková, R., Fernacová, A., & Labuda, J. (2009). Disposable DNA biosensor with the carbon nanotubes-polyethyleneimine interface at a screen-printed carbon electrode for tests of DNA layer damage by quinazolines. *Analytical and Bioanalytical Chemistry, 394*(3), 855-861.

Gao, L., Zhuang, J., Nie, L., Zhang, J., Zhang, Y., Gu, N., Wang, T., Feng, J., Yang, D., Perrett, S., & Yan, X. (2007). Intrinsic peroxidase-like activity of ferromagnetic nanoparticles. *Nature nanotechnology*, *2*(9), 577–583.

Gonchar, M. V., Maidan, M. M., Pavlishko, H. M., & Sibirny, A. A., (2001). A new oxidase–peroxidase kit for ethanol assays in alcoholic beverages. *Food Technology & Biotechnology, 39* (1), 37–42.

Goswami, P., Chinnadayyala, S.S.R., Chakraborty, M., Kumar, A.K. & Katoki, A. (2013). An overview on alcohol oxidases and their potential applications. *Applied Microbiology and Biotechnology, 97,* 4259-4275.

Groves, J. T. & Kruper, W. J. (1985). Metalloporphyrins in oxidative catalysis. oxygen transfer reactions of oxochromium porphyrins. *Israel Journal of Chemistry, 25*(2), 148-154.

Gui, Q., Lawson, T., Shan, S., Yan, L., & Liu, Y. (2017). The Application of Whole Cell-Based Biosensors for Use in Environmental Analysis and in Medical Diagnostics. *Sensors (Basel, Seitzerland)*, *17*(7), 1623.

Gvozdev, A. R., Tukhvatullin, I. A., & Gvozdev, R. I. (2010). Purification and properties of alcohol oxidase from *Pichia putida. Biochemistry (Moscow), 75*(2), 242-248.

Hao, J., Zhang, Z., Yang, W., Lu, B., Ke, X., Zhang, B., & Tang, J. (2013). *In situ* controllable growth of $CoFe_2O_4$ ferrite nanocubes on graphene for colorimetric detection of hydrogen peroxide. *Journal of Materials Chemistry A*, *1*(13), 4352-4357.

Harrison, H. R., Hodder, O. J. R. & Hodgkin, C. D. (1971) Crystal and molecular structure of 8,12-diethyl-2,3,7,13,17,18-hexamethylcorrole. *Journal of the Chemical Society B: Physical Organic, 0*, 640-645.

Hasunuma, T., Kuwabata, S., Fukusaki, E., & Kobayashi, A. (2004). Real-time quantification of methanol in plants using a hybrid alcohol oxidase−peroxidase biosensor. *Analytical Chemistry*, *76*(5), 1500-1506.

Heller, A. (1996). Amperometric biosensor. *Current Opinion in Biotechnology, 7*(1), 50-54.

Heme (n.d.). In *Wikipedia.* http://en.wikipedia.org/wiki/Heme.

Henriksen, A., Smith, A. T., & Gaihede, M. (1999). The structures of the horseradish peroxidase C-ferulic acid complex and the ternary complex with cyanide suggest how peroxidases oxidize small phenolic substrates. *Journal of Biological Chemistry, 274*, 35005-35011.

Heymann, H. & Ebeler, S.E. (2016). *Sensory and Instrumental evaluation of alcoholic Beverages* (1st ed.). Elsevier

Hua, E., Wang, L., Jing, X., Chen, C., & Xie, G. (2013). One-step fabrication of integrated disposable biosensor based on ADH/NAD$^+$/meldola's blue/graphitized mesoporous carbons/chitosan nanobiocomposite for ethanol detection. *Talanta, 111*, 163-169.

Hui, W., Yang, Z., Fang, K., Wu, M., Mu, W., Zhao, C., Xue, D., Zhu, T., Li, X., Gao, M., Lu, Y., & Yan, K. (2022). Hemin with Peroxidase Activity Can Inhibit the Oxidative Damage Induced by Ultraviolet A. *Current issues in molecular biology, 44*(6), 2683–2694.

Janshoff, A., Galla, H. J., & Steinem, C. (2000). Piezoelectric Mass-sensing Devices as Biosensors-An Alternative to Optical Biosensors?. *Angewandte Chemie (International ed. in English), 39*(22) 4004-4032.

Janssen, F. W., & Ruelius, H. W., (1968). Alcohol oxidase, a flavoprotein from several Basidiomycetes species crystallization by fractional precipitation with polyethylene glycol. *Biochimica et Biophysica Acta, 151*(2), 330–342.

Josephy, P., Eling, T., & Mason, R., (1982). The horseradish peroxidase-catalyzed oxidation of 3,5,3',5'-tetramethylbenzidine. Free radical and charge-transfer complex intermediates. *Journal of Biological Chemistry, 257*(7), 3669—3675.

Kadir, M. K.., & Tothill, I. E. (2010). Development of an electrochemical immunosensor for fumonisins detection in foods. *Toxins, 2*(4), 382-398.

Kanlayakrit, W., Boonranasawettatham, s. (2004, February). *Identification of yeasts and molds isolated from Thai tradition fermentation starter (Lookpang) for Sato industry* [Paper Presentation]. The 42nd Kasetsart University Annual conference, Kasetsart University Bangkok.

Kanlayakrit, W., Boonranasawettatham, s. (2005, February). *Identification of yeasts and molds isolated from Thai tradition fermentation starter (Lookpang) for Sato industry* [Paper Presentation]. The 43rd Kasetsart University Annual conference, Kasetsart University Bangkok.

Kaur, J., Choudhary, S., Chaudhari, R., Jayant DR. & Joshi, A. (2019). Enzyme-based biosensors. In Sandeep Choudhary (Eds.), *Bioelectronics and Medical Devices.* (pp. 1-31).

Kawai, H., Kitazumi, Y., Shirai, O., & Kano, K. (2019). Performance analysis of an oxidase/peroxidase-based mediatorless amperometric biosensor. *Journal of Electroanalytical Chemistry*, *841*, 73-78.

Kessler, M. A., Jurgen, G. G., & Wolfbeis, O. S. (1991). Optical sensor for on-line determination of solvent mixtures based on a fluorescent solvent polarity probe. *Sensor & Actuators B: Chemical, 3*(4), 267-272.

Kissinger, P. T. (2005). Biosensors-a perspective. *Biosensors & bioelectronic 20*(12), 2512-2516.

Kondo, H., Nara, J. & Ohno, T. (2011). Possibility of Gas Sensor Using Electronic Transport Properties of Iron−Porphyrin Molecular Junction System. *The Journal of Physical Chemistry C, 115*(14), 6886–6892.

Koenig, B., & Gratzel, M. (1993). Detection of viruses and bacteria with piezoelectric immunosensors. *Analytical Letters, 26*, 1567-1575.

Krueger, D. A., (2012). Composition of pomegranate juice. *Journal of AOAC International, 95*(1), 63-68.

Kruse, J. A. (1992). Methanol Poisoning. *Intensive Care Medicine, 18*(7), 391-397.

Kudo, H., Sawai, M., Suzuki, Y., Wang, X., Gessei, T., Takahashi, D., Arakawa, T., & Mitsubayashi, K. (2010). Fiber-optic bio-sniffer (biochemical gas sensor) for high-selective monitoring of ethanol vapor using 335 nm UV-LED. *Sensors & Actuators B: Chemical, 147*(2), 676-680.

Kurwanna, P. (2001). Factors and Opportunities in the community alcoholic beverages production. *Food, 1,* 23-27.

Kuswandi, B. (2003). Simple optical fibre biosensor based on immobilised enzyme for trace heavy metal ion monitoring. *Analytical & Bioanalytical Chemistry, 376*(3), 1104 -110.

Kuswandi, B., Irmawati, T., Hidayat, M. A., Jayus & Ahmad, M. (2014). A simple visual ethanol biosensor based on alcohol oxidase immobilize onto polyaniline film for halal verification of fermented beverage samples. *Sensors, 14*(2), 2135-2149.

Labib, M., Hedstrom, M., Amin, M., & Mattiasson, B. (2009). A capacitive immunosensor for detection of cholera toxin. *Analytica Chimica acta, 634*(2), 255-261.

Lammer, A. D., Cook, M. E. & Sessler, J. L. (2015). Synthesis and anti-cancer activities of a water soluble gold(III) porphyrin. *Journal of Porphyrins and Phthalocyanines, 19*(1-03), 398–403.

Lau, O. W., & Luk, S. F. (2007). Spectrophotometric method for the determination of ethanol in beverages and beer samples using cerium (IV) as reagent. *International Journal of Food & Technology, 29*(4), 469-472.

Lee, C.-S., Kim, S., & Kim, M. (2009). Ion-sensitive field-effect transistor for biological sensing. *Sensors, 9*(9), 7111-7131.

Li, M., Xiong, Y., Xiaotian, L., Bo, X., Zhang, Y., Han, C., & Guo, L. (2015). Facile synthesis of electrospun $MFe_2O_4$ (M = Co, Ni, Cu, Mn) spinel nanofibers with excellent electro-catalytic properties for oxygen evolution and hydrogen peroxide reduction. *Nanoscale*, *7*(19), 8920-8930.

Li, Q., Mathur, G., Gowda, S., Surthi, S., Zhao, Q., Yu, L., Lindsey, J. S., Bocain, D. F., & Misra, V. (2004). Multibit memory using self-assembly of mixed ferrocene/porphyrin monolayers on silicon. *Advanced Material, 16*(2), 133-137.

Lin, X. Q., Deng, H. H., Wu, G. W., Peng, H. P., Liu, A. L., Lin, X. H., Xia, X. H., & Chen, W. (2015). Platinum nanoparticles/graphene-oxide hybrid with excellent peroxidase-like activity and its application for cysteine detection. *The Analyst*, *140*(15), 5251–5256.

Liu, F., He, J., Zeng, M., Hao, J., Guo, Q., Song, Y., & Wang, l. (2016). Cu–hemin metal-organic frameworks with peroxidase-like activity as peroxidase mimics for colorimetric sensing of glucose. *Journal of Nanoparticle Research*, *18*(5), 106.

Liu, Q., Li, H., Zhao, Q., Zhu, R., Yang, Y., Jia, Q., Bian, B., & Zhuo, L. (2014). Glucose-sensitive colorimetric sensor based on peroxidase mimics activity of porphyrin-$Fe_3O_4$ nanocomposites. *Materials science & engineering. C, Materials for biological applications*, *41*, 142–151.

Liu, Q., Yang, Y., Li, H., Zhu, R., Shao, Q., Yang, S., & Xu, J. (2015). NiO nanoparticles modified with 5,10,15,20-tetrakis(4-carboxyl phenyl)-porphyrin: Promising peroxidase mimetics of $H_2O_2$ and glucose detection. *Biosensors & Bioelectronic, 64*, 147-153. (a)

Liu, Q., Zhang, L., Li, H., Jia, Q., Jiang, Y., Yang, Y., & Zhu, R. (2015). One-pot synthesis of porphyrin functionalized $\gamma$-$Fe_2O_3$ nanocomposites as peroxidase mimics for $H_2O_2$ and glucose detection. *Materials Science and Engineering. C, Material for Biological Application, 55*, 193-200. (b)

Liu, Q., Zhu, R., Du, H., Yang, Y., Jia, Q., & Bian, B. (2014) Higher catalytic activity of porphyrin functionalized Co3O4 nanostructures for visual and colorimetric detection of $H_2O_2$ and glucose. *Materials Science and Engineering. C, Material for Biological Application, 43*, 321-329.

Liu, Z., Yuan, R., Chai, Y., Zhuo, Y., Hong, C., & Yang, X. (2008). Highly sensitive, reagentless amperometric immunosensor based on a novel redox-active organic-inorganic composite film. *Sensors & Actuators B: Chemical, 134*(2), 625-631.

Lu, W., Liao, F., Luo, Y., Chang, G., & Sun, X. (2011). Hydrothermal synthesis of well-sTable silver nanoparticles and their application for enzymeless hydrogen peroxide detection. *Electrocimica Acta, 56*(5), 2295-2298.

Luangkhlaypho, A., Pattaragulwanit, K., Leepipatpiboon, N., & Yompakdee, C. (2014). Development of a defined starter culture mixture for the fermentation of sato, a Thai rice-based alcoholic beverage. *Science, Asia 40*, 125-134.

Lucarelli, F., Marrazza, G., Turner, A. P., & Mascini, M. (2004). Carbon and gold electrodes as electrochemical transducers for DNA hybridization sensors. *Biosensors & Bioelectronics, 19*(6), 515-530.

Maicas, S. (2020). The Role of Yeasts in Fermentation Processes. *Microorganisms*, *8*(8), 1142.

Malhotra, R., Patel, V., Vaque, JP., Gutkind, JS., & Rustling, JF. (2010). Ultrasensitive electrochemical immunosensor for oral cancer biomarker IL-6 using carbon nanotube forest electrodes and multilabel amplification. *Analytical Chemistry, 82*(8), 3118-3123.

Mangos, T .J., & Haas, M. J. (1996) Enzymatic determination of methanol with alcohol oxidase, peroxidase, and the chromogen 2,2'-azinobis(3-ethylbenzthiazoline-6-sulfonic acid) and its application to the determination of the methyl ester content of pectins. *Journal of Agricultural and Food Chemistry, 44*, 2977-2981.

Mani V., Chikkaveeraiah, B. V., Patel, V., Gutkind, J. S., & Rusling, JF. (2009). Ultrasensitive immunosensor for cancer biomarker proteins using gold nanoparticle film electrodes and multienzyme-particle amplification. *ACS Nano, 3*(3), 585-594.

Marsh, EN.(1999). Coenzyme B12 (cobalamin)-dependent enzymes. *Essays in Biochemistry, 34*, 54-139.

Marshall, R. W., & Gibson, T. D. (1992). Determination of sub-nanomole amounts of hydrogen peroxide using an immobilized enzyme flow cell. Application to the determination of ethanol. *Analytica Chimica Acta*, *266*(2), 309-315.

Martelli, C., Canning, J., Reimers, J. R., Sintic, M., Stocks, D., Khoury, T., & Crossley, M. J. (2009). Evanescent-field spectroscopy using structured optical fibers: detection of charge-transfer at the porphyrin-silica interface. *Journal of American Chemical Society*, *131*(8), 2925-2933.

Mathew, S., Yella, A., Gao, P., Humphry-Baker, R., Curchod, B. F., Ashari-Astani, N., Tavernelli, I., Rothlisberger, U., Nazeeruddin, M. K., & Grätzel, M. (2014). Dye-sensitized solar cells with 13% efficiency achieved through the molecular engineering of porphyrin sensitizers. *Nature chemistry*, *6*(3), 242–247.

Matsumoto, K., & Waki, K. (1999). Simultaneous biosensing of ethanol and glucose with combined use of a rotating bioreactor and a stationary column reactor. *Analytica Chimica Acta, 380*(1), 1-6.

McNaught A. D., & Wilkinson A. (1997) IUPAC. *Compendium of Chemical Terminology* (2nd ed. (the "Gold Book"). Blackwell Scientific Publications, Oxford.

Messerschmidt, A., Huber, R., Poulos, K. & Wieghardt K. (2001). *Handbook of metalloproteins*, vols 1 & 2. John Wiley & Sons, Ltd, Chichester

Milgrom L. R. (1997). *The colours of life: an introdruction to the chemistry of porphyrins ann related compounds*. Oxford University Press, Oxford.

Modijtahedi, A., Amirfazil, A., &Farhad, S. (2016) Low catalyst loaded ethanol gas fuel sensor. *Sensor & Actuators B: Chemical, 234*(2), 70-79.

Mohanty, S. P., & Kougianos, E. (2006). Biosensors: a tutorial review. *IEEE potentials, 25*(2), 35-40.

Monošík, R., Stred'anský, M., & Šturdík, E. (2012). Application of electrochemical biosensors in clinical diagnosis. *Journal of clinical laboratory analysis, 26*(1), 22-34.

Montalve, S. I., & Ingle, J. D. (1993). Chemiluminescence during the oxidation of alcohols by permanganate: Application to the determination of ethanol in gin. *Talanta, 40*(2), 167-172.

Mu, J., Wang, Y., Zhao, M. & Zhang, L. (2012). Intrinsic peroxidase-like activity and catalase-like activity of $Co_3O_4$ nanoparticles. *Chemical communication, 19*(48), 2540-2542.

Naresh, V. & Lee, N. (2021). A review on biosensors and recent development of nanostructured materials-enabled biosensors. *Sensor, 21,* 1109.

Nguyen, H. H., Lee, S. H., Lee, U. J., Femin, C.D. & Kim, M. (2019). Immobilized enzymes in biosensor applications. *Materials, 12*(1)*,* 121.

Nirala, N. R., Abraham, S., Kumar, V., Bansal, A., Srivastava, A., & Saxena, P. S. (2015). Colorimetric detection of cholesterol based on highly efficient peroxidase mimetic activity of graphene quantum dots. *Sensors and Actuators B: Chemical, 218*, 42-50.

Opwis, K., Kiehl, K., & Gutmann, J. S. (2016). Immobilization of peroxidase on textile carrier materials and their use in bleaching processes. *Chemical Engineering Transaction, 49*, 67-72.

Otles, S. (n.d.). *Structure and functions of biosensors*. http://eng.ege.edu.tr/~otles/Biyosensorler/structure.html

Ovádeková, R., Jantová, S., Letasiová, S., Stepánek, I., & Labuda, J.  (2006). Nanostructured electrochemical DNA biosensors for detection of the effect of berberine on DNA from cancer cells. *Analytical & Bioanalytical Chemistry, 386*(7-8), 2055-2062.

Pandey, V. P., Awasthi, M., Singh, S., Tiwari, S., & Dwivedi, U. (2017). A Comprehensive Review on Function and Application of Plant Peroxidases. *Biochemistry & Analytical Biochemistry*, *6*(1), 1-16.

Patel, N. G., Meier, S., Cammann, K., & Chemitius, G. (2001). Screen-printed biosensors using different alcohol oxidases. *Sensors & Actuators B: Chemical, 75*(1-2), 101-110.

Pickl, M., Fuchs, M., Glueck, S. M., & Faber, K. (2015). The substrate tolerance of alcohol oxidases. *Applied microbiology and biotechnology*, *99*(16), 6617–6642.

Pimpen, P.& Nitiya, R., (n.d). *Krachae.* https://www.foodnetworksolution.com/wiki/ word/3211.

Pimpen, P.& Nitiya, R., (n.d). *Lao U.* https://www.foodnetworksolution.com/wiki/ word/ 3169.

Porphyrin-http://shodhganga.inflibnet.ac.in/bitstream/10603/323/3/06_ chapter1.pdf.

Prabowo, B. A., Cabral, D. P., Freitas, P., & Fernandes, E. (2019). The challenges of developing biosensors for clinical assessment: A review. *Chemosensors, 9*(11), 299.

Rahman, M., & Harmon, H. J. (2006). Absorbance change and static quenching of fluorescence of meso-tetra(4-sulfonatophenyl)porphyrin (TPPS) by trinitrotoluene (TNT). *Spectrochimica acta. Part A, Molecular and biomolecular spectroscopy*, *65*(3-4), 901-906.

Reisner, D. E., Brauer, S., Zheng, W., Vulpe, C., Bawa, R., Alvelo, J., & Gericke, M. (2014). Bionanotechnology. *1*, 31-86.

Rodionov, Y. V., Keppen, O. I., & Sukhacheva, M. V. (2002). A photometricassay for ethanol. *Applied Biochemistry  &  Microbiology, 38*(4), 395–396.

Rothemund, P. (1935). Formation of porphyrins from pyrrole and aldehydes. *Journal of the American Chemical Society, 57*(10), 2010-2011.

Rothemund, P. (1936). A new porphyrin synthesis. The synthesis of porphyrin. *Journal of the American Chemical Society, 58*(4), 625-627.

Salgado, A. M., Folly, R. O. M., Valdman, B., Cos, O., & Valero, F. (2000). Colorimetric method for the determination of ethanol by Flow Injection Analysis. *Biotechnology letters, 22,* 327-330.

Sanpamongkolchai, W. (n.d.). *Thai traditional alcoholic beverage "Sato".* https://koreascience.kr/article/CFKO200635161995448.pdf.

Sansuk, S., Juntarakod, P., Tongphoothorn, W., Sirimungkala, A., & Somboon, T. (2020). Visual chemo-chronometric assay for quantifying ethanol in alcoholic drinks by the colorimetric Belousov-Zhabotinsky oscillator. *Food Control*, *110*, 107042.

Simon, D. N., Ache, H. J. (1995). Doped sol-gel films for the development of optochemical. *Thin Solid Films*, *260*(1), 107-110.

Shigeto, J., & Tsutsumi, Y. (2016). Diverse functions and reactions of class III peroxidases. *The New Phytology, 209*(4)*,* 1395-1402.

Shin, K. S., & Lee, Y. J. (2000). Purification and characterization of a new member of the laccase family from the white-Rot basidiomycete Coriolus hirsutus. *Archives of Biochemistry and Biophysics*, *384*(1), 109-115.

Shukla, S. K., Govender, P., & Tiwari, A. (2016). Polymeric micellar structures for biosensor technology. In A. Iglic, C. V. Kulkarni, & M. Rappolt (Eds.), Advances in Biomembranes and Lipid Self-Assembly (1st ed., pp. 143–161). Academic Press.

Smith, J. A., & Johnson, R. B. (2018). Infrared spectroscopy-based sensors for alcohol detection. *Sensors and Actuators B: Chemical, 243,* 123-135.

Smith, J. A., & Johnson, R. B. (2019). Development of an alcohol oxidase-based biosensor for ethanol detection. *Sensors and Actuators B: Chemical, 245,* 125-130.

Smith, J. A., Johnson, M. B., & Lee, C. K. (2020). Recent Advances in Fluorescence-based Sensors for Heavy Metal Ion Detection. *Analytical Chemistry, 92*(5), 3667-3680.

Somboon, T., & Sansuk, S. (2018). An instrument-free method based on visible chemical waves for quantifying the ethanol content in alcoholic beverages. *Food chemistry, 253*, 300-304.

Sternberg, E. D., Dolphin, D., & Brückner, C. (1998). Porphyrin-based Photosensitizers for Use in Photodynamic Therapy. *Tetrahedron, 54*(17), 4151-4202.

Stojiljkovic, I., Evavold, B.D. & Kumar, V. (2001). Antimicrobial properties of porphyrins. *Expert Opinion on Investigational Drugs, 10*(2), 309–320.

Tan, H., Ma, C., Gao, L., Li, Q., Song, Y., Xu, F., Wang, T., & Wang, L. (2014). Metal-organic framework-derived copper nanoparticle@carbon nanocomposites as peroxidase mimics for colorimetric sensing of ascorbic acid. *Chemistry (Weinheim an der Bergstrasse, Germany)*, *20*(49), 16377–16383.

Tan, J. & Xu, J. (2020). Applications of electronic nose (e-nose) and electronic tongue (e-tongue) in food quality-related properties determination: A review. *Artificial intelligence in agriculture. 4*, 104-115.

Tayler-Smith, K. (2017). *The properties of biological sensors.* https://www.azosensors.com/article.aspx?ArticleID=1700.

Tetyana, P., Shumbula P. M., & Niengele-Tetyana, Z. (2021). Biosensors: Design, development and applications. *Nanopores*, 1-20.

Thévenot, D. R., Toth, K., Durst, R. A., & Wilson, G. S. (2001). Electrochemical biosensors: recommended definitions and classification. *Biosensors & bioelectronics*, *16*(1-2), 121–131.

Tian, J., Liu, S., Luo, Y., & Sun, X. (2012). Fe(III)-based coordination polymer nanoparticles: peroxidase-like catalytic activity and their application to hydrogen peroxide and glucose detection. *Catalysis Science & Technology.*, *2*, 432-436

Tombelli, S., Minunni, M., & Mascini, M. (2005). Piezoelectric biosensors: strategies for coupling nucleic acids to piezoelectric devices. *Methods, 37*(1), 48-56.

Tossapon, P. (2015). *Synthesis and characterization of meso-tetraphenylporphyrin derivatives and their copper(II) complexes* [Master Thesis]. Thammasat University.

Tromberg, B. J., Sepaniak, M. J., Vo-Dinh, T., & Griffin, G. D. (1987). Fiber-optic chemical sensors for competitive binding fluoroimmunoassay. *Analytical chemistry, 59*(8), 1226-1230.

Twala, P.P., Mitema, A., Buram, C., & Feto, N. A., (2020). Breakthroughs in the discovery and use of different peroxidase isoforms of microbial origin. *AIMS Microbiology, 6*(3), 330-349.

Types of alcohol. (n.d.). https://www.alcoholrehabguide.org/alcohol/types/.

Ukeda, H., Ohira, M., & Sawamura, M. (1999). Immobilized enzyme-based microtiter plate assay for ethanol in alcoholic beverages. *Analytical Sciences, 15*(5), 447–450.

Vanícková, M., Lehotay, J., Cizmárik, J., & Labuda, J. (2005). Kinetic study of the degradation of a potential local anesthetic drug in serum using the DNA-based electrochemical biosensor. *Bioelectrochemistry (Amsterdam, Netherlands)*, *66*(1-2), 125–127.

Velasco-Garcia, M. N. (2009). Optical biosensors for probing at the cellular level: A review of recent progress and future prospects. *Seminars in Cell & Development Biology, 20*(1), 27-33.

Vitamin B12 (n.d.). In *Wikipedia.* http://en.wikipedia.org/wiki/VitaminB12.

Vo-Dinh, T., & Cullum, B. (2000) Biosensor and biochips: advances in biological and medical diagnostics. *Journal of analytical chemistry, 366*(6-7), 540-551.

Vo-Dinh, T., Tromberg, BJ., Griffin, G. D., Ambrose, K. R., Sepaniak, M. J., & Gardenhire, E. M. (1987). Antibody-based fiberoptics biosensor for the carcinogen benzo(a)pyrene. *Applied Spectroscopy, 41*(5), 735-738.

Volschenk, H., Vuuren H. J. & Viljoen-Bloom, M., (2006). Malic acid in wine: Origin, function and metabolism during vinification. *South African journal of enology and viticulture, 2*, 123-136.

Vonck, J., & van Bruggen, E. F., (1990). Electron microscopy and image analysis of two-dimensional crystals and single molecules of alcohol oxidase from *Hansenula polymorpha. Biochimica et Biophysica Acta, 1038*(1), 74–79.

Vorþáková, K., ŠtČpánková, S., Zoriþ, P., Sedlák, M., Metelka, R., & VytĜas, K. (2017). Application of electrochemical sensors for determination of anticholinesterase activity and immobilization of enzyme. *Sensing in electroanalysis, 7,* 409-422.

Waltera, M. G., Rudineb, A. B. & Wamser, C .C. (2010). Porphyrins and phthalocyanines in solar photovoltaic cells. *Journal of Porphyrins and Phthalocyanines, 14*(9), 759–792.

Wang, S. G., Wang, R., Sellina, P. J., & Zhang, Q. (2004). DNA biosensors based on self-assembled carbon nanotubes. *Biochemical & Biophysical Research Communications, 325*(4), 1433-1437.

Wen, G., Li, Z., & Choi, M. M. (2013). Detection of ethanol in food: A new biosensor based on bacteria. *Journal of Food Engineering*, *118*(1), 56-61.

Wen, G., Zhang, Y., Shuang, S., Dong, C., & Choi, M. M. (2007). Application of a biosensor for monitoring of ethanol. *Biosensors and Bioelectronics*, *23*(1), 121-129.

Werner G. (2008). *Alcoholic beverages.* file:///C:/Users/jitti/Downloads/Alcoholic_Beverages.pdf.

WHO (2014). *Global status report on alcohol and health*. http://www. who.int/substance_abuse/publications/global_alcohol_report/en/.

Wikins, E., & Atanasov, P. (1996). Glucose monitoring: state of the art and future possibilities. *Medical Engineering & Physics, 18*(4), 273-288.

Williams, M. B., & Reese, H. D. (1950). Colorimetric determination of ethyl alcohol. *Analytical Chemistry, 22*(12), 1556-1561.

Wine (n.d.). In *Wikipedia.* http://en.wikipedia.org/wili/Wine.

Wu, L., Lei, J., Zhang, X., & Ju, H. (2008). Biofunctional nanocomposite of carbon nanofiber with water-soluble porphyrin for highly sensitive ethanol biosensing. *Biosensors and Bioelectronics*, *24*(4), 644-649.

Xie, X., Suleiman, A. A., Guilbault, G. G., Yang Z. M., & Sun Z. A. (1992). Flow-injection determination of ethanol by fiber-optic chemiluminescence measurement. *Analytica Chimica Acta, 266*(2), 325-329.

Yang, Y. R., Ren, Y. F., Dong, G. M., Yang, R. J., Liu, H. X., Du, Y. H., & Zhang, W. Y. (2016). Determination of Methanol in alcoholic beverages by two-dimensional near-infrared correlation spectroscopy. *Analytical Letters, 49*(14), 2279-2289.

Yoon, I., Li, J. Z. & Shim, Y. K. (2013). Advance in photosensitizers and light delivery for photodynamic therapy. *Clinical Endoscopy, 46*(1), 7–23.

Zhang, L., Peng, D., Liang, R. P., & Qiu, J. D. (2015). Graphene Quantum Dots Assembled with Metalloporphyrins for "Turn on" Sensing of Hydrogen Peroxide and Glucose. *Chemistry (Weinheim an der Bergstrasse, Germany)*, *21*(26), 9343–9348.

Zhang, T., Lu, Y., & Luo, G. (2014). Synthesis of hierarchical iron hydrogen phosphate crystal as a robust peroxidase mimic for sTable $H_2O_2$ detection. *ACS Applied Materials & Interfaces*, *6*(16), 14433–14438.

Zhang, Y., He, X., Li, J., Maio, Z., & Huang, M. (2008). Fabrication and ethanol-sensing properties of micro gas sensor based on electrospun $SnO_2$ nanofibers. *Sensors & Actuators B: Chemical 132*(1), 67-73.

Zhao, D., Chen, C., Lu, L., Yang, F., & Yang, X. (2015). A label-free colorimetric sensor for sulfate based on the inhibition of peroxidase-like activity of cysteamine-modified gold nanoparticles. *Sensors and Actuators B: Chemical, 215*, 437-444

Zhou, W., Cao, Z., Jiang, S., Huang, H., Deng, L., Liu, Y., Shen, P., Zhao, B., Tan, S., & Zhang, X. (2012). Porphyrins modified with a low-band-gap chromophore for dye-sensitized solar cells. *Organic Electronics*, *13*(4), 560-569.

# APPENDICES

# APPENDIX A
# BIOSENSOR MODEL

Solution I
AOX + O.1M PBS
(pH7)
Keep in 4 ºC

Solⁿ I 400 µL + Sample 100 µL

Total Volume 600 µL
Incubate at 37 ºC
for 20 min
(Treated Sample)

Solution II
TMB + FeTOMPP +
0.1 mM NaAc
buffer (pH 6.0)
Keep at room temp

Solⁿ II 1.4 mL + TSample 600 µL

Total Volume 2 mL
Incubate at 30 ºC
for 10 min

Compare with chart color

0-3%

4-6%

7-9%

10-12%

13-15%
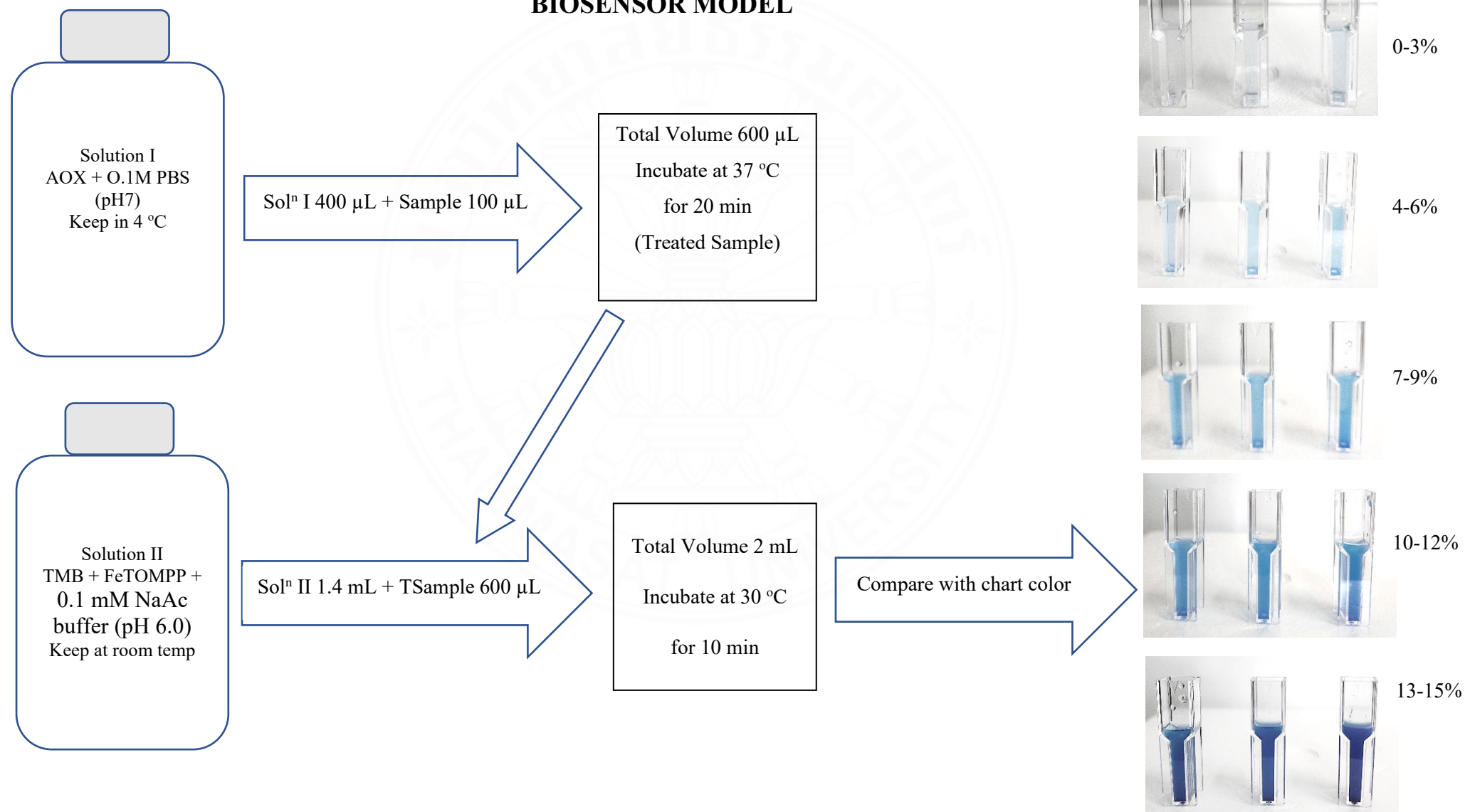
**APPENDIX B**

**PHOPHYRINS AND METALLOPORPHYRIN**

**CHARACTERISTICS**

**1. Structure of porphyrin and metalloporphyrin**



Formula $C_{44}H_{30}N_4$

Tetraphenylporphyrin

TPP

Formula $C_{48}H_{38}N_4O_4$

Tetrakis(4-methoxyphenyl)phenylporphyrin

TOMPP

Formula $C_{60}H_{62}N_4O_4$

Tetrakis(4-butyloxyphenyl)phenylporphyrin
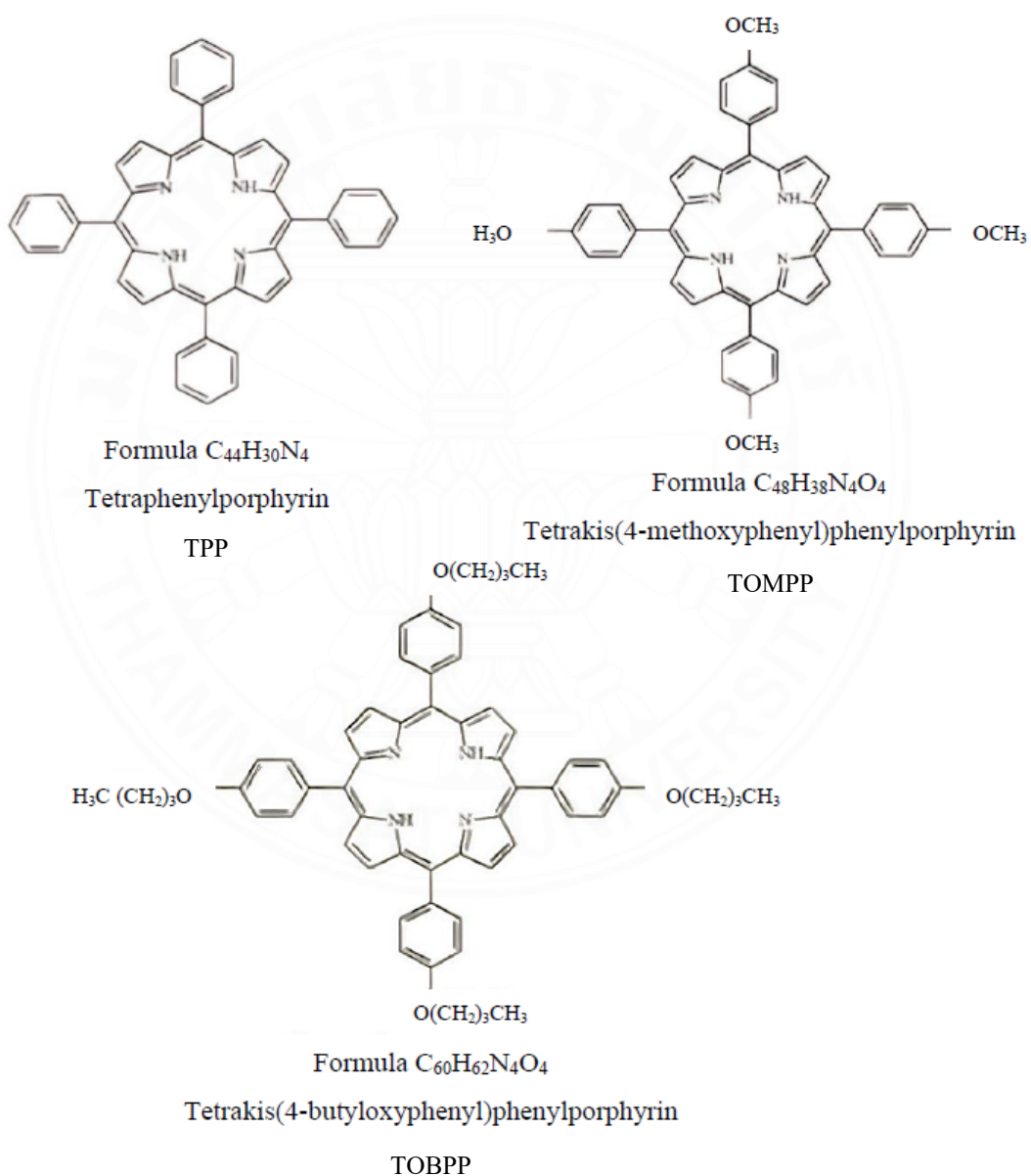
TOBPP

**Figure B.1** The structure of TPP, TOMPP and TOBPP

Formula CuC$_{44}$H$_{28}$N$_4$
Tetraphenylporphyrinatocopper(II)
CuTPP

Formula CuC$_{48}$H$_{36}$N$_4$O$_4$
Tetrakis(4-methoxyphenyl)phenylporphyrinatocopper(II)
CuTOMPP

Formula CuC$_{60}$H$_{60}$N$_4$O$_4$
Tetrakis(4-butyloxyphenyl)phenylporpl
rinatocopper(II)
CuTOBPP

Formula FeC$_{50}$H$_{41}$O$_6$N$_4$
Tetrakis(4-methoxyphenyl)phenylporphrinatoiron(III)
FeTOMPP
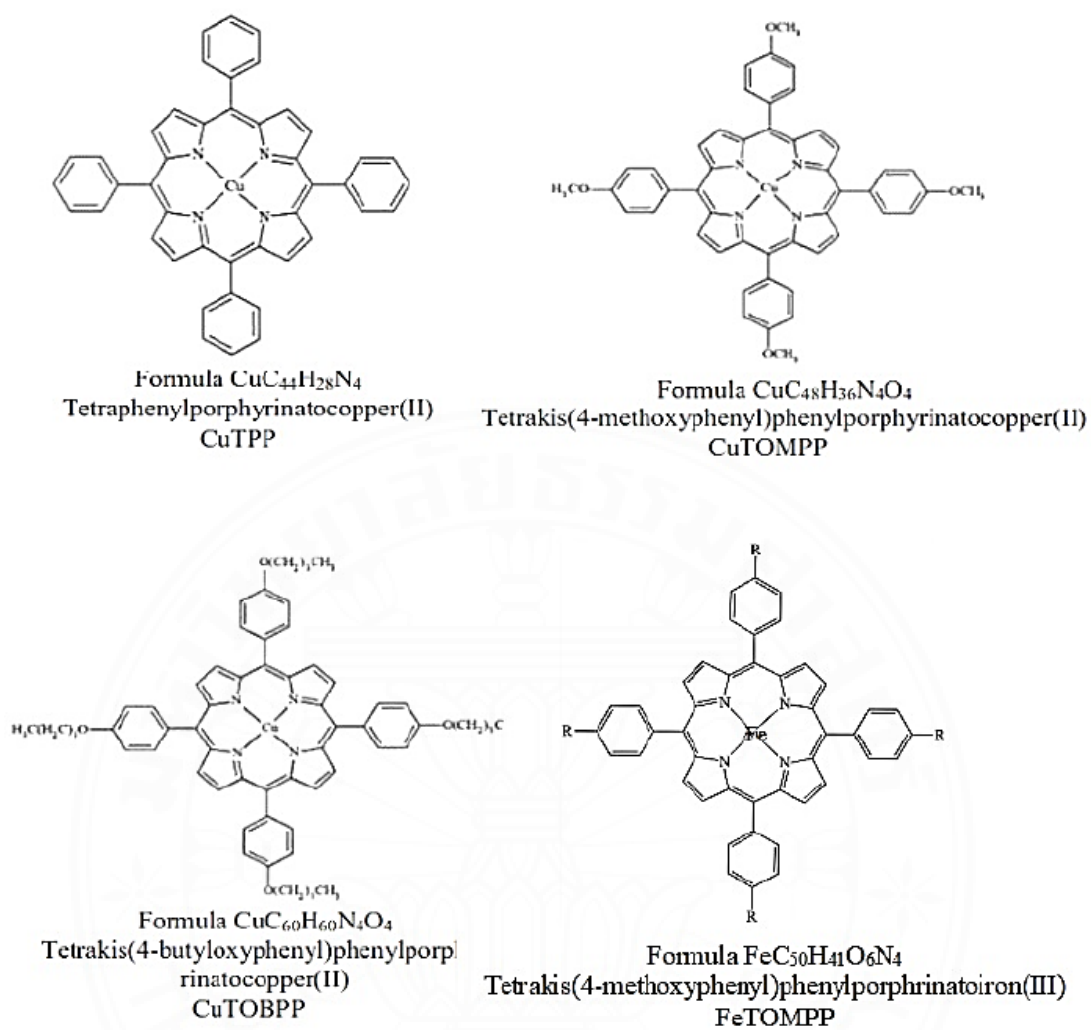
**Figure B.2** Structure of CuTPP, CuTOMPP, CuTOBPP and FeTOMPP

## 2. Mass spectrometry

**Table B.1** Characteristic data of free base porphyrins, copper(II) porphyrins, and iron(III) porphyrin

| Compounds | Empirical formula | Yield (%) | Formula weight [a] | Elemental analysis (b) % | | | MS (m/z) |
|---|---|---|---|---|---|---|---|
| | | | | C | H | N | |
| TPP | $C_{44}H_{30}N$ | 22 | 614.7 | 85.9(86) | 4.9(4.0) | 9.1(9.1) | 615.0 |
| TOMPP | $C_{48}H_{38}N_4O_4$ | 26 | 734.84 | 5.75(5.21) | 7.42(7.62) | 7.42(7.62) | 735.4 |
| TOBPP | $C_{60}H_{62}N_4O_4$ | 9 | 903.16 | 79.44(79.79) | 6.55(6.92) | 5.83(6.20) | 903.6 |
| CuTPP | $CuC_{44}H_{28}N_4$ | 93 | 676.27 | 76.90(78.15) | 3.94(4.17) | 8.18(8.28) | 677.0 |
| CuTOMPP | $CuC_{48}H_{36}N_4O_4 \cdot 2.5CH_2C_{12}$ | 92 | 796.38 | 60.42(60.14) | 4.17(4.07) | 6.22(5.55) | 797.4 |
| CuTOBPP | $CuC_{60}H_{60}N_4O_4$ | 71 | 964.70 | 74.51(74.77) | 6.25(6.23) | 5.76(5.82) | 965.6 |
| FeTOMPP | $FeC_{50}H_{41}O_6N_4$ | 70.3 | 848.84 | 70.42(70.84) | 4.88(4.64) | 6.29(6.61) | 766.0 |
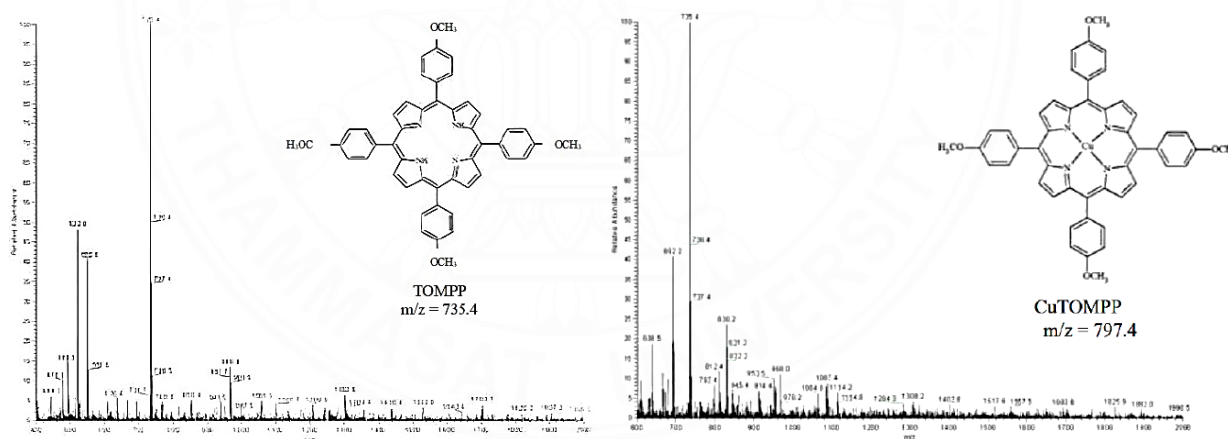


**Figure B.3** The mass spectrum of TOMPP and CuTOMPP

## 3. NMR spectroscopy

**TableB.2** ^{1}H and ^{13}C NMR spectroscopic data for free base porphyrins

| Porphyrins | ^{1}H NMR (ppm), proton | | | | | | | | | |
|---|---|---|---|---|---|---|---|---|---|---|
| | Pyrole, $\beta$-**H** | Phenyl, *o*-**H** | Phenyl, *m*-**H** | Phenyl, *p*-H | OC**H**$_3$ | OC**H**$_2$ | OCH$_2$C**H**$_2$ | C**H**$_2$CH$_3$ | CH$_2$C**H**$_2$CH$_2$ | C**H**$_3$ |
| TPP 4 | 8.85 | 8.20 | 7.77 | 7.52 | - | - | - | - | - | - |
| TOMPP 5 | 8.86 | 8.12 | 7.29 | - | 4.10 | - | - | - | - | - |
| TOBPP6 | 8.86 | 8.11 | 7.28 | - | - | 4.24 | 1.98 | 1.30 | 1.26 | 0.88 |

| Porphyrins | ^{13}C NMR (ppm), carbon | | | | | | | | | | | | |
|---|---|---|---|---|---|---|---|---|---|---|---|---|---|
| | Phenyl, *p*\*-**C** | $\alpha$-**C** | Phenyl, *o*-**C** | $\beta$-**C** | Phenyl, *p*-**C** | *Meso*-**C** | Phenyl, *m*-**C** | OC**H**$_3$ | OC**H**$_2$ | OCH$_2$C**H**$_2$ | CH$_2$C**H**$_2$CH$_2$ | C**H**$_2$CH$_3$ | C**H**$_3$ |
| TPP 4 | 127.70 | - | 134.56 | 131.12 | 142.22 | 120.15 | 126.67 | - | - | - | - | - | - |
| TOMPP 5 | 158.75 | 134.68 | 133.99 | 129.97 | 127.89 | 188.83 | 111.44 | 54.65 | - | - | - | - | - |
| TOBPP6 | 159.09 | 135.32 | 134.74 | 130.70 | 128.76 | 119.7 | 112.84 | - | 68.14 | 31.49 | - | 23.98 | 13.84 |

## 4. Infrared spectroscopy

**TableB.3** Infrared spectroscopic data of free base porphyrins

| Compounds | N-H str. In porphyrin | C-H str. In phenyl and long chain | C=C str. In phenyl | C-N str. In porphyrin | C-O str. In long chain | N-H bend in porphyrin | C-H bend in porphyrin | N=O str. |
|---|---|---|---|---|---|---|---|---|
| TPP | 3310 | - | 1597, 1469 | 1212 | - | 966 | 794 | - |
| TOMPP | 3316 | 2931, 2834 | 1607, 1509 | 1248 | 1174 | 966 | 804 | - |
| TOBPP | 3320 | 2931, 2868 | 1607, 1509 | 1245 | 1174 | 966 | 802 | - |
| CuTPP | - | - | 1600, 1441 | 1345 | - | - | 793 | - |
| CuTOMPP | - | 2929, 2835 | 1607, 1499 | 1248 | 1173 | - | 804 | - |
| CuTOBPP | - | 2930, 2869 | 1607, 1502 | 1246 | 1174 | - | 799 | - |
| FeTOMPP | - | 2943, 2868 | 1581, 1500 | 1237 | 1173 | - | 725 | - |

Unit $Cm^{-1}$

## 5. UV-vis spectroscopy
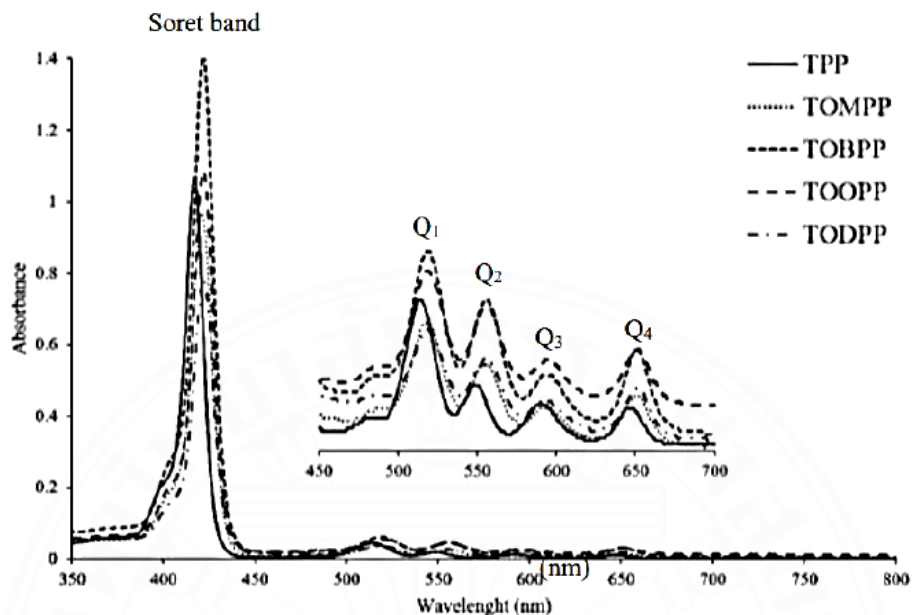


**FigureB.4** UV-Vis absorption spectra of free base porphyrins in dichloromethane (CH$_2$Cl$_2$) solution

**Table B.4** Absorption data of all compounds

| Porphyrin | Dichloromethane[a] | | | |
|---|---|---|---|---|
| | S band (nm) | Q band (nm), $\varepsilon$(M$^{-1}$cm$^{-1}$) | | |
| | | Q$_1$ | Q$_2$ | Q$_3$ | Q$_4$ |
| TPP | 417 | 514, 14122 | 548, 6140 | 590, 4605 | 649, 399 |
| TOMPP | 421 | 518, 11941 | 555, 8266 | 595, 3980 | 650, 5205 |
| TOBPP | 422 | 519, 22955 | 556, 17310 | 595, 8655 | 651, 11665 |
| CuTPP | 415 | - | 540, 13863 | - | - |
| CuTOMPP | 419 | - | 541, 18914 | - | - |
| CuTOBPP | 419 | - | 541, 24599 | - | - |
| FeTOMPP | 417 | - | 578, 17453 | - | - |

## 6. Fluorescence spectroscopy
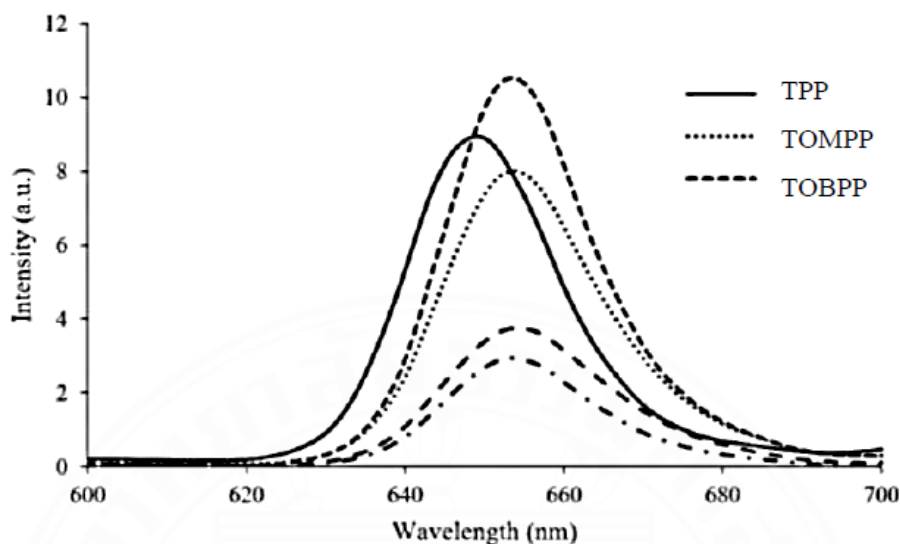


**FigureB.5** Emission spectra of free base ligands in dichloromethane ($CH_2Cl_2$) solution

**Table B.5** Absorption-Emission wavelength and estimated energy gap of free base porphyrins in dichloromethane

| Porphyrin | Dichloromethane | | |
|---|---|---|---|
| | Absorption wavelength (nm) | Emission wavelength (nm) | Egap (ev) |
| TPP | 529 | 649 | 1.92 [76] |
| TOMPP | 534 | 654 | 1.90 |
| TOBPP | 534 | 654 | 1.90 |
| CuTPP | 556 | 605 | 2.17[a] |
| CuTOMPP | 556 | 654 | 2.16[a] |
| CuTOBPP | 556 | 604 | 2.17[a] |

[a] Calculate by using average of wavelength between Q-band and emission band

## 7. Thermal gravimetric analysis (TGA)

**Table B.6** Decomposition temperatures of free base porphyrins and copper(II) porphyrins

| Compounds | Stage I | | Stage II | |
|---|---|---|---|---|
| | $T_{decomp}$/K | Weight loss/% (Tf/K) | $T_{decomp}$/K | Weight loss/% (Tf/K) |
| TPP | 671 | 74.4 (680) | - | - |
| TOMPP | 680 | 18.7 (738) | 738 | 81.6 (973) |
| TOBPP | 688 | 60.1 (763) | - | - |
| CuTPP | 808 | 88.2 (859) | - | - |
| CuTOMPP | 732 | 49.2 (773) | - | - |
| CuTOBPP | 748 | 42.7 (777) | - | - |

# APPENDIX C
# REAL SAMPLE MEASUREMENT SUPPLEMENT DATA

**Table C.1** The alcoholic beverages that use for GC and biosensor measurements

| Symbol | Product |
|---|---|
| Beer 1 | Cheer X-tra Beer |
| Beer 2 | Chang Beer |
| Beer 3 | Singha Beer |
| Beer 4 | Leo Beer |
| Sato 1 | Local Sato |
| Sato 2 | Sato Bangma |
| Sato 3 | Sato Siam |
| Krachae | Local Krachae |
| Soju 1 | Soju Chamisul grapefruit |
| Soju 2 | The Nanda soju peach |
| Wine 1 | Spy Wine cooler white |
| Wine 2 | Spy Wine cooler classic |
| Wine 3 | Penfolds Koonung Hill Chrdonay |
| Liquor 1 | Sangsom |
| Liquor 2 | White spirit |

**Table C.2** The analysis of ethanol in commercial beverage sample using GC

| Product | Area ratio | | | |
|---|---|---|---|---|
| | **No.1** | **No.2** | **No.3** | **Average** |
| Beer 1 | 6.4101 | 6.4023 | 6.4195 | 6.4106 ± 0.0086 |
| Beer 2 | 5.4819 | 5.5012 | 5.4567 | 5.4799 ± 0.0223 |
| Beer 3 | 5.1299 | 5.1201 | 5.1545 | 5.1348 ± 0.0177 |
| Beer 4 | 5.1701 | 5.1523 | 5.1798 | 5.1674 ± 0.0139 |
| Sato 1 | 6.4994 | 6.5623 | 6.4769 | 6.5129 ± 0.0443 |
| Sato 2 | 7.4786 | 7.5225 | 7.4513 | 7.4841 ± 0.0359 |
| Sato 3 | 6.5519 | 6.6034 | 6.5271 | 6.5608 ± 0.0389 |
| Krachae | 10.3134 | 10.2786 | 10.3687 | 10.3202 ± 0.0454 |
| Soju 1 | 7.5247 | 7.2786 | 7.8261 | 7.5431 ± 0.2742 |
| Soju 2 | 8.2672 | 8.4619 | 8.1859 | 8.3050 ± 0.1418 |
| Wine 1 | 4.335 | 4.4687 | 4.2188 | 4.3408 ± 0.1251 |
| Wine 2 | 4.2104 | 4.5813 | 4.3312 | 4.3743 ± 0.1892 |
| Wine 3 | 6.7351 | 6.9812 | 6.6451 | 6.7871 ± 0.1740 |
| Liquor 1 | 4.8896 | 4.7245 | 5.0231 | 4.8791 ± 0.1496 |
| Liquor 2 | 4.6291 | 4.3908 | 4.8891 | 4.6363 ± 0.2492 |

**Table C.2** Relationship between ethanol concentration and area ratio of ethanol and iso-butanol

| Ethanol conc. (%) | Area ratio | | | |
|---|---|---|---|---|
| | No.1 | No.2 | No.3 | Average |
| 0.5 | 0.2749 | 0.3708 | 0.2749 | 0.3069 ± 0.0452 |
| 1 | 0.8029 | 0.8108 | 0.8403 | 0.8180 ± 0.161 |
| 2 | 1.6795 | 1.6551 | 1.6223 | 1.6523 ±0.234 |
| 3 | 2.6978 | 2.6978 | 2.6088 | 2.6681 ± 0.042 |
| 4 | 3.6815 | 3.6514 | 3.3489 | 3.5606 ±0.1502 |
| 5 | 4.9746 | 4.992 | 5.1213 | 5.0293 ±0.0654 |
| 6 | 5.9928 | 6.0236 | 6.2114 | 6.0759 ± 0.0966 |
| 7 | 7.3231 | 7.4018 | 7.3329 | 7.3526 ± 0.0350 |
| 8 | 8.7987 | 8.8992 | 8.5437 | 8.7472 ± 0.1496 |
| 9 | 10.1261 | 10.5726 | 10.0028 | 10.2338 ± 0.2448 |
| 10 | 11.5346 | 11.8276 | 11.9928 | 11.7850 ± 0.1895 |
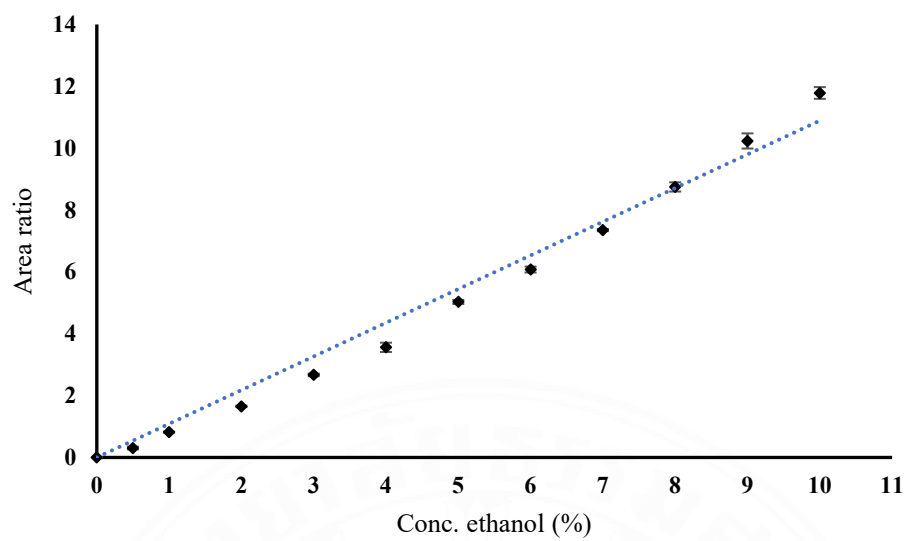
**Figure C.1** Calibration curves for ethanol using iso-butanol as an internal standard.

# BIOGRAPHY

Name                                    MS. Jittima Khorungkul

Educational Attainment        2003: Bachelor of Science in Biotechnology,
                                            Mahidol University
                                            2007: Master of Science in Environmental
                                            Technology, Mahidol University

Publication

Paper publishing in Heritage Journal in science and technology volume 18 no.2 (2023).

Paper publishing in Trends in Science volume 21 (2024).